UNIVERSIDAD COMPLUTENSE DE MADRID
FACULTAD DE CIENCIAS MATEMÁTICAS

Departamento de Matemática Aplicada

ORIENTACIÓN Y SISTEMAS ECOLÓGICOS MEDIANTE SEÑALES LOCALES

MEMORIA PARA OPTAR AL GRADO DE DOCTOR
PRESENTADA POR

María Vela Pérez

Bajo la dirección de los doctores
Juan José López Velázquez
Marco Antonio Fontelos López

Madrid, 2011

ISBN: 978-84-694-8496-8

Orientación y sistemas ecológicos mediante señales locales

Tesis doctoral realizada por:

D.ª María Vela Pérez

Bajo la dirección de:

Dr. D. Juan José López Velázquez
Dr. D. Marco Antonio Fontelos López

2011

Departamento de Matemática Aplicada

Facultad de Ciencias Matemáticas
Universidad Complutense de Madrid

D. Juan José López Velázquez, Profesor Catedrático de la Universidad Complutense de Madrid del Departamento de Matemática Aplicada e Investigador del ICMAT y D. Marco Antonio Fontelos López, Investigador del ICMAT, AUTORIZAN:

La presentación de la Tesis Doctoral titulada ***Orientación y sistemas ecológicos mediante señales locales***, realizada por D.ª María Vela Pérez bajo nuestra dirección en el Departamento de Matemática Aplicada y que presenta para la obtención del grado de Doctor, con Mención Europea, por la Universidad Complutense de Madrid.

En Madrid, a dia de mes de año

Juan José López Velázquez

Marco Antonio Fontelos López

A mi familia

Agradecimientos

En primer lugar, a mis directores de tesis Juan José López Velázquez y Marco Antonio Fontelos López, por su gran esfuerzo y dedicación durante estos años. Gracias por vuestros sabios consejos y acertadas correcciones, por todo el tiempo que me habéis dedicado, por vuestra total implicación y tremendo entusiasmo, sin las cuales este trabajo no hubiera sido posible. Y sobre todo, por vuestra infinita paciencia.

Gracias a la Fundación Ramón Areces por concederme una beca para realizar parte de este trabajo y a la URJC por contratarme como profesora ayudante.

Gracias a mis compañeros de la URJC que siempre me han apoyado. En especial, a Javi con quien he tenido la suerte de compartir despacho y aprender un poquito de rigor y orden. Gracias también a Marek, Fabricio, Juan y Juan-Antonio.

Gracias a mis compañeros cataneses Roberta, Alessio, Giuseppe y Enzo. Y en especial, a Vito, por hacerme sentir en casa desde el primer día y por preocuparse de mi. También a mis compañeros del Instituto Max Planck, con los que tanto disfruté en Leipzig.

Gracias a todos mis amigos: a los que están y a los que decidieron dejar de estar. A mis amigas de toda la vida Ángela C., Ángela L., Ana e Iris. A mis compañeros de la Orquesta Sinfónica Chamartín, con los que tengo el privilegio de disfrutar de la buena música en directo en cada concierto. A mis colegas del grupo Verona 9, por los buenos ratos en el local dándole fuerte a la batería. A mis compañeros y amigos de la carrera Carlos G., Joaco, Pablo (Vero y Marcos), María, Nacho, Esti, Bea, Pedro, Carlos P., Carlos F. y Sonia. En especial, a Grego, gracias por estar siempre ahí, en lo bueno y en lo malo.

Por último, quiero dedicar esta tesis a toda mi familia que son lo mejor: mis padres, mis tíos, mis primos, mi abuela y, en especial, a mi hermano José. Sin vosotros yo no estaría aquí. Y finalmente, a Ignacio Luengo "no-matemático" por existir, ser único y demostrármelo cada día; gracias por pintar mi vida con tantos colores.

Index

Prólogo

Desde la aparición de las ecuaciones de Lotka Volterra en el siglo XIX para la modelización de la dinámica de poblaciones, se han producido numerosos avances en el campo de la biología matemática. Problemas tan dispares como el modelado de neuronas, la génesis y el crecimiento de un cáncer, la mecánica de los tejidos biológicos, el funcionamiento de los sistemas fisiológicos o modelos multi-escala del corazón han sido tratados con mayor o menor éxito combinando técnicas matemáticas con experimentos biológicos.

En particular, en el campo de la Ecología, la ciencia que estudia a los seres vivos, se han desarrollado numerosos modelos. Entre otras cosas, estos modelos nos permiten comprender mejor el funcionamiento de los seres vivos que habitan a nuestro alrededor, así como, copiar y trasladar el funcionamiento de sus mecanismos a productos creados por el hombre. No es de extrañar que el ser humano analice la Naturaleza y aproveche su perfección a la hora de desarrollar, por ejemplo, redes de comunicación más eficientes.

La presente monografía está dedicada a la modelización y estudio de geodésicas en sistemas formados por hormigas.

En el Capítulo 1 se introducen los problemas matemáticos más interesantes relacionados con el estudio a desarrollar. En concreto, se revisan los modelos de desarrollo de patrones biológicos, haciendo un hincapié especial en los modelos de agregación de tipo Keller-Segel. A continuación, se revisan los patrones de formación en la morfogénesis. En particular, se revisa la morfogénesis de redes vasculares. Posteriormente, se describen brevemente los algoritmos de optimización de colonia de hormigas. Después, se revisan modelos de ecuaciones diferenciales para describir el comportamiento de las hormigas cuando salen del hormiguero en busca de comida. Se estudian los casos particulares de modelos mediante ecuaciones estocásticas y simulaciones de Montecarlo. Finalmente, se exponen los resultados fundamentales de la tesis.

En el Capítulo 2 se recopilan los datos experimentales para diferentes tipos de hormigas. Entre otras, se estudian las hormigas Argentinas (*Iridomyrmex humilis*), las hormigas Faráon (*Monomorium pharaonis*), las hormigas Lasius niger (*Hymenoptera, Formicidae*) y las hormigas soldado (*Eciton burchelli*).

En el Capítulo 3 se realizan simulaciones en grafos sencillos. Dichos grafos representan laberintos simples en los que otros autores han realizado estudios experimentales. Compara-

mos los resultados de nuestras simulaciones con dichos resultados experimentales, y obtenemos conclusiones sobre los mecanismos básicos para la formación de caminos de longitud mínima.

En el Capítulo 4 se desarrolla un estudio analítico para redes con reforzamiento de dos y tres nodos. El resultado fundamental obtenido para una red de tres nodos y dos hormigas es que son necesarias dos condiciones, reforzamiento y direccionalidad de las hormigas, para obtener caminos geodésicos entre el hormiguero y la comida.

En el Capítulo 5 se realizan simulaciones en redes más complicadas. Entre otras, en una red de ocho nodos, en redes polarizadas y no polarizadas y en mallados regulares e irregulares. En estas últimas, se estudia en detalle el problema en las fronteras de las redes y las condiciones que son necesarias para reproducir los resultados experimentales.

En el Capítulo 6 se realizan simulaciones de Montecarlo. Considerando el plano, se sitúan el hormiguero y la comida y se estudian dos algoritmos distintos para encontrar caminos geodésicos.

En el Capítulo 7 se destacan las conclusiones más importantes que se derivan de esta tesis, se resumen sus principales aportaciones y se comentan algunas líneas futuras de investigación.

Objetivos de la tesis

- Formular y describir detalladamente un problema de búsqueda de geodésicas que ha sido, por el momento, tratado experimentalmente en la literatura especializada.
- Estudiar los posibles modelos para el problema numérica y analíticamente.
- Desarrollar algoritmos capaces de simular el problema en forma óptima (en tiempo y capacidad de proceso).
- Encontrar soluciones analíticas para casos sencillos y demostrar resultados rigurosos en algunos de esos casos.
- Realizar una extensa experiencia computacional empleando diversos modelos y presentar, relacionar y comentar en detalle los resultados obtenidos.
- Como objetivo global, demostrar que la acción combinada de reforzamiento y persistencia en caminos aleatorios de múltiples individuos da lugar a caminos de longitud mínima entre dos puntos.

Summary

- We will describe some interesting experimental results for 4 different types of ants.
- We will describe in detail some models appeared in the literature.
- We will solve analytically some models for networks of two and three nodes for one ant.
- We will solve analytically the model for a three node network without reinforcement and with directionality constraint for two ants.
- We will solve analytically the model for a three node network with reinforcement and with directionality constraint for two ants.
- We will develop numerical algorithms and perform extensive numerical computations in various situations: simple networks, complex networks and Monte Carlo simulations to show that both directionality constraint and reinforcement are needed in order for the ants to follow the shortest paths. Moreover, we will develop a model for the motion of ants in a general planar domain and solve it numerically to show the tendency for the ants to create shortest paths.
- We will compare our results with the ones appeared in the literature.

Chapter 1

Introduction

Goals of this chapter

- General discussion on chemotaxis and aggregation models.
- General discussion on morphogenesis. In particular, morphogenesis of vascular networks.
- General discussion on minimal paths in graphs.
- General discussion on mathematical models for ants.
- Main results of this thesis.

In recent times, one of the main emphasis in mathematical biology studies lies in the study of development, differentiation and morphogenesis (development of the shape) of living things. The forms of organisms arise by complex dynamic processes that show many levels of organization. How individual organisms establish connection and coordinate to develop a higher order of organization (in the form of pluricellular entities, organs, etc.) or collective behavior (in the form of swarms, flocks, etc.) is one of the main problems in current theoretical and mathematical biology. Despite a still incomplete understanding, some broad concepts are now recognized as underlying principles [39, 49]. In this thesis, we propose a set of simple principles that are minimal for the formation of swarms of ants and show, by means of mathematical analysis and numerical simulations, that they are necessary for the formation of paths of minimal length between a nest of ants and food source.

Our models for ant foraging follow various ideas derived from the study of chemotactic movements where random walkers emit signals (the chemoattractant that can influence the motion of other individuals). Of special importance is the well known Keller-Segel model which is the first system of partial differential equations (PDE's) that was proposed to account for

the formation of aggregates under the influence of chemical signals. It can be deduced from a random walk process which is in the spirit of the ones proposed by us in chapters 2 to 6. In fact, the rigorous justification of the PDE's from discrete processes is a very active area of research. In the thesis, we have focused on the discrete processes and generated PDE's in certain limits which are very much in the spirit of models a la Keller-Segel. In the context of vasculogenesis, various models that combine chemotactic processes and persistence effects, understood as the tendency for random walker to follow straight lines, have been proposed in the past. Since one of our findings is that persistence is also crucial for the formation of minimal paths, we present in this introduction some of the main ideas behind chemotaxis and vasculogenesis. More directly related to the motion of ants, we will discuss later in this chapter the most relevant early models that are based in systems of differential equations, and indicate what in our view are their limitations.

We first study different models for ant's behavior in terms of differential equations in section 1.1. Then, we describe the main results of this thesis. After, since there are many different models and theories for differentiation and morphogenesis (due to the variety of aspects of the phenomena) we will focus on some models for development and morphogenesis in subsections 1.3.1 and 1.3.2. Finally, some interesting algorithms appeared in the field of artificial intelligence that employ ant optimization algorithms are reviewed in subsection 1.3.3.

1.1 Mathematical models for ants

Social insects are an important example of complex collective behavior. In particular, ant colonies develop different tasks as foraging, building and allocation [28]. This collective behavior might be regulated either by a centralized mechanism (the queen) or a distributed control where the local interactions between the individuals determine the collective behavior [10]. In the subsequent sections we review some stochastic models and Monte Carlo simulations to model this collective behavior.

1.1.1 Stochastic equations models for ants

In [22], a series of experiments have been done with *Iridomyrmex humilis* (Argentine ant). The main question the authors aimed to answer is: how can an animal with only limited and local navigational information achieve to find the shortest path between nest and food? As it is well known, Argentine ant has a limited individual capacity for orientation. Hence, they need to cooperate via pheromone trails with other ants in order to find the shortest path to the food source.

Different differential equations models have been proposed since 1989 trying to catch the key points in ants's behavior observed in the experiments:

1. The first ant finds the food source (F), via any way (a), then returns to the nest (N), leaving behind a trail pheromone (b).

2. Ants can follow four possible ways, but the strengthening of the runway makes more attractive the shortest route.

3. The shortest route is selected for almost all the ants.

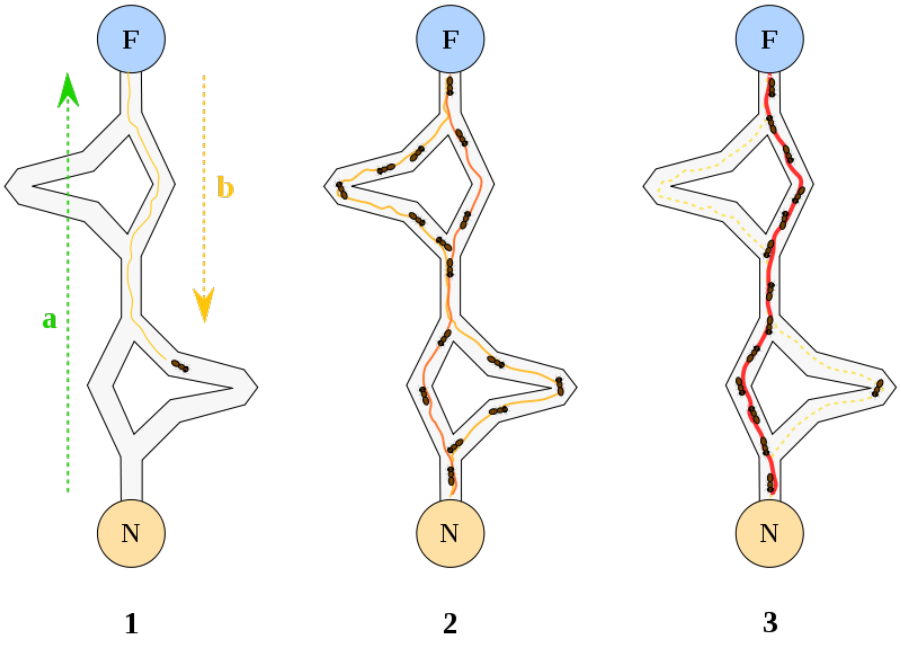

Figure 1.1: A colony of I. humilis selecting the short branches

In [22] the authors consider that Φ ants cross the bridge in each direction per second laying one pheromone unit. When ants arrive to one of the choice points ($j = 1, 2$), each ant selects the short or long branch with probability $p_{s,j}$ and $p_{l,j}$ respectively. These probabilities depend on the quantities S_j and L_j of pheromone on the two branches at that choice point (see figure 1.2).

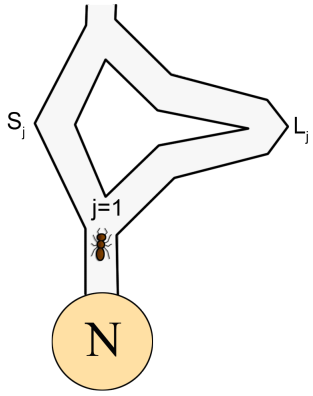

Figure 1.2: Ant at choice point

It takes 20 seconds to arrive to the next choice point for those ants selecting the short path, whereas it takes $20r$ seconds to cross the long one, where r is the ratio of the length of the long branch to the short one. The evaporation of pheromone is ignored because the time scale of the experiments is of order of the mean lifetime of the pheromone. Hence, at time t the average equations for the stochastic model are:

$$\frac{dS_j}{dt} = \Phi p_{s,j'}(t-20) + \Phi p_{s,j} t, \tag{1.1}$$

$$\frac{dL_j}{dt} = \Phi p_{l,j'}(t-20r) + \Phi p_{l,j} t, \tag{1.2}$$

$$p_{s,j} = \frac{(20-S_j)^2}{(20-S_j)^2 + (20-L_j)^2}, \tag{1.3}$$

where if $j = 1, j' = 2$ and if $j = 2, j' = 1$, and the probabilities satisfy $p_{s,j} + p_{l,j} = 1$. Equation (1.3) is the choice function based on the experimental results appeared in [9]. This stochastic model is solved numerically by employing Monte Carlo simulations. It shows that the colony's probability of selecting the shortest path increases with the difference between the two branches. For two equally sized branches, one of the two is randomly selected. Furthermore, if the short branch is only present after the trail on the long branch has been established, the colony cannot switch to the short branch. Finally, if the workers leave pheromone when returning to the nest, as some species do, it is not possible for the colony to select the short branch more times than the long one. This is due to the lack of double marking in the short branch at the initial period. A summary of the results is the following:

- If both branches are equal ($r = 1$), there is not a significant preference.
- If one branch is a bit longer than the other ($r = 1.4$), ants select more times the short branch (15/18).
- If one branch is much longer than the other ($r = 2$), ants select almost always the short branch (14/14).

Overall, the main limitation of system (1.1-1.2) is its poor justification in terms of stochastic processes which results in the need to have a number of ad-hoc assumptions. Moreover, it is very specific to the geometry depicted in figure 1.1 and it is not clear how to extend it to more general situations, and in particular, to motions in a planar domain.

1.1.2 Monte Carlo simulations for ant models

There are not many studies concerning motions of ants in the plane. The most relevant one concerns the particular army ant *Eciton burchelli*. These colonies of ants are huge (may have a million of workers) and carnivores, and form traffic lanes in their main foraging columns. In [7] it is shown that the movement rules of individual ants can produce a collective behavior creating distinct traffic lanes that minimize congestion and maximize traffic flow. This is done assuming pre-existing pheromone concentration with fix profile. A general model of ant behavior is developed, in terms of individual-based simulation approach. To do so, it is studied first the behavior of individual ants in the absence of interactions with other ants. After so, the collective properties of the model during the generation of spatial patterns are investigated.

N ants are simulated. Each ant i has a position vector $\mathbf{c}_i(t)$ and a direction vector $\mathbf{v}_i(t)$ at time t; the head is at $\mathbf{c}_i(t) + \frac{1}{2}\beta\mathbf{v}_i(t)$, where β is the ant body length. Each antennae is extended a distance ϕ from the head at an angle 45° to the ant's body orientation. One of the key points of this model is that it takes into account the abilities of ants to detect and avoid colliding with other ants. In order to do that, there are defined two local areas (interaction zone). The first one is a circle of radius r_d with center at $\mathbf{c}_i(t)$, representing the proximity to the body of the ant. The second one is an arc extending from $\mathbf{c}_i(t)$ a distance r_p and with an internal angle α, representing either a local visual field in some species or the tactile range of the antennae. Figure (1.3) shows the representation of the flow chart for the algorithm.

The algorithm is as follows:

1. At each time step t, all the ants are moved simultaneously. For each ant i, it is calculated the desired vector $\mathbf{d}_i$, provided that there are other ants j within the interaction zone of ant i:

$$\mathbf{d}_i(t+\Delta t) = \sum_{j\neq i} \frac{\mathbf{c}_i(t) - \mathbf{c}_j(t)}{|\mathbf{c}_i(t) - \mathbf{c}_j(t)|}. \tag{1.4}$$

   The ant is able to turn through an angle of, at most, $\theta_a\Delta t$ degrees in time Δt. The value of θ_a is an input value for the algorithm. If the angle between $\mathbf{v}_i(t)$ and $\mathbf{d}_i(t+\Delta t)$ is less than the maximum turning angle then $\mathbf{v}_i(t+\Delta t) = \mathbf{d}_i(t+\Delta t)$, that is it achieves alignment with the desired vector. Otherwise, it turns $\theta_a\Delta t$ towards it. In this way, individuals are able to turn away from others. They also try to slow down to avoid collisions with a constant acceleration, $-\mu$, unless they are not at the minimum speed $u_{\min}$.

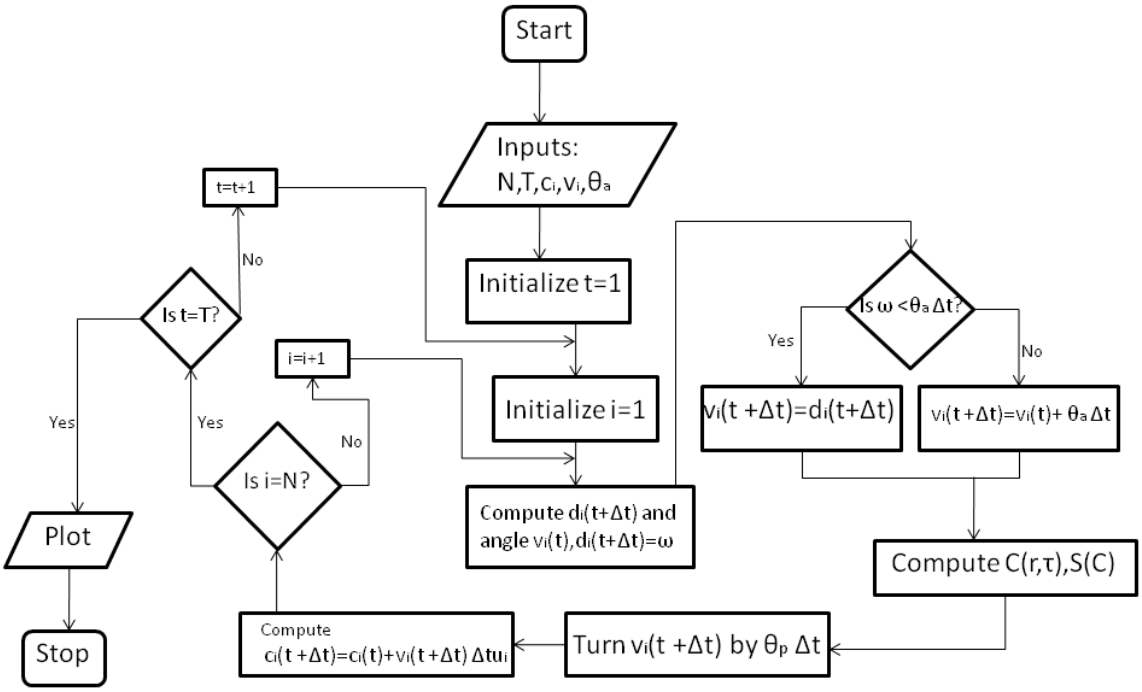

Figure 1.3: Representation of flow chart of the Algorithm appeared in [7].

2. If there is not any ant in the interaction zone of ant i, it responds to pheromone concentration defined as:

$$C(r,\tau) = \frac{Q}{2\pi D\tau} e^{-\frac{r^2}{4D\tau}}, \tag{1.5}$$

where Q is the amount of pheromone deposited (g/cm) and D is the diffusion coefficient ($D = 0.01cm^2/s$ is the typical value measured experimentally). Since the aim of the model is to study the movement of ants along a pre-existing trail, the concentration profile is fixed after setting time τ.

3. For each ant i, it is defined the stimulus intensity function as:

$$S(C) = \frac{\arctan\left(k(\frac{C}{C_{\max}})\right)}{\frac{\pi}{2}}, \tag{1.6}$$

where $C_{\max}$ is the saturate concentration for antennae and k is a constant that controls the rate at which the concentration approaches its maximal value ($k = 100$). Ant i follows the direction of highest pheromone concentration. To do so, it turns its direction by $\theta_p \Delta t$. This turning is subject to an error and so vector $\mathbf{v}_i(t + \Delta t)$ is rotated an angle ϵ by employing a Gaussian- distributed random number, centered at zero and with a standard

deviation of 0.5 radians. If ant i is not avoiding collisions it accelerates with acceleration μ until it reaches its desired speed u_{des}.

4. For the special study of sense of direction, it is defined a directional preference by employing an internal unit vector $\mathbf{g}_i(t+\Delta t)$, with a weight of ω and replacing $\mathbf{d}_i(t+\Delta t)$ by $\mathbf{d}'_i(t+\Delta t)$ as follows:

$$\mathbf{d}'_i(t+\Delta t) = \frac{\mathbf{d}_i(t+\Delta t) + \omega \mathbf{g}_i(t+\Delta t)}{|\mathbf{d}_i(t+\Delta t) + \omega \mathbf{g}_i(t+\Delta t)|}. \tag{1.7}$$

5. For each ant i, the new position vector is given by

$$\mathbf{c}_i(t+\Delta t) = \mathbf{c}_i(t) + \mathbf{v}_i(t+\Delta t)\Delta t u_i, \tag{1.8}$$

where u_i is the current speed. In this process the time is partitioned into discrete steps with spacing $\Delta t = 0.02$s.

There are several parameters that have been measured by employing some video analysis for the army ants and are summarized in table 1.1.

Table 1.1: Experimental data measured for the model

Parameter	**Value**
r_d	0.4 cm
r_p	1.2 cm
β	0.8 cm
ϕ	0.4 cm
u_{des}	13 cm/s
u_{min}	2 cm/s
μ	50 cm/s^2

The study has three parts: the behavior of individual ants, the collective selection of a direction and the bi-directional traffic with lane formation (where it is applied equation (1.7)). The mains results for the behavior of individual ants are:

- The distance that an individual ant moves along a trail before losing it is a complex function of the pheromone concentration of that trail. Intermediate values maximize the accuracy of trail following. The saturation level, C_{max}, changes the position of the peak of the distribution of the pheromone concentration.

- The error, σ, does not change the position of the peak, but when increasing the error the covered distance by ants before losing the trail decreases. This noise has a greater influence on ant's behavior when there is a small difference between the concentrations at each antennae.

- If pheromone concentration is very low and trails are very narrow, any error made by an ant may cause it to lose the trail.

For the case of the collective selection of a direction, by employing periodic boundary conditions, it is found that the flow F of ants is strongly influenced by the avoidance turning rate, θ_a, and the internal angle of the perception zone ahead of an ant, α. At intermediate values of these parameters, ants are sufficiently sensitive to the positions of others and can select a direction collectively ($\alpha = 90°$).

Finally, for the bi-directional traffic with lane formation, it is suggested that army ants have a sense of direction. This is based on the observations in [23] and in the proposed model. Furthermore, there is a qualitative difference in the behavior of those ants leaving the nest and returning to it, but the flow of ants, F, is quite similar. This flow is dependent on the strength of directional preference, ω, and the magnitude of the asymmetry of avoidance turning rate, $\Delta\theta_a$. Regardless of $\Delta\theta_a$, F is maximum when $\omega = 1$ (same weight for local conditions and directional preference), whereas it has low values when ω tends to zero. For high values of ω ants are forced to slow down through long-lasting collisions resulting in congestion. At intermediate values, increasing $\Delta\theta_a$ causes an asymptotic increase in F. This increase is due to the fact that outbound ants occupy the periphery whereas returning ones occupy the center.

In this model it is shown how local interactions and individual movement rules can strongly influence the organization of traffic over a large spatial scale. Nevertheless, it does not constitute a full self-consistent model due to the fact that pheromone concentration is assumed to be fixed in time and it is not clear whether reinforced random walks of ants are able to produce lanes of minimal length.

1.2 Main results of this thesis

Problem description and previous results in the literature

- We will describe some interesting experimental results for 4 different types of ants.
- We will describe in detail some models appeared in the literature.

Analytical results

- We will solve analytically some models for networks of two and three nodes for one ant.
- We will solve analytically the model for a three node network without reinforcement and with directionality constraint for two ants.
- We will solve analytically the model for a three node network with reinforcement and with directionality constraint for two ants.

Computational experiments

- We will develop numerical algorithms and perform extensive numerical computations in various situations: simple networks, complex networks and Monte Carlo simulations to show that both directionality constraint and reinforcement are needed in order for the ants to follow the shortest paths. Moreover, we will develop a model for the motion of ants in a general planar domain and solve it numerically to show the tendency for the ants to create shortest paths.

- We will compare our results with the ones appeared in the literature.

In the subsequence sections, we discuss some classical models of pattern formation in mathematical biology. Although the subjects mentioned in the next subsections will not be studied in this thesis, these mathematical models have inspired us for the derivation of our model.

1.3 General background

1.3.1 Development of biological patterns: aggregation

There are many relevant biological processes that involve chemotaxis, a process in which many cells react to chemical stimuli moving towards an increasing or decreasing chemical gradient. A particular case of chemotaxis has deserved attention of many scientists such as biologists, physicists and mathematicians. This particular process is chemotactic aggregation.

Aggregation in cellular slime molds: the Keller-Segel model

Slime molds have fascinated biologists for many decades. A particular species has been the most frequently studied: *Dictyostelium discoideum* (Dd). This unicellular organism under certain conditions of environmental stress begins a complex cascade of chemical processes. The main consequence is the release away from the cell of a chemical substance having chemoattractant properties in the cells themselves. The key points of this process can be summarized as follows:

1. When food becomes scarce, the amoebae enter a phase of starvation. An initially uniform cell distribution develops what is called *aggregation sites*, some kind of centers of organization.

2. Cells are attracted to the aggregation sites and move in a wavelike manner towards them.

3. Contacts begin to form between neighbors and streams of cells converge in a single site forming a multicellular shapeless mass.

4. The aggregate changes its shape several times; at some time it takes the appearance of a slug that moves in a characteristic way.

5. The cells in the forward portion become somewhat different biochemically from the ones on the rear. A process of differentiation has taken place; there are two types of cells: prespore and prestalk.

6. The collection of cells executes a crawling motion adopting different shapes until it seems a reverse fountain. The stalk bears a spore-filled capsule at its top, hardening its cells that eventually die.

7. The spore cells can be dispersed by air currents and thus propagate the species. Since individual cells do not reproduce after the onset of aggregation, a fraction of cells must die always.

The life cycle of Dictyostelium discoideum is represented in figure 1.4.

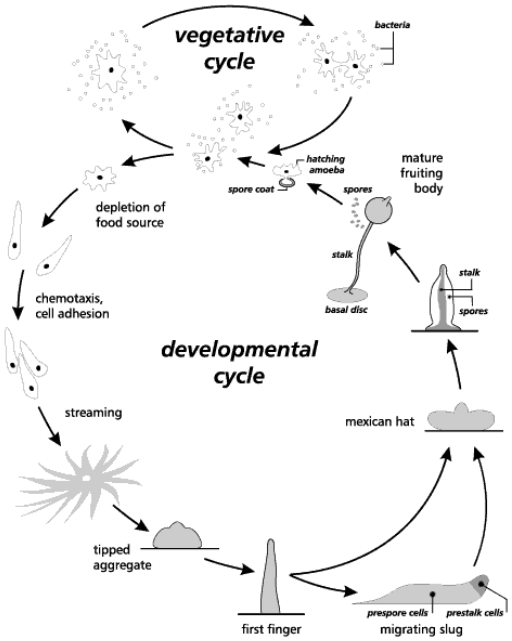

Figure 1.4: Life cycle of Dictyostelium discoideum

The earliest attempt to describe chemotactic aggregation employing a two dimensional system of PDEs was the Keller-Segel model (see [35] and [36]). It is a continuum model that describes the aggregation process for Dd and contains the fundamental biological knowledge from the experiments (for further details on the experiments see [4]). It is assumed that there are only two relevant variables:

- the cell concentration n=n(x,t),
- the chemical concentration of the substance c=c(x,t) that propagates the signals between the cells, called cAMP.

The functions are assumed to be, during the aggregation process, functions of the Petri dish x as well as time t. In order to have a valid description with this assumption, the functions n and c have to be measured in a length scale larger than the typical distance between cells. Then, the model is the following:

$$\frac{\partial n}{\partial t} + \nabla \cdot (j_n) = 0, \tag{1.9}$$

$$\frac{\partial c}{\partial t} + \nabla \cdot (j_c) = f(n, c), \tag{1.10}$$

where j_n, j_c are the cell fluxes and chemical fluxes respectively. The function $f(n, c)$ describes the production of chemical by the cells as well as the decay of the concentration of c due to its interaction with the environment. These fluxes can be described by assuming that diffuse according to the classical Fick's law:

$$j_c = -D_c \nabla c, \tag{1.11}$$

$$j_n = -D_n \nabla n + \chi n \nabla c, \tag{1.12}$$

where D_c, D_n are the diffusion coefficients for the chemical and the cells respectively, and χ is the chemotactic sensitivity. In order to define the function $f(n, c)$, two important facts have to be taken into account. The first one is that the molecules of cAMP degrade with a characteristic life-time, due to their interaction with the molecules of the enviroment. The second one is that, if the chemical production of each cell is assumed to be independent from the others, the production of chemical per unit area is proportional to the cell concentration n. Hence, the function $f(n, c)$ would be

$$f(n, c) = \alpha n - \beta c, \tag{1.13}$$

with $\alpha > 0, \beta > 0$. Putting together equations (1.9-1.13), we find the following system of PDEs:

$$\frac{\partial n}{\partial t} = D_n \Delta n - \chi \nabla \cdot (n \nabla c), \tag{1.14}$$

$$\frac{\partial c}{\partial t} = D_c \Delta c + \alpha n - \beta c. \tag{1.15}$$

All the effects demonstrated in the analysis depend on the functional forms of the three main processes during chemotactical movement. They are:

- The sensing of the chemoattractant which has an effect on the oriented movement of the species.
- The production of the chemoattractant by a mobile species or an external source.
- The degradation of the chemoattractant by a mobile species or an external effect.

For a complete review on this topic see [29], [30] and [50]. There have been many studies of chemotaxis in Keller-Segel models. In [25] it is shown, by means of matched asymptotic expansions techniques, that there exist radial solutions exhibiting chemotactic collapse. In [26] and [27] it is found a class of solutions for a two dimensional Keller-Segel model under certain assumptions, for which chemotactic collapse occurs and can be described in a precise manner. In [33], for a class of initial values, explosion of the bacteria concentration in finite time is shown in two space dimensions and radially symmetric situations. In [24] a rigorous mathematical characterization for early pattern formation in the Keller-Segel model is given.

Aggregation and reinforced random walks

As seen above, in some biological systems, the movement of an organism in response to a signal can be modeled by diffusion equations with advection terms (see also [48]). Other biological systems are best modeled in terms of random walkers that deposit a nondiffusing signal. In [34] and [55] it is given an introduction to open problems and recent studies of classes of partial differential equations for chemotactic problems. In [31] and [47] a complete study of those systems is done, showing a variety of possible dynamics as aggregation, blowup or collapse. To do so, partial differential equations that approximate several different reinforced jump processes are derived and analyzed. The aim of [47] is to understand the qualitative behavior of the continuous equations and establish a correspondence between the asymptotic behavior of the PDEs and the results for the reinforced random walk appeared in [8]. In [31] a class of space-jump processes explaining the mechanisms by which mysobacteria propel themselves on the substrate and aggregates is analyzed.

Different models are considered in [47]. We only explain in detail those that produce some kind of aggregation at some point. In order to describe the models, a master equation for a continuous-time and discrete-space random walk in one dimension is considered. It is assumed that the transition rates depend on the density of a control or modulator species W and jumps are one step long. If we denote the conditional probability $p_n(t)$ that a walker is at $n \in \mathbb{Z}$ at time t, conditioned on the fact that it begins at $n = 0$ at $t = 0$, then the continuous-time master equation is

$$\frac{\partial p_n}{\partial t} = \hat{\mathcal{T}}^+_{n-1}(W)p_{n-1} + \hat{\mathcal{T}}^-_{n+1}(W)p_{n+1} - (\hat{\mathcal{T}}^+_n(W) + \hat{\mathcal{T}}^-_n(W))p_n, \tag{1.16}$$

where $\hat{\mathcal{T}}^\pm_n(\cdot)$ are the transition probabilities per unit time for a one-step jump to $n \pm 1$, and $(\hat{\mathcal{T}}^+_n(W) + \hat{\mathcal{T}}^-_n(W))^{-1}$ is the mean waiting time at the nth site. The vector W is given by

$$W = (\ldots, \omega_{-n-\frac{1}{2}}, \omega_{-n}, \omega_{-n+\frac{1}{2}}, \ldots, \omega_0, \omega_{\frac{1}{2}}, \ldots). \tag{1.17}$$

That is, the density of the control species ω is defined on the embedded lattice of half the step size.

The first model we review is a barrier and nearest-neighbor model, where the ω-dependence of the transition rate at site n is localized at $n \pm \frac{1}{2}$ and produces a bias on the transition rate. That is, $\hat{\mathcal{T}}^\pm_n(W) = \hat{\mathcal{T}}(\omega_{n\pm\frac{1}{2}})$. Then, by employing an appropriate scaling equation (where $\hat{\mathcal{T}}(\omega) = \lambda\mathcal{T}(\omega)$), (1.16) becomes

$$\frac{\partial p}{\partial t} = D\nabla \cdot (\mathcal{T}(\omega)\nabla p), \tag{1.18}$$

where p is the probability density, ω is the control substance, $\mathcal{T}(\omega)$ is the transition probability in an homogeneous and isotropic medium and

$$D = \lim_{\substack{h\to 0 \\ \lambda\to\infty}} \lambda h^2$$

exists, being h the mesh size. The average particle velocity is given by

$$\mathbf{u} = -D\mathcal{T}(\omega)\frac{\nabla p}{p}. \tag{1.19}$$

This process contains only a diffusional component and depending on the initial data, there may be a transient aggregation. But, it does not persist and so it is sometimes called pseudochemotaxis.

Within the framework of PDEs models, stable aggregation can occur with local modulation of the transition rates (see [47] for further details). The model is a barrier model with linear response function and renormalized transition rates. The governing equation for the particle density is:

$$\frac{\partial p}{\partial t} = D\frac{\partial}{\partial x}\left(\frac{\partial p}{\partial x} - \frac{p}{\omega}\frac{\partial \omega}{\partial x}\right), \tag{1.20}$$

for $x \in (0,1)$, with Neumann boundary conditions and production rate for ω given by:

$$\frac{d\omega}{dt} = \frac{p\omega}{1+\nu\omega} - \mu\omega + \gamma_r\frac{p}{1+p}. \tag{1.21}$$

Equation (1.21) represents saturation growth, which is more realistic in the biological context. There, the production can locally be very large if ν is sufficiently small, but eventually saturates. The computational results show that the probability density p can reach a stable, stationary, nonconstant solution, whereas the control substance ω continues to growth (see figure 1.5 where $\nu = 1 \times 10^{-5}, \mu = 0$ and $\gamma_r = 0$). If the decay rate μ is zero, the density converges to a stable aggregation whereas for $\mu = 1$ it blows up (see figure 1.6). This is due to the fact that at large μ the production of ω never saturates.

Nevertheless, equations (1.20, 1.21) are for walkers which do not interact directly but only indirectly via ω and the contact interaction observed experimentally is not included in the model. Moreover, in the absence of diffusion of ω the asymptotic behavior of p strongly depends on the history of the process and, in particular, on the initial data.

1.3.2 Pattern formation in morphogenesis

The processes underlying morphogenesis are complex, spanning subcellular to multicellular levels within the individual. During almost one century, they have been studied both experimentally and theoretically. Despite many advances have been done, understanding how global patterns of tissue movement and deformation emerge from the combined activities of many individual cells remains a central unsolved problem in developmental biology. We will review the pioneering paper by Turing in the following subsection and we will focus on morphogenesis in vascular networks. The latter topic is quite related to our investigations with ants, since in many models it is proposed that persistence and chemotaxis are key factors for the models.

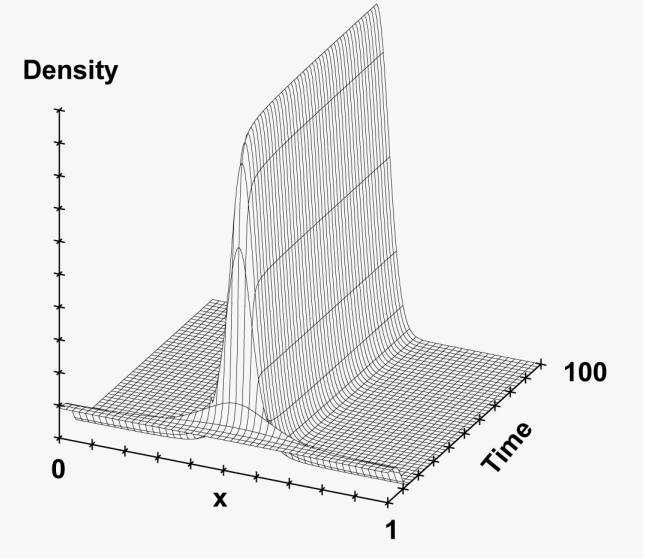

Figure 1.5: The evolution of p in (1.20,1.21) as a function of time for $D = 0.036$, $\nu = 10^{-5}$, and $\mu = \gamma_r = 0$. Figure from [47].

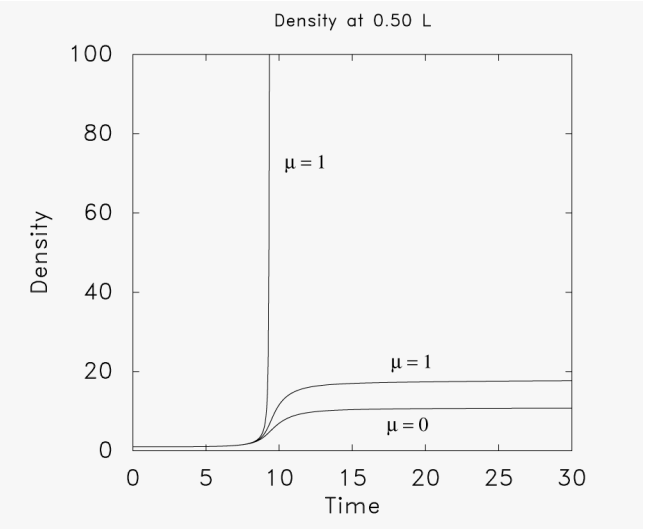

Figure 1.6: The evolution of p for the solution of (1.20,1.21) at the midpoint of the interval as a function of time for the indicated values of the decay rate μ. Figure from [47].

Chemical basis for morphogenesis

In 1952 Turing proposed in a pioneering paper [59] that the potential of diffusion lead to chemical morphogenesis. It was an astonishing result in which diffusion engenders chemical gradients and fosters nonuniform chemical patterns.

The main necessary elements for chemical pattern formation are [17]:

- Two or more chemical species.

- Different rates of diffusion for the participants.
- Chemical interactions. There is one activator and one inhibitor substance.

In this way, chemical patterns can arise as a destabilization of a uniform chemical distribution with a proper combination of these factors. Turing suggested that during stages in the development of an organism, chemical constituents generate a pre-pattern that is later interpreted as a signal for cellular differentiation. After Turing's paper, chemical substances playing a role in cellular differentiation are called *morphogen*. In [51] it is proposed the following model that captures these instabilities:

$$\frac{\partial C_1}{\partial t} = R_1(C_1, C_2) + D_1 \frac{\partial^2 C_1}{\partial x_2}, \tag{1.22}$$

$$\frac{\partial C_2}{\partial t} = R_2(C_1, C_2) + D_2 \frac{\partial^2 C_2}{\partial x_2}, \tag{1.23}$$

where $C_1 = C_1(x,t), C_2 = C_2(x,t)$ are the concentrations of the chemicals, D_1, D_2 are the diffusion coefficients and $R_1(C_1, C_2)$ is the rate of production of C_1 and $R_2(C_1, C_2)$ is the rate of production of C_2.

Morphogenesis of vascular networks

Endothelial Cells (ECs) are able to organize themselves to form capillary-like networks when cultured *in vitro* in a suitable environment. It is interesting to notice that this characteristic is also shared by melanoma cells [60], although the morphogenetic process depends on the specific experimental setting [2]. In [19] it is proposed a nonlinear system of PDEs to model the process of angiogenesis in tumor growth, a process consisting on sprout new blood vessels from a pre-existing vascular network initiated by release of chemicals by the tumor.

The formation of vascular networks in vitro develops two stages [57]: early migration-dominated stage where the main features of the pattern emerges and a subsequent stage where the mechanical interaction of the cells with the substratum stretches the network. Hence, there are two main approaches to model vasculogenesis: chemical models based on the concepts of cell persistence and endogenous chemotaxis, and mechanical models based on the interactions with the substratum. Furthermore, in [57] it is proposed a unified approach for the morphogenetic process in terms of physical mechanisms and mathematical modeling.

In [21] and [52] it is proposed a vascular network formation model for the early development based on the basic assumption that persistence and chemotaxis are the key features determining the size of the structure. Here, the mechanical interactions are neglected. It is described the behavior of the system during the first $3-6$ hours.

The mathematical model is constructed taking into account the following assumptions:

1. Persistence is shown in the motion of endothelial cells.

2. A soluble growth factor provides communication between endothelial cells via release and absorption. This chemical factor can be identify with VEGF-A[52].

3. The chemical factors released by cells diffuse and degrade in time.

4. During the process, endothelial cells neither duplicate nor die.

5. Due to the interaction with the fixed substratum cells are slowed down by friction.

6. Closely packed cells mechanically respond to avoid overcrowding.

Three state variables are considered:

- The density n of endothelial cells.
- The velocity $\mathbf{v}$ of the endothelial cells.
- The density c of chemoattractant.

These assumptions lead to the following set of equations

$$\frac{\partial n}{\partial t} + \nabla \cdot (n\mathbf{v}) = 0, \tag{1.24}$$

$$\frac{\partial n\mathbf{v}}{\partial t} + \nabla \cdot (n\mathbf{v} \otimes \mathbf{v}) = \mathbf{f}, \tag{1.25}$$

$$\frac{\partial c}{\partial t} = D\Delta c + \alpha n - \frac{1}{\tau}c. \tag{1.26}$$

Equations (1.24) and (1.25) are Euler's equations, the ones governing inviscid fluids in fluid dynamics. Equation (1.24) is a mass conservation equation. It is assumed that cells do not undergo mitosis (cell division) or apoptosis (process of programmed cell death). Equation (1.26) is a diffusion equation for the chemical factor which is produced at a rate α and degrades with a half life τ. Equation (1.25) assumes that cell motion can be obtained on the basis of a suitable force balance. It includes the divergence of a dyadic product, and may be clearer in subscript notation ($j = 1, 2, 3$)

$$\frac{\partial (nv_j)}{\partial t} + \sum_{i=1}^{3} \frac{\partial (nv_i v_j)}{\partial x_i} = \mathbf{f}_j, \tag{1.27}$$

where i and j label the three Cartesian components for vectors $\mathbf{v} = (v_1, v_2, v_3), \mathbf{x} = (x_1, x_2, x_3)$ and $\mathbf{f} = (f_1, f_2, f_3)$. Although the second term in the l.h.s of equation (1.25) reminds the convective flux of cellular matter, it should be understood as a term modeling persistence; that is, the inertia in changing cell direction. There are several reasons which may cause a change in cell persistence that are modeled by the force term $\mathbf{f}$. The main ones are:

1. A chemotactic body force
$$\mathbf{f}_{chem} = \beta n \nabla c, \tag{1.28}$$
where β measures the intensity of cell response per unit mass. Since each cell senses a similar chemotactic action, the dependence on n is linear.

2. A dissipative interaction with the substrate
$$\mathbf{f}_{diss} = -\gamma n \mathbf{v}, \tag{1.29}$$
where again the linear dependence on n is due to the fact that each cell is subject to the same dissipative forces.

3. The resistance of closely packed cells to compression
$$\mathbf{f}_{surf} = -\nabla[n\pi(n)]. \tag{1.30}$$

Rearranging terms and employing some algebra, equations (1.24-1.26) can be written as
$$\frac{\partial n}{\partial t} + \nabla \cdot (n\mathbf{v}) = 0, \tag{1.31}$$
$$\frac{\partial \mathbf{v}}{\partial t} + \mathbf{v} \cdot \nabla \mathbf{v} = \beta \nabla c - \gamma \mathbf{v} - \nabla \varphi(n), \tag{1.32}$$
$$\frac{\partial c}{\partial t} = D\Delta c + \alpha n - \frac{1}{\tau} c, \tag{1.33}$$
where $\varphi(n)$ is defined by
$$\varphi = \int \frac{1}{n} \frac{d}{dn}(n\tau) dn.$$
Equations (1.31-1.33) are known as PEC model (Persistence and Endogenous Chemotaxis). It is interesting to notice that assuming immediate adjustment of the cells to the limit velocity (by dropping the pressure and persistence terms in (1.32)) one has the classical chemotactic models (see [47]), where blow-up in finite time is possible.

The PEC model was solved numerically in [2] by integrating equations (1.31-1.33) with the following initial conditions:
$$n(\mathbf{x}, t=0) = \frac{1}{2\pi r^2} \sum_{j=1}^{M} e^{-\frac{(\mathbf{x}-\mathbf{x}_j(\omega))^2}{2r^2}}, \tag{1.34}$$
$$\mathbf{v}(\mathbf{x}, t=0) = \mathbf{0}. \tag{1.35}$$
These initial conditions represent M Gaussian bumps for cell density; they are centered at random locations $\mathbf{x}_j$ distributed with uniform probability on a square of size L and average cell radius $r \simeq 20\mu m$. Periodic boundary conditions are imposed and the initial velocity is zero.

The results of the simulations are in agreement with the experimental data (see figures 1.7 and 1.8, taken from [2]).

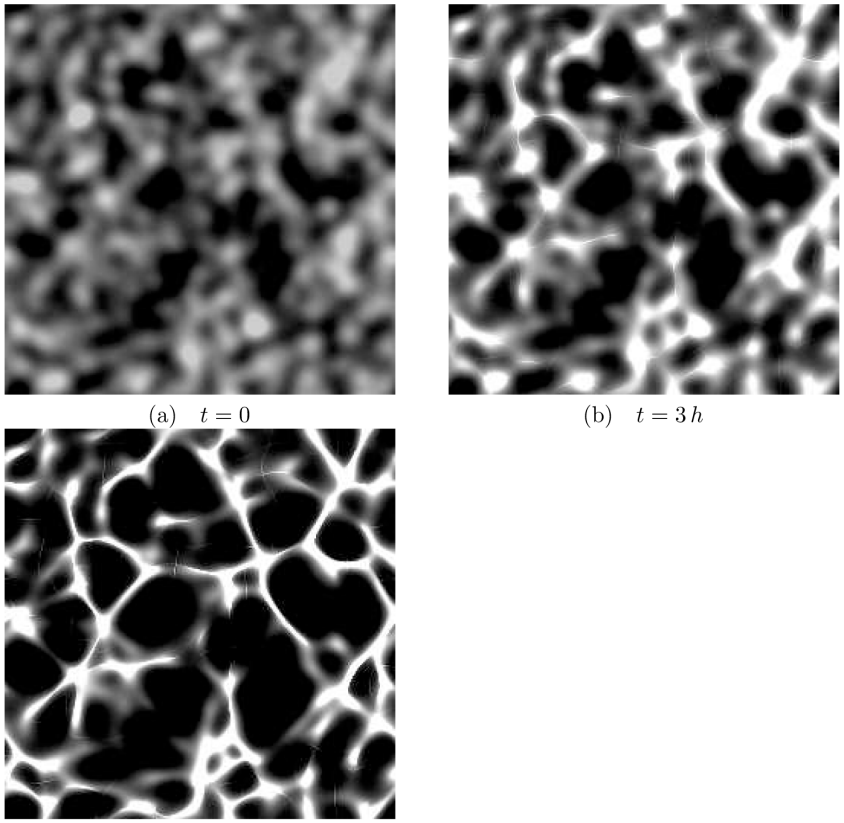

(a) $t = 0$ (b) $t = 3\,h$

(c) $t = 6h$

Figure 1.7: Simulation of the initial development of vascular networks. Figure from [2].

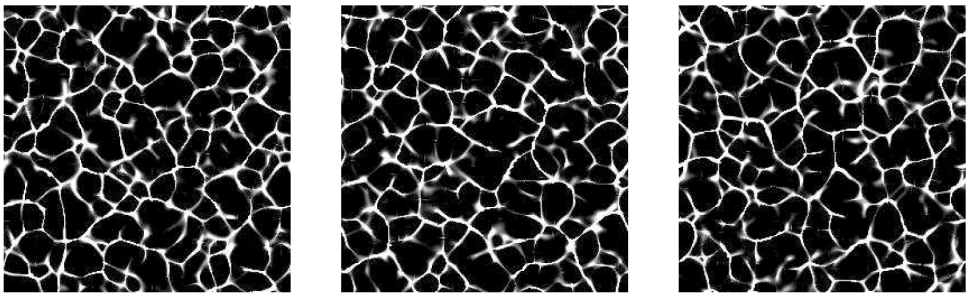

Figure 1.8: Dependence of the specific network structure on the initial conditions. Figure from [2].

The process of network formation is as follows:

- Initially, the random inhomogeneities of the density function enforce non zero velocities built up by the chemoattractant term.
- Density inhomogeneities are translated to places where details of scales of the character-

istic length $\ell = \sqrt{D\tau}$ are averaged out.

- The cellular matter moves toward the ridges of concentration of the chemoattractant factor.

- In the concentration landscape the ridges are sharpened and the valleys are emptied out by a non linear mechanism as in fluid dynamics. A network structure characterized by a length scale of order ℓ is produced.

We can remark that there is a dependence of the characteristics of the structure on the density of seeded cells and on the transitions occurring at small and large densities respectively (see figure 1.8). Furthermore, there must exist a precise mechanism controlling the average chord length during vascular formation, like the one hypothesized in model (1.24-1.26).

The PEC model describes very well the early migration dominated stages of network formation. Its basic assumption is that the mechanisms of persistence and endogenous chemotaxis govern the size of the capillary structure through the diffusion coefficient D and the chemoattractant half-life τ. The predicted average size of formed network structures $\ell \simeq \sqrt{D\tau}$ agrees the obervations *in vivo* and measurements *in vitro*. Furthermore, PEC numerical simulations reproduce the percolative transition around $n_c \simeq 100\ cell/mm^2$, that distinguish when the functional network is formed and when it is not properly connected. PEC model describes in a proper way the case when a moderate number of cells is seeded on the substratum.

In [18], [38], [41], [42], [43], [44] and [46] appear some mechanical models describing the formation of capillary network. The pioneering paper [44] was mainly devoted to mesenchymal (a type of loose connective tissue) morphogenesis based on some experiments regarding the interaction between Extracellular Matrix (ECM, the extracellular part of animal tissue that usually provides structural support to the animal cells) and fibroblasts (a type of cell with a strong pulling force). The main assumptions of the mechanical models are the following ones:

1. Cells exert traction forces onto the ECM, which is a viscoelastic material.

2. The Petri dish exerts a drag force on the matrix.

3. Cells may move because of haptotaxis (directional motility of cells) or chemotaxis.

Three state variables are considered:

- The density n of endothelial cells.

- The density ρ of ECM.

- The displacement $\mathbf{u}$ of ECM from its original position.

All the mathematical models inspired on the model proposed in [44] can be written as follows:

$$\frac{\partial n}{\partial t} + \nabla \cdot \mathbf{J} = \Gamma, \tag{1.36}$$

$$\frac{\partial \rho}{\partial t} + \nabla \cdot (\rho \mathbf{w}) = -\Delta, \tag{1.37}$$

$$-\nabla \cdot \mathbf{T}_n - \nabla \cdot \mathbf{T}_\rho = \mathbf{F}, \tag{1.38}$$

where $\mathbf{w} := \frac{d\mathbf{u}}{dt}$ is the ECM velocity, $\mathbf{J}$ is the cellular flux, Γ refers to the (possible) generation and death of cells, Δ is the (possible) digestion of ECM by the cells, $\mathbf{T}_n$ is the cell traction stress and $\mathbf{T}_\rho$ is the stress in the deformed ECM. Finally, $\mathbf{F}$ is the force due to the interaction between the ECM and the Petri-dish. Equations (1.36) and (1.37) are mass balance equations. Cells may duplicate or die during the process and ECM is degraded and produced by cells. In most cases (1.36) and (1.37) are written as conservation laws by neglecting cell duplication/apoptosis and ECM production/degradation. Equation (1.38) is a force balance equation for the whole system, the mixture of cells and matrigel. The term $\mathbf{T}_n$ represents the internal forces of the system due to cell traction whereas $\mathbf{T}_\rho$ accounts for the elastic response of the matrix. Equations (1.36-1.37) are known as the elasto-mechanical model. It can be identified four types of contributions for the cellular flux $\mathbf{J}$:

- A passive motion due to the attachment of the cells on the moving ECM, $\mathbf{J}_\omega$=n$\mathbf{w}$.
- A strain dependent motion $\mathbf{J}_d = -\nabla \cdot [D(\mathbf{I} + dev(\mathbf{E}))n]$, where $dev(\mathbf{E}) = E - \frac{tr\mathbf{E}}{2}\mathbf{I}$ and $\mathbf{E} = \frac{1}{2}(\nabla \mathbf{u} + \nabla \mathbf{u}^T)$ is the strain tensor and $tr\mathbf{E} = E_{xx} + E_{yy}$.
- A haptotactic motion along the adhesive ECM density gradients $\mathbf{J}_\rho = kn\nabla\rho$.
- A chemotactic motion along the gradients of a specific chemical factor c, $\mathbf{J}_c = \chi n \nabla c$.

Although the first two contributions are always present, haptotaxis is only considered in [58] and [45], and chemotaxis is only considered in [37]. Furthermore, in [40] Murray states that "One of the initially surprising and important finding is that random motility of cells was not necessary for the formation of patterns. Networks would still form provided that the seeding density was sufficiently large." Thus, from the point of view of linear stability and numerical simulations, we can consider the minimal traction-induced vasculogenesis model as:

$$\frac{\partial n}{\partial t} + \nabla \cdot (n\mathbf{w}) = 0, \tag{1.39}$$

$$\tau \nabla \Sigma(n) - \frac{E}{1+\nu} \nabla \cdot \left(\mathbf{E} + \frac{\nu}{1-2\nu} tr(\mathbf{E})\mathbf{I} \right) = \mathbf{F}, \tag{1.40}$$

where the anchoring force can be either represented as an elastic restoring force or as a viscous drag.

Numerical simulations may suggest that the formation of patterns in the mechanical models starts with the formation of regions with less cells surrounded by regions with more cells.

Elasto-mechanical models describe the phenomenon of pattern formation starting from monolayer initial conditions. They describe the interaction with the substratum and a viscoelastic regime which is not accessible by the PEC model.

A model combining physical mechanisms and mathematical modeling is proposed in [57]. It is proposed a unified view of the whole morphogenetic process of vascular networks, including both amoeboid-type migration driven by chemical factors such as Vascular Endothelial Growth Factor (VEGF) and mesenchymal migration when Endothelial Cells (ECs) detect the stress field of the underlying layer and move on the surface along the tensional lines [20]. ECs and ECM are described as a two-layers system in which the vertical dimension can be neglected provided a suitable rearrangement of the equations. The model is in good agreement with the experiments done in [52] and [3].

Three state variables are considered in two dimensions with $\mathbf{x} = (x, y)$:

- The density field $\rho(\mathbf{x}, t)$.
- The horizontal displacement of the substratum $\mathbf{u}(\mathbf{x}, t)$.
- The horizontal velocity field $\mathbf{v}(\mathbf{x}, t)$ of the cells.

After some computations, the mathematical model can be written as follows:

$$\frac{\partial \rho}{\partial t} + \nabla \cdot (\rho \mathbf{v}) = 0, \tag{1.41}$$

$$\frac{\partial (\rho \mathbf{v})}{\partial t} + \nabla \cdot (\mathbf{v} \otimes \rho \mathbf{v}) + \nabla p(\rho) = \kappa(\rho)(\mathbf{u} - \mathbf{u}_c) + \beta \rho \nabla c, \tag{1.42}$$

$$-F\frac{1-\nu}{2}\nabla^2 \mathbf{u} - F\frac{1-\nu}{2(1-2\nu)}\nabla(\nabla \cdot \mathbf{u}) = -\kappa(\rho)(\mathbf{u} - \mathbf{u}_c), \tag{1.43}$$

$$\frac{\partial c}{\partial t} - D\nabla^2 c = \alpha(\rho)\rho - \frac{c}{\tau}, \tag{1.44}$$

$$\frac{\partial \mathbf{u}_c}{\partial t} = \mathbf{v}. \tag{1.45}$$

When $\kappa = 0$, the dynamics of ECs and ECM are decoupled and one recovers the chemotactic model by [1] (see figure 1.9, taken from [57]).

First of all, the chemotactic field is created after random seeding of the cells. After this, due to the chemotactic force, cells start moving along the chemical gradient. The cellular matter preserve its initial direction motion due to persistence and hence it generally does not move towards larger density points. In this way, clusters are avoided and a density pattern with spatial characteristics dictated by the typical length $\ell \simeq \sqrt{D\tau}$ emerges. Once a sufficiently large density is obtained, the traction between the cellular layer and the gel starts driving the cells to stretch the substratum.

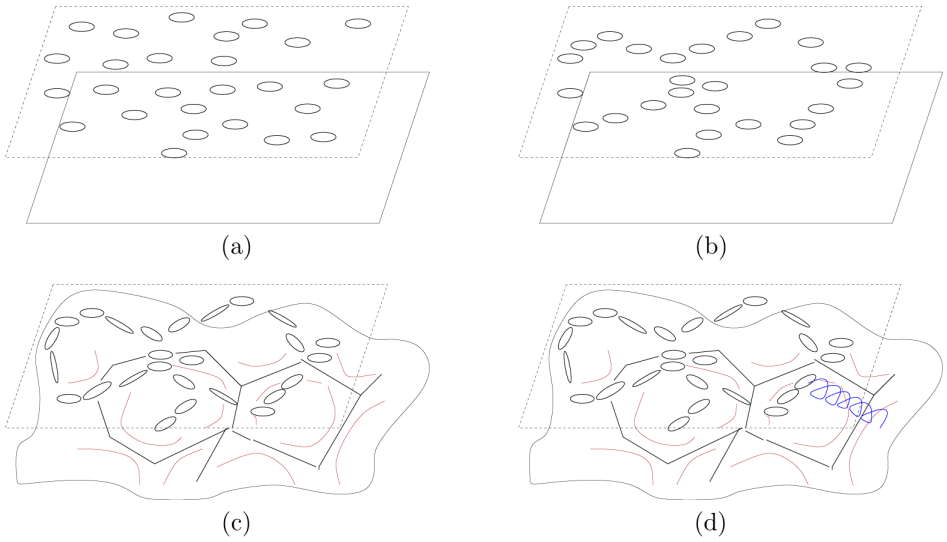

Figure 1.9: Random seeding of cells (a), amoeboid cell migration following the concentration gradient (b), traction between the cellular layer and the gel (c), ideally spring connecting the two layers (d). Figure from [57].

Curiously, the models presented above were introduced by the authors in analogy to some models in cosmology, where the chemoattractant density plays the role of the gravitational potential. Despite the numerical simulations corroborate some interesting pattern formation (for instance, the formation of filaments in the development of vascular networks), many assumptions lack a fully satisfactory justification and the models rely mainly on the analogy with models aiming to describe the formation of filamentary structures in the distribution of matter in the universe.

1.3.3 Ant colony optimization algorithms

Transport networks are ubiquitous in both social and biological systems. Biological networks have inspired many different algorithms and are likely to yield reasonable solutions to combinatorial optimization problems. Furthermore, they develop without centralized control and can be employed for growing networks in general. A recent work appeared in Science [56], is a good example of man-made networks inspired on biological systems; it is shown that the slime mold *Physarum polycephalum* forms efficient and robust networks comparable to the real-world infrastructures (Tokio rail system in the article). Despite the importance of these operational research problems, we will not study them in this thesis.

Inspired by the behavior of ants, a metaheuristic optimization technique was developed in 1992 (see [6], [11] and [15]). A metaheuristic algorithm consists on a computational method

that optimizes a problem by iteratively trying to improve a candidate solution with regard to a given measure of quality. In particular, the ant colony optimization algorithm (ACO) is a probabilistic technique for solving computational problems which can be reduced to finding good paths through graphs. The ACO algorithm is based on the behavior of ants when seeking a path between their colony and a source of food.

When ants start to forage for food, they initially wander randomly; once they have found a food source, they return to their colony while laying down pheromone trails. If other ants find such a path, instead of keeping to traveling at random, they are likely to follow that path, returning and reinforcing it if they eventually find food. In the meanwhile, the pheromone trail starts to evaporate, reducing thus its attractive strength. The more time it takes for an ant to travel down the path and back again, the less quantity of pheromone it senses. A short path, by comparison, gets marched over faster, and thus the pheromone density remains high. Pheromone evaporation has also the advantage of avoiding the convergence to a locally optimal solution. If there were no evaporation at all, the paths chosen by the first ants would tend to be excessively attractive to the following ones. In that case, the exploration of the solution space would be constrained.

Once one ant finds a short path from the nest to a food source, other ants are more likely to follow that path, and positive feedback eventually leads to all the ants following a single path. The idea of the ant colony algorithm is to mimic this behavior with "simulated ants" walking around the graph representing the problem to solve.

Ant colony optimization algorithms have been applied to many combinatorial optimization problems, ranging from quadratic assignment (QA) to fold protein or vehicles routing problems (VRP), and a lot of derived methods have been adapted to dynamic problems in real variables, stochastic problems, multi-targets and parallel implementations. It has also been used to produce near-optimal solutions to the traveling salesman problem (TSP). They have an advantage over genetic algorithm approaches of similar problems when the graph may change dynamically; the ACO can be run continuously and adapt to changes in real time. This is of interest in network routing and urban transportation systems.

The first ACO algorithm was called the ant colony system (ACS) [15] and it was aimed to solve the TSP (see [13] and [14]), in which the goal is to find the shortest round-trip to link a series of cities. The general algorithm is relatively simple and based on a set of ants, each making one of the possible round-trips along the cities. Ants cooperate using an indirect form of communication mediated by a pheromone they deposit on the edges of the TSP graph while building solutions. At each stage, the ant chooses to move from one city to another according to some rules:

1. Each city has to be visited once;

2. A distant city has less chance of being chosen;

3. The probability of an edge is proportional to the pheromone laid on it;

4. Once the ant has completed its journey, it deposits pheromone on the edges it traversed, provided that it has selected the shortest path;

5. After each iteration, pheromone trails evaporate.

Recent studies employ hybrid algorithms combining ACO algorithm with others algorithms (see [5] and [32]). Moreover, in [53] it is proposed an extension of ACO so that it can be applied to both continuous and mixed-variable optimization problems. In [54] it is discussed the inter-cell layout problem and a mathematical formulation for material flow between the cells is presented by employing an ant algorithm. For a complete review on ACO see [12] and [16].

For some versions of the algorithm, it is possible to prove that it is convergent (i.e. it is able to find the global optimum in a finite time). However, like for most metaheuristics, it is very difficult to estimate the theoretical speed of convergence. Furthermore, it is not guaranteed an optimal solution is ever found or even a satisfactory near-optimal solution.

Bibliography

[1] D. Ambrosi, A. Gamba and G. Serini, Cell directionality and chemotaxis in vascular morphogenesis. Bull. Math. Biol. **66(6)** (2004), 1851-1873.

[2] D. Ambrosi, F. Bussolino and L. Preziosi, A review of vasculogenesis models. J. Theor. Med. **6** (2005), 1-19.

[3] I. B. Bischofs and U. S. Schwarz, Cell organization in soft media due to active mechanosensing. PNAS **100** (2003), 9274-9279.

[4] J. T. Bonner, *The cellular slime mold*, Princeton University Press, Princeton NJ, 1967.

[5] G. Di Caro, F. Ducatelle and L. .M. Gambardella, AntHocNet: An Adaptive Nature-Inspired Algorithm for Routing in Mobile Ad Hoc Networks. ETT, Special Issue on Self Organization in Mobile Networking **16(5)** (2005), 443-455.

[6] A. Colorni, M. Dorigo and V. Maniezzo, Distributed optimization by ant colonies. Proceedings of ECAL'91, European Conference on Artificial Life, Elsevier Publishing, Amsterdam (1991), 134-142.

[7] I. D. Couzin and N. R. Franks, Self-organized lane formation and optimized traffic flow in army ants. Proc. R. Soc. Lond. B **270(22)** (2003), 139-146.

[8] B. Davis, Reinforced random walk. Probab. Theory Related Fields **84(2)** (1990), 203-229.

[9] J. L. Deneubourg, S. Aron, S. Goss and J. M. Pasteels, The Self-Organizing Exploratory Pattern of the Argentine Ant. J. Insect Behav. **3(2)** (1990), 159-168.

[10] J. L. Deneubourg and S. Goss, Collective patterns and decision making. Ethol. Ecol. Evol. **1** (1989), 295-311.

[11] M. Dorigo, *Optimization, Learning and Natural Algorithms*, PhD thesis, Politecnico di Milano, Italy, 1992.

[12] M. Dorigo and C. Blum, Ant colony optimization theory: a survey. Theoretical Computer Science **344(2-3)** (2005), 243-278.

[13] M. Dorigo and L. M. Gambardella, Ant Colony System: A cooperative learning approach to the traveling salesman problem. IEEE Transactions on Evolutionary Computation **1(1)** (1997), 53-66.

[14] M. Dorigo and L. M. Gambardella, Ant colonies for the traveling salesman problem. BioSystems **43** (1997), 73-81.

[15] M. Dorigo, V. Maniezzo and A. Colorni, The ant system: an autocatalytic optimizing process. Technical Report Politecnico di Milano **TR91-016** (1991), .

[16] M. Dorigo and T. Stützle, *Ant colony optimization*, MIT Press, Cambridge, 2004.

[17] L. Edelstein-Keshet, *Mathematical Models in Biology*, SIAM, 2005.

[18] I. Ferrenq, L. Tranqui, B. Vailhe, P. Y. Gumery and P. Tracqui, Modelling biological gel contraction by cells: mechanocellular formulation and cell traction quantification. Acta Biotheoretica **45** (1997), 267-293.

[19] M. A. Fontelos, A. Friedman and B. Hu, Mathematical analysis of a model for the initiation of angiogenesis. SIAM Journal on Mathematical Analysis **33(6)** (2002), 1330-1355.

[20] P. Friedl and K. Wolf, Tumour-cell invasion and migration: diversity and escape mechanisms. Nature Rev. Cancer **3** (2003), 362-374.

[21] A. Gamba, D. Ambrosi, A. Coniglio, A. de Candia, S. Di Talia, E. Giraudo, G. Serini, L. Preziosi and F. Bussolino, Percolation, morphogenesis, and Burgers dynamics in blood vessel formation. Phys. Rev. Letters **90(11)** (2003), 118101/1-4.

[22] S. Goss, S. Aron, J. L. Deneubourg and J. M. Pasteels, Selforganized shortcuts in the Argentine ant. Naturwissenschaften **76** (1989), 579-581.

[23] W. H. Gotwals, *Army ants: the biology of social predation*, Ithaca, NY: Cornell University Press, 1995.

[24] Y. Guo and H. J. Hwang, Pattern formation (I): The Keller-Segel Model. JDE **249(7)** (2010), 1519-1530.

[25] M. A. Herrero and J. J. L. Velázquez, Chemotactic collapse for the Keller-Segel model. J. Math. Biol. **35** (1996), 177-196.

[26] M. A. Herrero and J. J. L. Velázquez, Singularity patterns in a chemotactic model. Math. Ann. **206** (1996), 583-623.

[27] M. A. Herrero and J. J. L. Velázquez, A blow-up mechanism for a chemotaxis model. Ann. Scuola Norm. Sup. Pisa Cl. Sci. **4(24)** (1997), 633-683.

[28] B. Hölldobler and K. Wilson, *The ants*, Berlin: Springer, 1990.

[29] D. Horstmann, From 1970 until present: the Keller-Segel model in chemotaxis and its consequences I. Jahresber. Dtsch. Math.-Ver. **105(3)** (2003), 103-165.

[30] D. Horstmann, From 1970 until present: the Keller-Segel model in chemotaxis and its consequences II. Jahresber. Dtsch. Math.-Ver. **106(2)** (2004), 51-69.

[31] D. Horstmann, K. J. Painter and H. G. Othmer, Aggregation under local reinforcement: From lattice to continuum. Eur. J. Appld. Math **15** (2004), 545-576.

[32] K. L. Huang and C. J. Liao, Ant colony optimization combined with taboo search for the job shop scheduling problem. Computers and Operations Research **35(4)** (2008), 1143-1154.

[33] W. Jäger and S. Luckhaus, On explosions of solutions to a system of partial differential equations modelling chemotaxis. Trans. Amer. Math. Soc. **329** (1992), 819-824.

[34] K. Kang, A. Stevens and J. J. L. Velazquez, Qualitative behavior of a Keller-Segel model with non-diffusive memory. Communications in PDE **35(2)** (2010), 245-274.

[35] E. F. Keller and L. A. Segel, Initiation of slime mold aggregation viewed as an instability. J. Theor. Biol. **26** (1970), 399-415.

[36] E. F. Keller and L. A. Segel, A model for chemotaxis. J. Theor. Biol. **30** (1971), 225-234.

[37] D. Manoussaki, A mechanochemical model of vasculogenesis and angiogenesis. Math. Model. Num. Anal. **37** (2004), 581-600.

[38] D. Manoussaki,S. R. Lubkin, R. B. Vernon and J. D. Murray, A mechanical model for the formation of vascular networks in vitro. Acta Biotheoretica **44** (1996), 271-282.

[39] J. D. Murray, *Mathematical Biology*, Springer-Berlag, 1989.

[40] J. D. Murray, On the mechanical theory of biological pattern formation with application to vasculogenesis. C. R. Biologies **326** (2003), 239-252.

[41] J. D. Murray, D. Manoussaki, S. R. Lubkin and R. B. Vernon, *A mechanical theory of in vitro vascular network formation in Vascular Morphogenesis: In Vivo, In Vitro and In Mente*, Eds. Birkhauser, 1998.

[42] J. D. Murray and G. F. Oster, Cell traction models for generation of pattern and form in morphogenesis. J. Math. Biol. **19** (1984), 265-279.

[43] J. D. Murray and G. F. Oster, Generation of biological pattern and form. J. Math. Appl. Med. Biol. **1** (1984), 51-75.

[44] J. D. Murray, G. F. Oster and A. K. Harris, A mechanical model for mesenchymal morphogenesis. J. Math. Biol. **17** (1983), 125-129.

[45] P. Namy, J. Ohayon and P. Traqui, Critical conditions for pattern formation and in vitro tubulogenesis driven by cellular traction fields. J. Theor. Biol. **227** (2004), 103-120.

[46] G. F. Oster, J. D. Murray and A. K. Harris, Mechanical aspects of mesenchymal morphogenesis. Cell traction models for generation of pattern and form in morphogenesis. J. Embryol. Exp. Morph. **78** (1983), 83-125.

[47] H. G. Othmer and A. Stevens, Aggregation, blowup, and collapse: the ABCs of taxis in reinforced random walks. SIAM J. Appl. Math. **57** (1997), 1044-1081.

[48] C. S. Patlak, Random walk with persistence and external bias. Bull. Math. Biophys. **15** (1953), 311-338.

[49] B. Perthame, *Transport Equations in Biology*, Birkhäuser Verlag, Basel-Boston-Berlin, 2007.

[50] B. Perthame, PDE models for chemotactic movements: parabolic, hyperbolic and kinetic. Appl. Math. **49(6)** (2004), 539-564.

[51] L. A. Segel and J. L. Jackson, Dissipative structure: An explanation and an ecological example. J. Theor. Biol. **37** (1972), 545-559.

[52] G. Serini, D. Ambrosi, E. Giraudo, A. Gamba, L. Preziosi and F. Bussolino, Modeling the early stages of vascular network assembly. EMBO J. **22** (2003), 1771-1779.

[53] K. Socha and M. Dorigo, Ant colony optimization for continuous domains. European Journal of Operations Research **185(3)** (2008), 1155-1173.

[54] M. Solimanpur, P. Vrat and R. Shankar, Ant colony optimization algorithm to the intercell layout problem in cellular manufacturing. European Journal of Operational Research **157** (2004), 592-606.

[55] A. Stevens and J. J. L. Velázquez, Partial differential equations and non-diffusive structures. Nonlinearity **21** (2008), 283-289.

[56] A. Tero, S. Takagi, T. Saigusa, K. Ito, D. P. Bebber, M. D. Fricker, K. Yumiki, R. Kobayashi and T. Nakagaki, Rules for biologically inspired adaptive network design. Science **327** (2010), 439-442.

[57] A. Tosin, D. Ambrosi and L. Preziosi, Mechanics and chemotaxis in the morphogenesis of vascular networks. Bull. Math. Biol. **68** (2006), 1819-1836.

[58] L. Tranqui and P. Traqui, Mechanical signalling and angiogenesis. The integration of cell-extracellular matrix couplings. C.R. Acad. Sci. Paris, Science de la Vie **323** (2000), 31-47.

[59] A. Turing, The chemical basis of morphogenesis. Phil. Trans. Roc. Soc. B **237** (1952), 37-72.

[60] B. Vailhe, D. Vittet and J. J. Feige, In vitro models of vasculogenesis and angiogenesis. Lab. Investig. **81** (2001), 439-452.

Chapter 2

Experimental data

Goals of this chapter

- Review of different experimental data for ants.
- Detailed descriptions found in the literature for Argentine ant (*Iridomyrmex humilis*) [1, 5, 8, 12], Pharaoh's ant (*Monomorium pharaonis*) [9, 11], Lasius niger (*Hymenoptera, Formicidae*) [2, 6, 10] and Army ant (*Eciton burchelli*) [3, 4, 7].
- Description of some models appeared in the literature to describe the dynamics of these organisms.

2.1 General introduction

Transport networks play an important role in different natural and man-made systems. In the last years many work has been done to understand collective patterns generated by the individual workers' trail laying, showing how complex collective structures in insect colonies may be based on self-organization and co-operation. Foraging ants find the shortest paths for initially unknown food sources in almost the minimum possible time for certain types of mazes. How can an animal with only limited and local information achieve this in such an efficient way? Many ants, having no more than a limited individual capacity for orientation are able to select the shortest path between nest and food source dodging many obstacles by just following the pheromone trail. Just as the functioning and success of modern cities are dependent on an efficient transportation system, the effective management of traffic is also essential to ant colonies. In this chapter, we review some experimental results related to different types of ants. We focus on the results for Argentine ant (*Iridomyrmex humilis*) [1, 5, 8, 12], Pharaoh's ant

(*Monomorium pharaonis*) [9, 11], Lasius niger (*Hymenoptera,Formicidae*) [2, 6, 10] and Army ant (*Eciton burchelli*) [3, 4, 7].

2.2 Argentine ant (Iridomyrmex humilis) [1, 5, 8, 12]

- Argentine ant follows chemical stimuli and not visual ones. The explorers follow the trail pheromone [1, 5].
- This ant lays just one pheromone, (Z)-9-Hexadecenal, when it leaves the nest to find food and when it comes back. Not only this pheromone is used for recruitment but also for exploring. The mean life is about 30 minutes [1, 5, 12].
- There are some differences between the trail-laying behavior by workers moving from and returning to the nest: when leaving the nest the streaks are shorter and more separated. When returning they are larger and more frequent [1].
- Around 40% of workers do not leave any trail. That is, the pheromone is not reinforced. Different data are summarized in tables 2.1, 2.2 ([1], n is the number of experiments):

Table 2.1: Trail-laying behavior

	Towards the nest	**Towards the arena**
Length of streaks(cm)	0.19 ± 0.03, n=13	0.10 ± 0.01, n=17
Distance between two streaks(cm)	0.31 ± 0.09, n=13	0.57 ± 0.07, n=17
Worker's velocity(cm/s)	1.09 ± 0.09, n=13	1.01 ± 0.07, n=17

Table 2.2: No trail-laying behavior

	Towards the nest	**Towards the arena**
Worker's velocity(cm/s)	1.11 ± 0.07, n=10	1.15 ± 0.08, n=13

- In [8] two different kind of mazes are considered: those which are regular lattices so that all the edges adjacent to any given vertex form identical angles (these will be called non polarized or NP mazes) and those for which edges adjacent to any given vertex do not form identical angles (these will be called polarized or P mazes). Individual and collective ant behavior are investigated when it crosses symmetrical bifurcations (non polarized, NP-mazes) and asymmetrical (polarized, P-mazes), see figure 2.1.

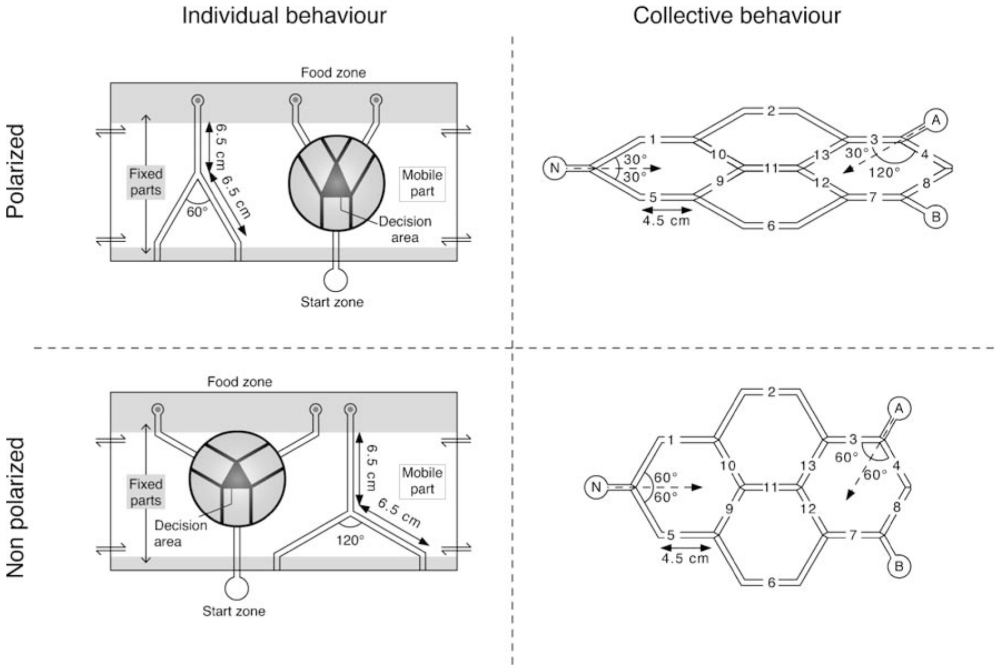

Figure 2.1: Schematic representation of the experimental setups for polarized maze (top) and non polarized maze (bottom). Notice that the nest is at the left edge of the maze and there are two possible food sources denoted by A and B. Picture from [8]

.

- There are not significant differences in the behavior between the ants that have eaten and those which have not. The mean number of ants in the network at each time frame grows for both P-mazes and NP-mazes. However, ants appear less dispersed in the first case [8].

- Ants, individually, behave in a different way depending on the bifurcation geometry. 66% of the ants chooses the branch that deviates less from the original direction. At a collective level, ants are spreaded and less able to select a path in non-polarized networks (symmetrical)[8].

- This shows that "persistence", that is the tendency to follow a path in the direction closest to the actual direction of motion, might play an important role in finding shortest paths. It is assumed for the model that all the ants leave a trail. The model employed in [8] is the following one:

$$F_e = \frac{k_0(k_1 + C_e)^m}{k_2 + (k_1 + C_e)^m}$$

where F_e is the flow of ants leaving the nest and entering the network at each time step and C_e corresponds to the total quantity of pheromone deposited by the ants at the entrance of the network.

Since at an asymmetrical bifurcation about $\frac{2}{3}$ of the ants choose the branch deviating less from their original direction, it is computed the probability p_a^* to select the branch a and p_b^* to select the branch b at an asymmetrical bifurcation as:

$$p_a^* = p_a + p_{pref}, \qquad p_b^* = 1 - p_a^*$$

with

$$p_{pref} = \ell(-4p_a^2 + 4p_a)$$

where ℓ is the tendency of an ant to follow the less deviating path.

Experimental data is summarized in table 2.3, where $p_{30^\circ}, p_{60^\circ}, p_{120^\circ}$ are the probabilities

Table 2.3: Experimental data for the motion in polarized and non polarized mazes

Parameter	**Value**
mean velocity(cm/s)	1.1 ± 0.25
ℓ	0.1666
$p_{30^\circ}, p_{60^\circ}, p_{120^\circ}$	$0.1; 0.26; 0.57$

to perform a U-turn after a rotation of $30, 60$ or 120 degrees. This quantifies the persistency effect.

- In [12] it is studied the behavior when recruiting. It is described in terms of a positive feedback (trail reinforcement) and a negative feedback (evaporation of the pheromone).

- The mean velocity of the ants is 1.06 ± 0.06 cm/s, within the range measured in [8]. The average time spent by the ants at the food source is 179.90 ± 39.04 s (mean values in the experiments [12]).

- Around 77% of the ants reaching an asymmetrical bifurcation proceeded on the branch that deviates less from their initial direction [12]. A new proof of the existence of a persistency effect.

- As a conclusion, the choice of the ants when arriving at a bifurcation depends on two parameters: the concentration of the pheromone and its deviation with respect to the original direction [12].

- If one defines the flow as the relative number of ants entering the maze per unit time, then one can attempt to write differential equations for the evolution of such flow. In [12], the flow is modeled by the logistic equation, although not justification for such a modeling is provided. Another shortcoming lies in the fact it is totally deterministic and it does not reflect the stochastic behavior. This is a phenomenological model that fits well

with experiments for appropriate choices of constants, but no theoretical justification is provided. The equation is

$$\frac{dF(t)}{dt} = rF(t)\left(1 - \frac{F(t)}{K}\right) \Rightarrow F(t) = \frac{F_{\max}}{1 + (F_{\max}/F_0 - 1)e^{-t/\tau}},$$

where the variables are estimated by the experiments [12] (see table 2.4).

Table 2.4: Experimental data for the model proposed in [12]

Parameter	**Value**
$F_{\max}$	0.42 (1/s)
F_0	5×10^{-4} 1/s
τ	127.4 s
k	20
n	4
$r_{pref} = \frac{k_{120}}{k_{30}}$	0.74

2.3 Pharaoh's ant (Monomorium pharaonis) [9, 11]

- Pharaoh's ant uses three types of foraging pheromone: long-term attractive pheromone, shorter-term attractive pheromone and a repellent pheromone. All of them have a role in trail choice. The repellent pheromone prevents random fluctuations. It is suggested that having a repellent pheromone is adaptive since it increases the robustness and flexibility of the colony's overall foraging response. The repellent pheromone has a key role in enabling the colony to refocus the foraging effort to the new location. If agents detect positive pheromone, they always lay more positive pheromone [11].

- The mean velocity is $15.1mm/s$, traffic flow rate is 1 ant per 3 seconds and the error rate at angle of deviation (the proportion of ants which choose a branch at random at a bifurcation) is 1% when the angle is of 120 degrees and 5% when the angle is 30 degrees [11]. The modeled environment consists of four cells: the nest, the stem of the trail and two trail branches (see figure 2.2).

- The mean lifetime of the pheromone is estimated as 9 minutes (on plastic) and 3 minutes (in paper). Trail decay is rapid and is affected strongly by trail substrate [9].

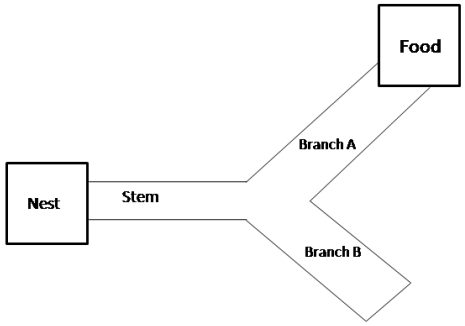

Figure 2.2: The four-cell environment in which simulated foraging takes place. The modeled environment consists of four cells: the nest, the stem of the trail and two trail branches

2.4 *Lasius niger (*Hymenoptera, Formicidae*) [2, 6, 10]*

- Ants lay a pheromone trail only after ingesting food. The recruited ants do not lay a trail on their first trip between the nest and the food source, but ants which leave the nest for their subsequent foraging also lay trail between the nest ant the food source. To increase even more the complexity of the problem, after a certain number of trips ants may stop laying trail, despite the fact that they are still foraging [2, 10].
- The mean lifetime of the trail pheromone is estimated to be 47 minutes [2].
- It is measured the quantity of pheromone on a trail as a function of food concentration. To do so, 3 different cases are studied: food concentration (drop of sucrose solution) at 1 M (Molarity, that is the number of moles of a given substance per liter of solution), 0.05 M and 0.1 M. Overall trail laying per passage is 43% greater for the first case than for the others [2].
- The % of ants choosing the food source $1M$ instead of one of the others is summarized in table 2.5:

Table 2.5: Quantity of pheromone on a trail as a function of food concentration, where n is the number of experiments.

Concentration of 2nd source	**n**	**%**
0.5	12	50
0.1	14	86
0.05	17	100

In [10] it is proposed a model to describe the evolution of the amount of pheromone on each link of the maze in terms on non linear functions F_i of the concentration of pheromone

in adjacent links and evaporation rates for the pheromone (the ant chooses between s different trails). The model is the following:

$$\frac{dc_i}{dt} = \Phi\sigma_i F_i(c_i) - v_i c_i, i = 1, \ldots, s; F_i = \frac{(k + c_i)^l}{\sum_{j=1}^{s}(k + c_j)^l}$$

where Φ is the total ant flow from the nest toward the trails (taken to be a constant), c_i is the pheromone concentration on trail i, σ_i is the quantity of pheromone deposed on the trail i, v_i is the corresponding evaporation rate and $F_i(c_i)$ is a function describing the relative attractiveness of trail i over the others, $i = 1, \ldots, s$.

2.5 Army ant (Eciton burchelli) [3, 4, 7]

- Ants form aggressive predatory foraging groups with a huge number of workers up to one million [4].
- They do not construct permanent nests and move almost incessantly over the time they exist [3].
- Ants lay pheromone trails both on the way out to the raid front and on the return journey [7].
- The running velocity of the ants is a sigmoidal function of the strength of their trail pheromone [7].
- A general model of ant behavior by employing an individual-based simulation approach appeared in [4] was described in section 1.1.2. This model takes into account the abilities of ants to detect and avoid colliding with others. Moreover, ants respond to local pheromone concentration [4].
- The main experimental results were summarized in table 1.1 in section 1.1.2. In particular the mean velocity is $7.5cm/s$ and the typical diffusion coefficient is $D = 0.01cm^2/s$.

2.6 Conclusions

- We have seen that different ants use one pheromone (Argentine ant, Lasius niger and Army ant) whereas others employ three types of pheromone (Pharaoh's).
- The mean lifetime of the pheromone is large compared to the time spent from nest to food source.

- The persistence effect has some importance as demonstrated by graphs with the same topology but different angles between edges.
- In general, mathematical theories involve equations that are not justified precisely. In particular, the problem has not been considered employing stochastic processes.
- Ants usually tend to follow shortest paths in the different tested mazes.
- All these observations pose the mathematical problem of determining a minimal set of rules so that a given number of ants following them tent to choose shortest paths between nest and food source. From the experimental observations it seems that such mechanism should include the presence of pheromone and the persistency (tendency to follow straights path in the absence of other effects). The main purpose of our work is to analyze this problem.

We summarize the main information in table 2.6:

Table 2.6: Summary of properties for different types of ants

Ant species	**Pheromone**	**Mean velocity** (cm/s)	**Mean lifetime pheromone trail** (min)
Argentine ant	One type	1.1 ± 0.25	30
Pharaoh's ant	One type	1.51	9 (plastic), 3 (paper)
Lasius niger	Three types	No data	47
Army ant	One type	7.5 ± 1.5	30

Bibliography

[1] S. Aron, J. M. Pasteels and J. L. Deneubourg, Trail-laying behaviour durign exploratory rescruitment in the Argentine and, Iridomyrmex humilis. Bio. of Behav **14**, (1989), 207-217.

[2] R. Beckers, J. L. Deneubourg and S. Goss, Modulation of Trail Laying in the Ant Lasius niger (Hymenoptera: Formicidae) and Its Role in the Collective Selection of a Food Source. J. Insect Behav. **6(6)**, (1993), 751-759.

[3] S. Brady, Evolution of the army ant syndrome: the origin and long-term evolutionary stasis of a complex of behavioral and reproductive adaptations. PNAS **100(11)**, (2003), 6575-6579.

[4] I. D. Couzin and N. R. Franks, Self-organized lane formation and optimized traffic flow in army ants. Proc. R. Soc. Lond. B **270(22)**, (2003), 139-146.

[5] J. L. Deneubourg, S. Aron, S. Goss and J. M. Pasteels , The Self-Organizing Exploratory Pattern of the Argentine Ant. J. Insect Behav. **3(2)**, (1990), 159-168.

[6] A. Dussutour, V. Fourcassié, D. Helbing and J. L. Deneubourg, Optimal traffic organization in ants under crowded conditions. Nature **428**, (2004), 70-73.

[7] N. R. Franks, N. Gomez, S. Goss and J. L. Deneubourg, The blind leading the blind in army ant raid patterns: Testing a model of self-organization (Hymenoptera: Formicidae). J. Insect Behav. **4(5)**, (1991), 583-607.

[8] S. Garnier, S. Guérécheau, M. Combe, V. Fourcassié and G. Theraulaz, Path selection and foraging efficiency in Argentine ant transport networks. Behav. Ecol. Sociobiol. **63**, (2009), 1167-1179.

[9] R. Jeanson, F. L. W. Ratnieks and J. L. Deneubourg, Pheromone trail decay rates on different substrates in the Pharaoh's ant, Monomorium pharaonis. Phys. Entom. **28**, (2003), 192-198.

[10] S. C. Nicolis and J. L. Deneubourg, Emerging Patterns and Food Recruitment in Ants: an Analytical Study. J. Theo. Biol. **198**, (1999), 575-592.

[11] E. J. H. Robinson, F. L. W. Ratnieks and M. Holcombe, An agent-based model to investigate the roles of attractive and repellent pheromones in ant decision making during foraging. J. of Theo. Biol. **255**, (2008), 250-258.

[12] K. Vittori, G. Talbot, J. Gautrais, V. Fourcassié, A. F. R. Araújo and G. Theraulaz, Path efficiency of ant foraging trails in artificial network. J. of Theo. Biol. **14**, (2005), 507-515.

Chapter 3

Numerical Simulations in simple graphs

Goals of this chapter

- Make simulations for reinforced random walks on two and three node networks to show in each case what is the minimum number of properties needed to reproduce ant's behavior.

3.1 General considerations

From the previous chapter, it is evident that both the pheromone laying and the geometry of mazes are essential factors for ants to find minimal paths. In some sense, the importance of these two elements is pretty intuitive and can be explained by the underlying biological assumptions: on one hand, ants need to communicate with each other when approaching a path between nest and food source so that they collectively are able to transport food in the most efficiently possible way. This communication is through the deposition of pheromones, acting as chemoattractants, and must be such that higher concentrations of them are created around the paths of minimal length between the nest and the food source. On the other hand, once in a region of high concentration of pheromone, ants must avoid to enter into cycles where several ants keep chasing each other. This kind of behavior is observed, for instance, in non polarized mazes. In order to avoid this phenomenon ants must have some preference to keep straight directions instead of turning around in circles. It is in this sense that a certain bias when choosing a direction to follow among several possible ones with the same amount of pheromone, so that the one that implies a minimal change in the direction is preferred, is natural. Based on this experimental observations, we develop in this chapter a model consisting of a set of random walkers (the ants) moving from edge to edge of a network according to some probabilities that depend on the amount of pheromone that ants deposit on each edge when moving through it.

We study numerically the collective behavior of a variable number of ants in networks in the form of graphs with E edges, $w_1, w_2, \ldots, w_E$. The experiments are done using a Monte Carlo method with the random number generator *binornd* from MATLAB. This random number generator returns numbers from a binomial distribution with parameters N (number of Yes/No experiments) and p (probability of success). We do a certain number of simulations for a different number of time steps and for a number H of ants.

For a two node network as in figure 3.1, let p_{W_1} be the probability of moving from node 1 to node 2 through the edge W_1 and p_{W_2} be the probability of moving from node 1 to node 2 through the edge W_2.

Following [2], we take the probabilities at step t to be

$$p_{W_1}(t) = \frac{(k+\omega_1(t))^\alpha}{(k+\omega_1(t))^\alpha + (k+\omega_2(t))^\alpha},$$

$$p_{W_2}(t) = \frac{(k+\omega_2(t))^\alpha}{(k+\omega_1(t))^\alpha + (k+\omega_2(t))^\alpha},$$

where $\omega_1(t), \omega_2(t)$ are the quantities of pheromone at each link W_1, W_2 respectively at time t, k is a positive constant and α is the exponent of the non-linearity. The value of $\omega_1(t)$ (resp. $\omega_2(t)$) is increased in one unit each time the ant moves along the edge W_1 (resp. W_2), representing the deposit of pheromone by the ant.

For the case of a three node network as in figure 3.8 with reinforcement we have the following probabilities at step t:

$$p_{1,2}(t) = \frac{(k+\omega_1(t))^\alpha}{(k+\omega_1(t))^\alpha + (k+\omega_2(t))^\alpha}, \qquad p_{1,3}(t) = \frac{(k+\omega_2(t))^\alpha}{(k+\omega_1(t))^\alpha + (k+\omega_2(t))^\alpha},$$

$$p_{2,1}(t) = \frac{(k+\omega_1(t))^\alpha}{(k+\omega_1(t))^\alpha + (k+\omega_3(t))^\alpha}, \qquad p_{2,3}(t) = \frac{(k+\omega_3(t))^\alpha}{(k+\omega_1(t))^\alpha + (k+\omega_3(t))^\alpha},$$

$$p_{3,1}(t) = \frac{(k+\omega_2(t))^\alpha}{(k+\omega_2(t))^\alpha + (k+\omega_3(t))^\alpha}, \qquad p_{3,2}(t) = \frac{(k+\omega_3(t))^\alpha}{(k+\omega_2(t))^\alpha + (k+\omega_3(t))^\alpha}.$$

Moreover, if we impose the following directionality constraint: if the ant is at node 1 or 2, it can move to the other two nodes; if the ant is at node 3 and the previous node is node 1, then it must move to node 2; if the previous node is node 2, then it must move to node 1, we have four different states for the system: being at node 1 (with associated probability p_1), being at node 2 (with associated probability p_2), being at node 3 coming from node 1 (with associated probability $p_{3\uparrow 1}$) and being at node 3 coming from node 2 (with associated probability $p_{3\downarrow 2}$). The transition probabilities are $p_{i,j}$ probability of moving from node i to node j. If we denote by $\omega_i(t)$ the quantity of pheromone at link W_i, at time t ($i = 1, 2, 3$), then the probabilities at step t are given by:

$$p_{1,2}(t) = \frac{(k+\omega_1(t))^\alpha}{(k+\omega_1(t))^\alpha + (k+\omega_2(t))^\alpha}, \qquad p_{1,3}(t) = \frac{(k+\omega_2(t))^\alpha}{(k+\omega_1(t))^\alpha + (k+\omega_2(t))^\alpha},$$

$$p_{2,1}(t) = \frac{(k+\omega_1(t))^\alpha}{(k+\omega_1(t))^\alpha + (k+\omega_3(t))^\alpha}, \qquad p_{2,3}(t) = \frac{(k+\omega_3(t))^\alpha}{(k+\omega_1(t))^\alpha + (k+\omega_3(t))^\alpha}.$$

Due to the directionality constraint, since an ant in node 3 is forced to go to node 2 if it is coming from node 1 and to node 1 if it is coming from node 2, one must take $p_{3,1} = 1$ and $p_{3,2} = 1$. The value of $\omega_1(t)$ (resp. $\omega_2(t)$ and $\omega_3(t)$) is increased in one unit each time the ant moves along the edge W_1 (resp. W_2 and W_3), representing the deposit of pheromone by the ant.

Our purpose is to explain the behavior of ants choosing the shortest path in terms of reinforcement and directionality constraint. We will show that both are necessary to reproduce this behavior. We show in detail what is the role of each parameter and how they affect to the model.

The main consequence of the numerical simulations done in the subsequent sections is that in the case that the reinforcement mechanisms will be super-linear ($\alpha > 1$), ants get trapped in one of the paths. On the other hand, this behavior does not happen in the sub-linear case ($\alpha < 1$) because the ants remain spread.

3.2 Simulations for a two node network

We consider a two node network with reinforcement as in figure 3.1.

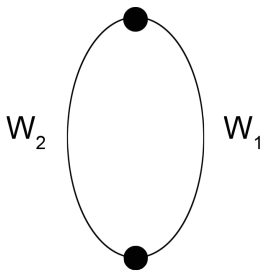

Figure 3.1: Two node network

We employ different MATLAB program simulations to create histograms with the behavior of one ant with different values for k and α. We consider one of the edges, say W_1 and a given number n of time steps. We repeat the experiment a certain number of times and plot the number of this experiments for which the edge W_1 has been crossed by the ants a given number of times. We can conclude from the graphics that

a) If the ratio k/α is small both branches are selected equivalently; i.e. the ant chooses one branch at the beginning and it goes almost all the times by this branch.

b) If we increase the ratio k/α then the distribution becomes Gaussian.

c) Final conclusion: for a given value of α, k plays the role of time scaling and so the greater the value of k, the more polarized are the histograms (almost all the ants go to the same branch). On the other hand, for a fixed value of k, the larger is α, the faster the histogram tends to a polarized state. These results agree with the rigorous mathematical results in [1] and [3] showing that for $\alpha > 1$ there is a path selection whereas for $\alpha < 1$ there is not preferentiability.

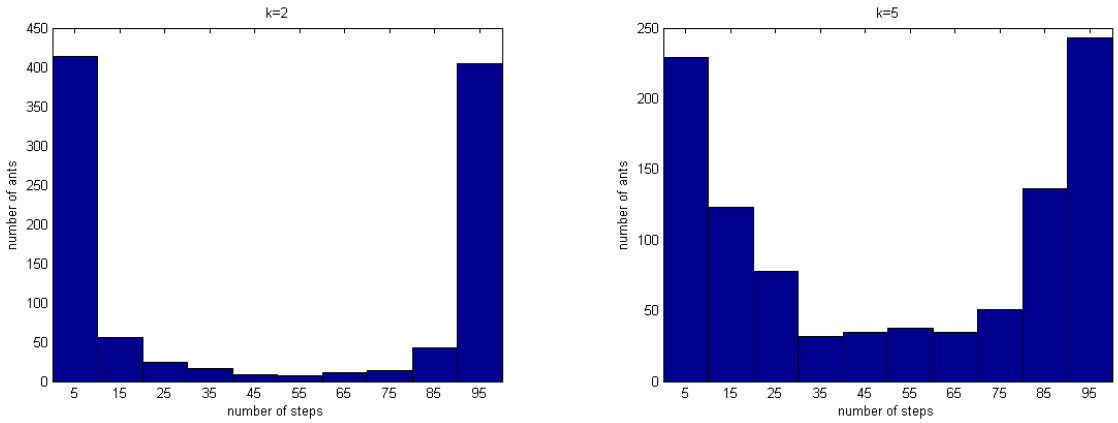

Figure 3.2: Histogram for $k = 2$ (left figure), $k = 5$ (right figure), $\alpha = 2$, $n = 100$ time steps. The experiment is repeated 1000 times and we represent the cumulative result.

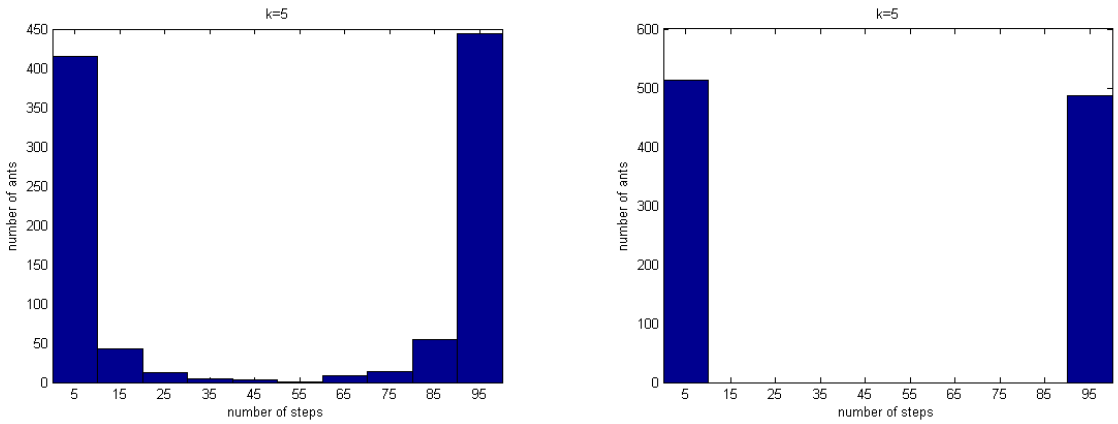

Figure 3.3: Histogram for $k = 5$, $n = 100$ time steps, $\alpha = 3$ (left figure), $\alpha = 10$ (right figure). The experiment is repeated 1000 times and we represent the cumulative result.

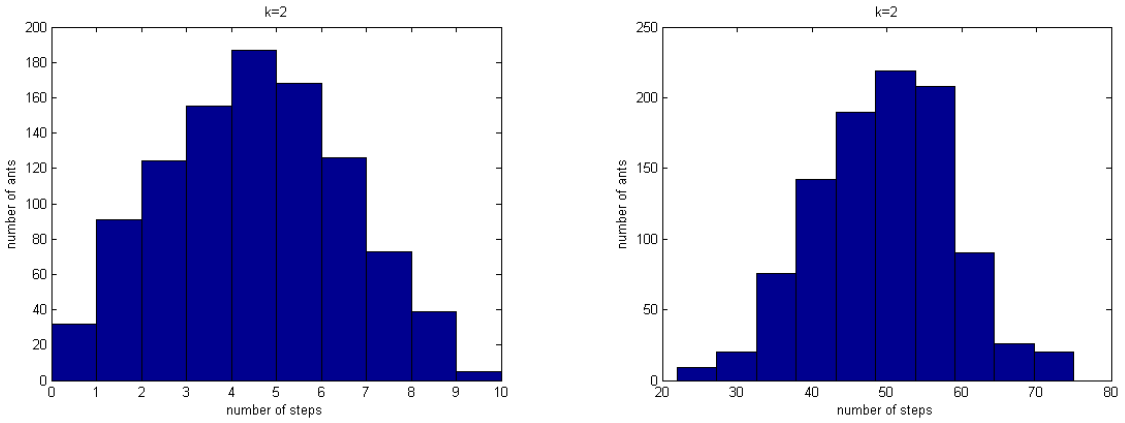

Figure 3.4: Histogram for $k = 2$, $\alpha = 0.5$, $n = 10$ time steps (left figure), $n = 100$ time steps (right figure). The experiment is repeated 1000 times and we represent the cumulative result.

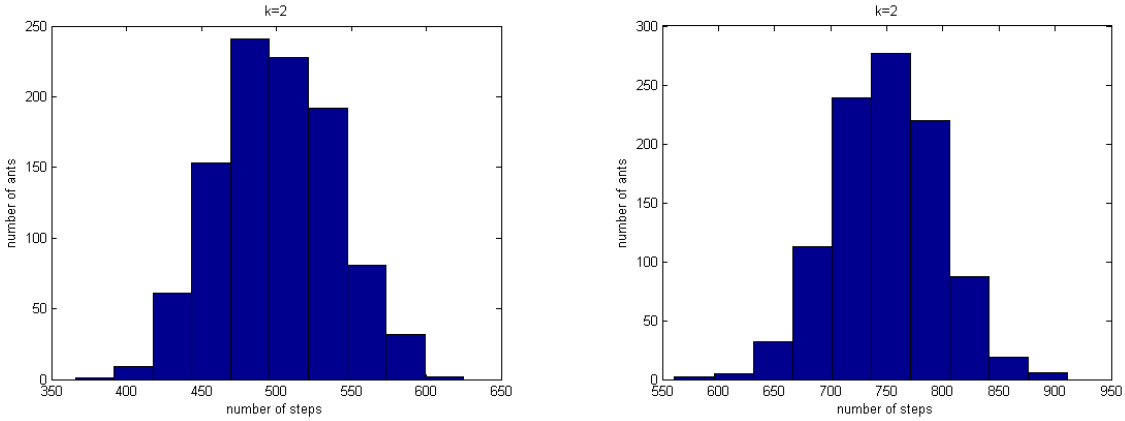

Figure 3.5: Histogram for $k = 2$, $\alpha = 0.5$, $n = 1000$ (left figure), $n = 1500$ time steps (right figure). The experiment is repeated 1000 times and we represent the cumulative result.

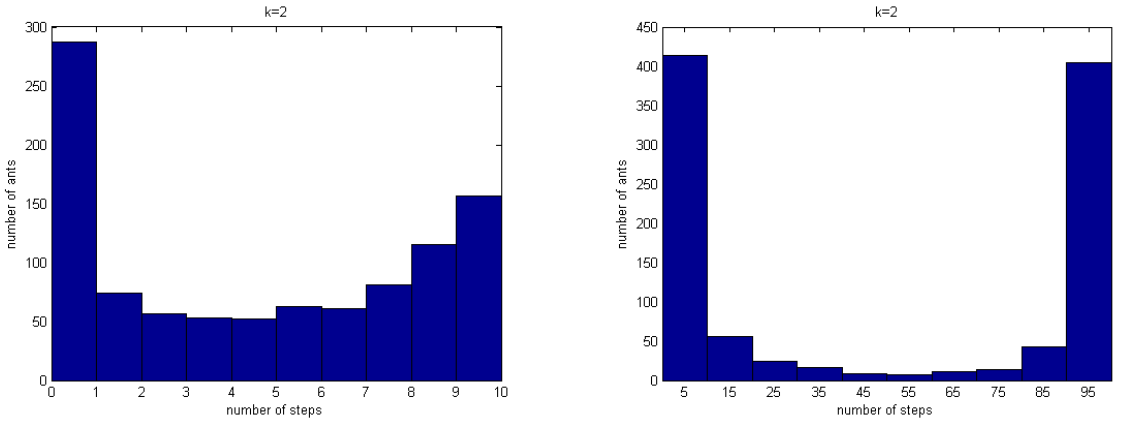

Figure 3.6: Histogram for $k = 2$, $\alpha = 2$, $n = 10$ time steps (left figure), $n = 100$ time steps (right figure). The experiment is repeated 1000 times and we represent the cumulative result.

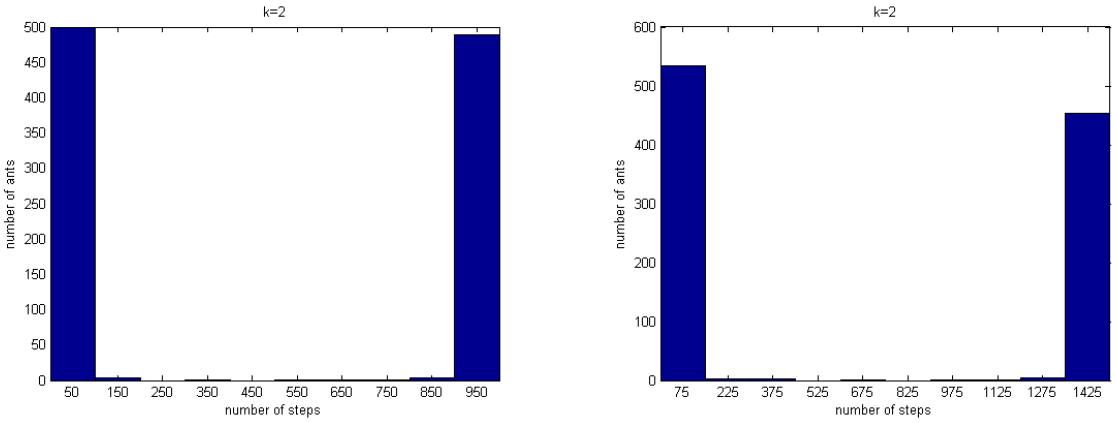

Figure 3.7: Histogram for $k = 2$, $\alpha = 2$, $n = 1000$ time steps (left figure), $n = 1500$ time steps (right figure). The experiment is repeated 1000 times and we represent the cumulative result.

3.3 Simulations for a three node network

In this section we consider a three node network as in figure 3.8. We distinguish two cases: non-constrained and directionality constrained. The directionality constraint is as follows: if the ant is at node 1 or 2, it can move to the other two nodes. If the ant is at node 3 and the previous node is node 1, then it must move to node 2; if the previous node is node 2, then it must move to node 1.

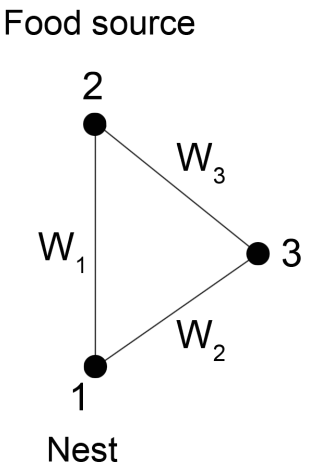

Figure 3.8: Three node network

We employ different MATLAB program simulations to show:

a) Temporal evolution graphics to show the relative number of times one ant goes through each branch without the directionality constraint. We conclude that reinforcement is not enough to obtain selection of the shortest paths, since for α sufficiently large, one particular edge is reinforced but it is not necessarily the shortest one. If α is small enough, no particular branch is selected (see figure 3.9).

b) Temporal evolution graphics to show the number of times one ant goes through each branch with the directionality constraint. We conclude that directionality constraint, with α sufficiently large, is sufficient to reinforce one particular path but this path is not necessarily the shortest one. If α is small enough, no particular branch is selected (see figure 3.10).

c) We consider more than one ant. For a certain number of numerical experiments n, we count the relative number of times that it is chosen the shortest path with respect to the number of times that it is chosen the longest path for each experiment. The result is a set of n numbers at each time t that we will call $r_i(t), i = 1, \ldots, n$, so that if $r_i(t) > 1$, then for the i-th experiment at time t the shortest path has been chosen most times and, on the contrary, if $r_i(t) < 1$ then the longest path has been chosen most times. Then, at any given time t, we count the number of cases among the n experiments for which the shortest path has been chosen (that is, those experiments for which $r_i(t) > 1$) and divide it by the number of times that the longest path has been chosen (that is, those experiments for which $r_i(t) < 1$). The result of these calculations is a measurement of the preferentiability of the shortest path with respect to the longest path. As we can see, the shortest path is chosen more often than the longest path for any number of ants. With two ants, the shortest path is chosen approximately 1.16 times more often than the longest path (see figures 3.11,3.12 left), for three ants it is approximately 1.11 (see figures 3.11,3.12 right) and for five ants it is around 1.5 times (see figure 3.13). Finally, for twenty ants is about 5.76 times and for fifty is nearly 165.66 (see figure 5.3). Notice that the convergence to a constant ratio is faster when the number of ants increases. In figure 3.15 we represent the limiting ratio as a function of the number of ants together with each logarithm. As we can see, the ratio clearly follows an exponential law as a function of the number of ants, implying a strong reinforcement of shortest paths when the number of ants is relatively large.

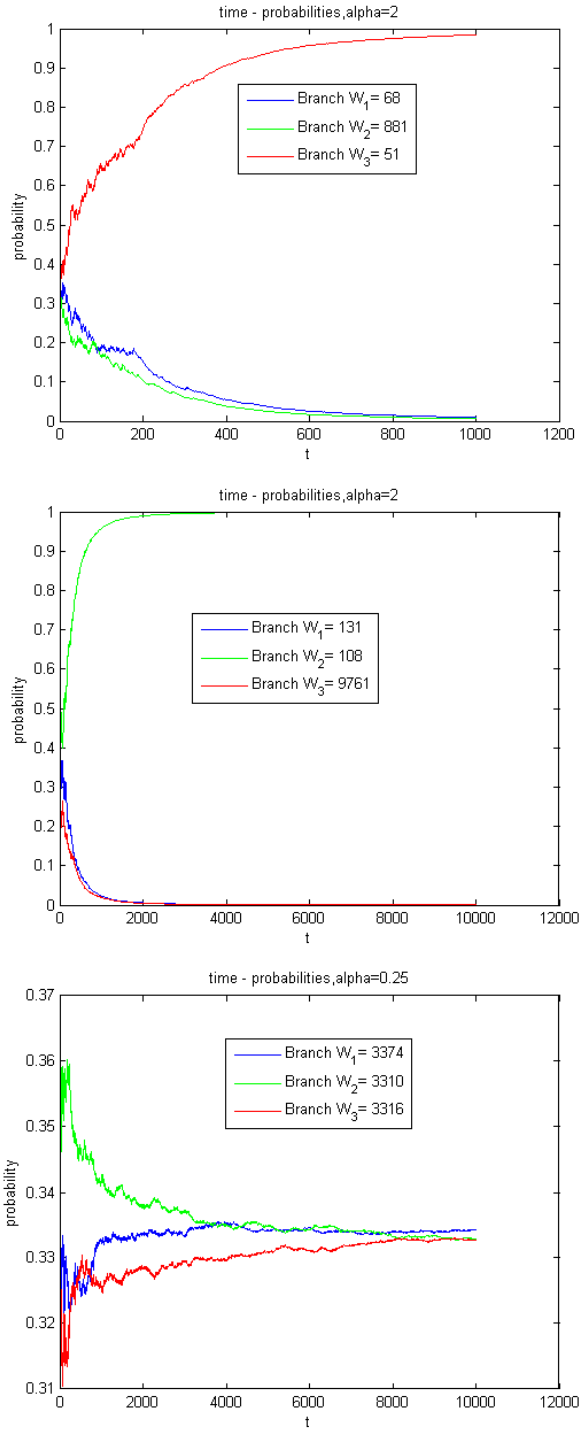

Figure 3.9: Temporal evolution for different experiments for $n = 1000$ time steps, $\alpha = 2$ (top figure); $n = 10000$ time steps, $\alpha = 2$ (center figure); $n = 10000$ time steps, $\alpha = 0.25$ (bottom figure); $k = 20$, network without directionality constraint. Conclusion: if α is sufficiently large, any branch can be selected; for α small enough, no particular branch is selected.

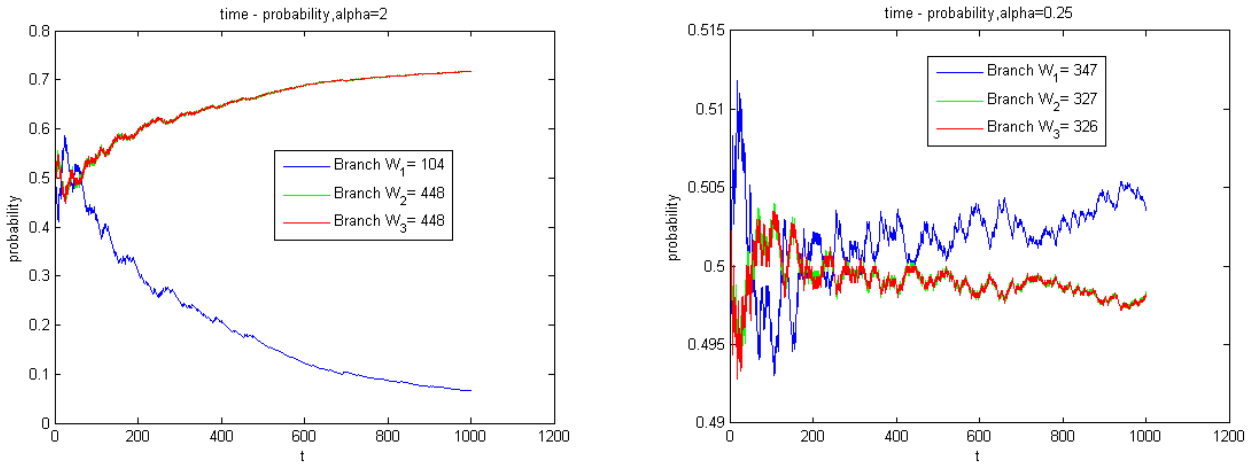

Figure 3.10: Temporal evolution for $n = 10000$ time steps, $k = 20$, $\alpha = 2$ (left figure), $\alpha = 0.25$ (right figure); network with directionality constraint. Conclusion: for α sufficiently large one of the branches can be selected, the short or the long path between the nest and the food source. In particular, with only one ant it can be selected the longest path.

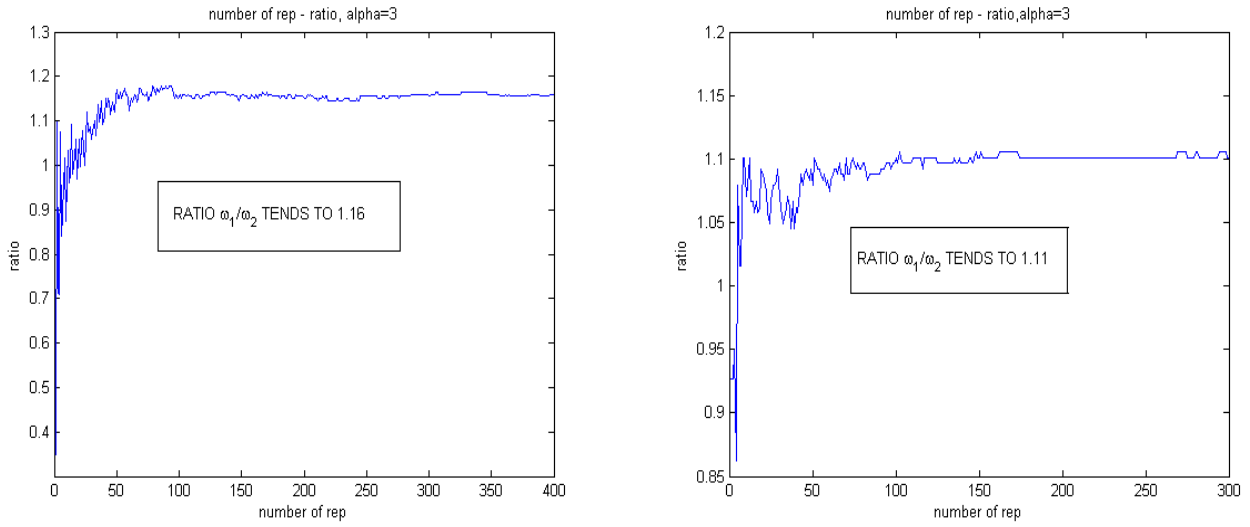

Figure 3.11: Temporal evolution of the ratio= $\frac{\omega_1}{\omega_2}$ for two ants (left figure), three ants (right figure), $k = 20$, $\alpha = 3$.

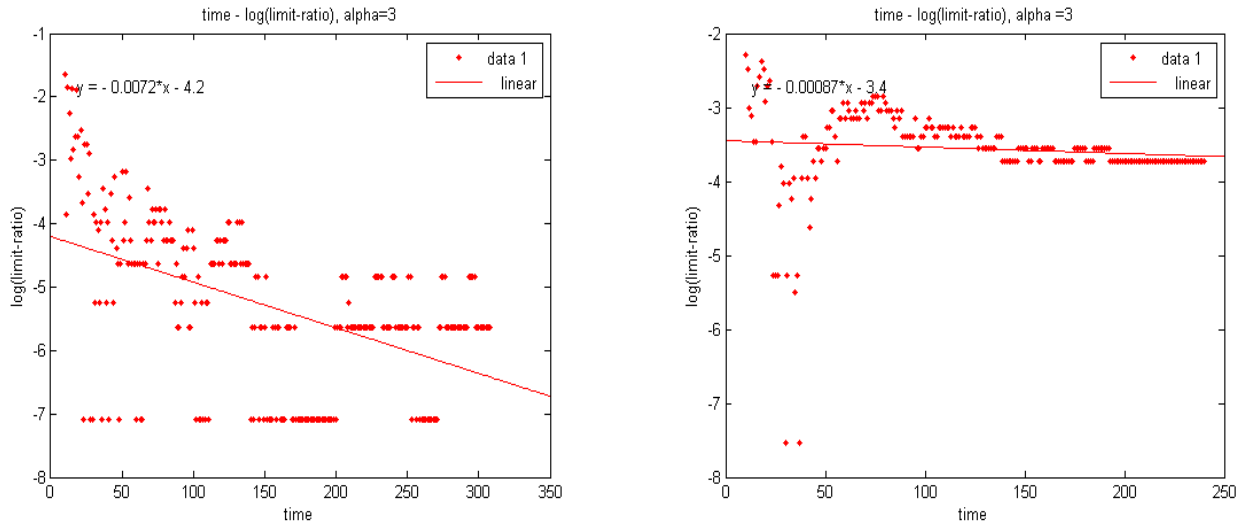

Figure 3.12: Logarithmic temporal evolution for the ratio= $\frac{\omega_1}{\omega_2}$ for two ants (left figure), three ants (right figure), $k = 20$, $\alpha = 3$. The convergence to the ratio is exponentially fast: $A \times e^{-7.2\times10^{-3}t}$ (left), $B \times e^{-0.8\times10^{-3}t}$ (right).

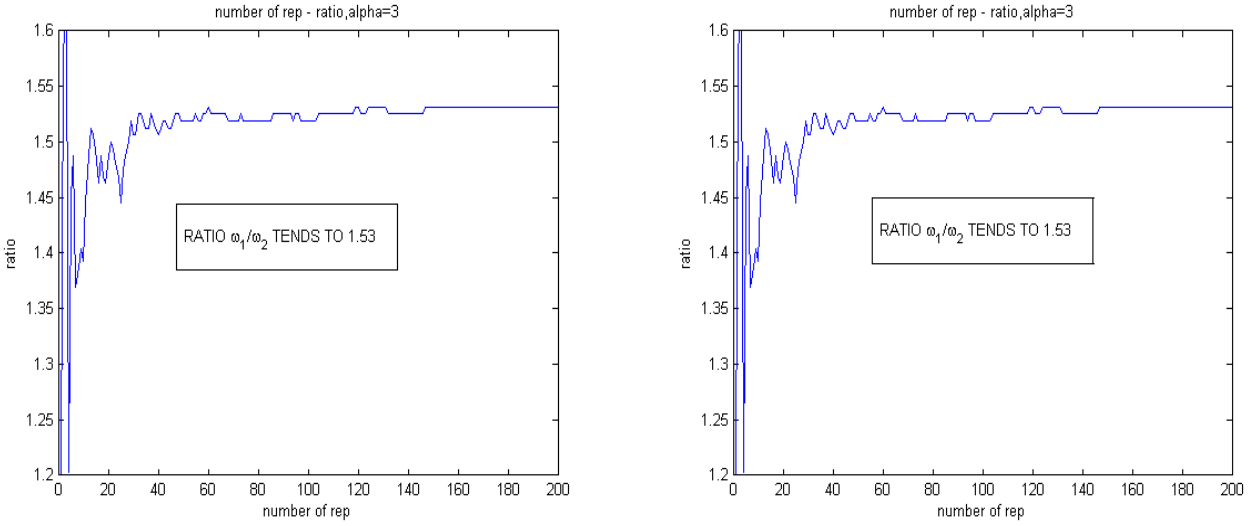

Figure 3.13: Temporal evolution of the ratio= $\frac{\omega_1}{\omega_2}$ for five ants, first ant (left figure), fifth ant (right figure), $k = 20$, $\alpha = 3$.

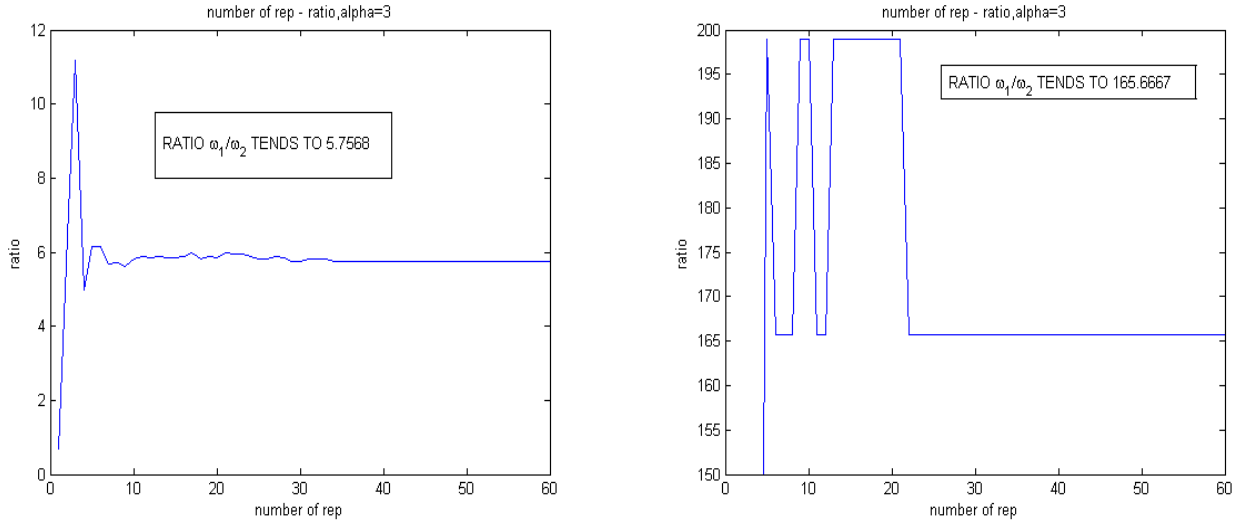

Figure 3.14: Temporal evolution of the ratio= $\frac{\omega_1}{\omega_2}$ for twenty ants (left figure), fifty ants (right figure), $k = 20$, $\alpha = 3$.

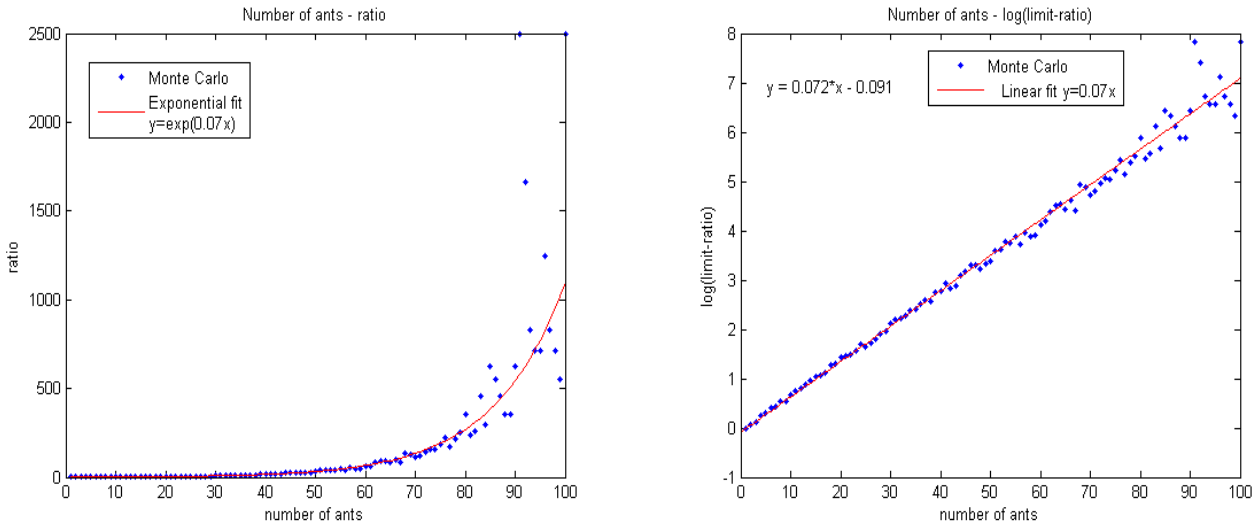

Figure 3.15: Ratio= ω_1/ω_2 (left figure) and logarithmic ratio (right figure) for the number of times that the short path is chosen with respect to the long path as a function of the number of ants. The parameters are $k = 20$, $\alpha = 3$. Notice that the relative number of times that the shortest path has been selected grows exponentially with the number of ants: $y = e^{0.07t}$.

As a result of the numerical simulations presented above, we conclude that reinforcement, persistence and a relatively large (in fact, more than one) number of ants are necessary for shortest selection in our three node network. The effect is stronger for large values of α (stronger nonlinearities) and increasing number of ants. In fact, the number of times that the shortest path is selected relative to the number of times the longest path is selected grows exponentially

with the number of ants (see figure 3.15) implying that a large number of ants will find the shortest path quickly.

Bibliography

[1] B. Davis, Reinforced random walk. Probab. Theory Related Fields **84(2)**, (1990), 203-229.

[2] S. Garnier, S. Guérécheau, M. Combe, V. Fourcassié and G. Theraulaz, Path selection and foraging efficiency in Argentine ant transport networks. Behav. Ecol. Sociobiol. **63**, (2009), 1167-1179.

[3] S. Volkov, Vertex-reinforced random walks on arbitrary graphs. Ann. Probab. **29(1)**, (2001), 66-91.

Chapter 4

Mathematical analysis of simple networks

Goals of this chapter

- Analytical study for a two node network with reinforcement.
- Study of a three node network with two ants and with non-reinforcement and directionality constraint to show that it is not enough to reproduce ant's behavior concerning choice of the shortest path.
- Study of a three node network with two ants with reinforcement and directionality constraint to show that it is enough to reproduce ant's behavior concerning choice of the shortest path.

In this chapter we consider a random walk process for H individuals (representing ants) along various simple graphs represented in figures (4.1) and (4.2). Each individual moves along an edge of the graph in each time step that we will take, without loss of generality, as $\Delta t = 1$. Hence, at the end of each time step, every individual will be located at a vertex of the graph. Another component of the random walk process is a set of i scalar quantities, $\omega_i(t)$ defined on the respective edges of the graph W_i. These quantities represent the cumulative amount of pheromone that is deposited by the ants on each edge. More precisely, when an ant runs through an edge W_i in one time step, it will increase $\omega_i(t)$ in one unit. Finally, once every individual ant is located at some vertex, it will decide which adjacent edge is going to move in the next time step by following a probability law of the form:

$$p_{W_i}(t) = \frac{(k + \omega_i(t))^\alpha}{\sum_j (k + \omega_j(t))^\alpha}.$$

Finally, in some cases we will impose directionality constraints so that U-turns (that is, running the same edge two consecutive time steps) is forbidden. In this chapter, we will prove that these ingredients are sufficient to create minimal paths.

4.1 Network with two nodes

We consider a two node network with reinforcement as in figure (4.1). Ants move one step at each time interval Δt that can be taken, without loss of generality as $\Delta t = 1$.

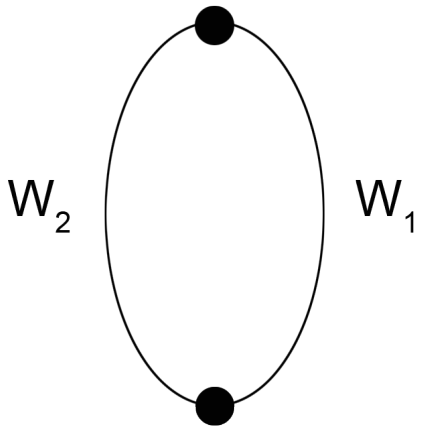

Figure 4.1: Two node network

Let p_{W_1} be the probability of moving from node 1 to node 2 through the edge W_1 and p_{W_2} be the probability of moving from node 1 to node 2 through the edge W_2.

Following [1] and [3], we have the probabilities at step t to be

$$p_{W_1}(t) = \frac{(k+\omega_1(t))^\alpha}{(k+\omega_1(t))^\alpha + (k+\omega_2(t))^\alpha}$$
$$p_{W_2}(t) = \frac{(k+\omega_2(t))^\alpha}{(k+\omega_1(t))^\alpha + (k+\omega_2(t))^\alpha},$$

where $\omega_1(t), \omega_2(t)$ are the quantities of pheromone at each link W_1, W_2 respectively at time t, k is a positive constant and α is the exponent of the non-linearity. The value of $\omega_1(t)$ (resp. $\omega_2(t)$) is increased in one unit each time the ant moves along the edge W_1 (resp. W_2), representing the deposit of pheromone by the ant.

For $k \gg 1, t \gg k, t \gg N\Delta t$, at a time scale $[t, t+N\Delta t]$, we can use a quasi-stationary approximation in the spirit of [2] and we have that

$$\omega_1(t+N\Delta t) - \omega_1(t) = Np_{W_1},$$

$$\omega_2(t+N\Delta t) - \omega_2(t) = Np_{W_2},$$

so that

$$\frac{\omega_1(t+N\Delta t) - \omega_1(t)}{N} = p_{W_1}, \qquad \frac{\omega_2(t+N\Delta t) - \omega_2(t)}{N} = p_{W_2}. \tag{4.1}$$

Asymptotically, using our choice of $\Delta t = 1$, we replace the left hand side of (4.1) by time derivatives and we then

$$\begin{cases} \dfrac{d\omega_1}{dt} = p_{W_1} \\ \dfrac{d\omega_2}{dt} = p_{W_2} \end{cases} \tag{4.2}$$

with $p_{W_1} + p_{W_2} = 1$, since we are working with probabilities, and $\omega_1 + \omega_2 = t$.

If we do the change $\omega_i = k\Omega_i, i = 1, 2, t = k\tau$ then system (4.2) becomes

$$\begin{cases} \dfrac{d\Omega_1}{d\tau} = \dfrac{(k\Omega_1 + k)^\alpha}{(k\Omega_1 + k)^\alpha + (k\Omega_2 + k)^\alpha} = \dfrac{(1 + \Omega_1)^\alpha}{(1 + \Omega_1)^\alpha + (1 + \Omega_2)^\alpha} \\ \dfrac{d\Omega_2}{d\tau} = \dfrac{(k\Omega_2 + k)^\alpha}{(k\Omega_1 + k)^\alpha + (k\Omega_2 + k)^\alpha} = \dfrac{(1 + \Omega_2)^\alpha}{(1 + \Omega_1)^\alpha + (1 + \Omega_2)^\alpha} \end{cases} \tag{4.3}$$

and $\Omega_1 + \Omega_2 = \tau$.

Now, to study the equilibrium points for system (4.3), we do the change $\phi_i = \frac{\Omega_i}{\tau}, i = 1, 2$; since $\phi_1 + \phi_2 = 1$, we only take into account branch ϕ_1. Notice that the unknowns ω_i grow linearly in time and it is the pre-factors ϕ_i of this linear law that can be expected to achieve stationary values. Hence

$$\frac{d\Omega_1}{d\tau} = \frac{d}{d\tau}(\tau\phi_1) = \phi_1 + \tau\frac{d\phi_1}{d\tau} = \frac{(1 + \tau\phi_1)^\alpha}{(1 + \tau\phi_1)^\alpha + (1 + \tau\phi_2)^\alpha}, \tag{4.4}$$

and so

$$\begin{aligned} \tau\frac{d\phi_1}{d\tau} &= \frac{1}{1 + \left(\frac{1+\tau\phi_2}{1+\tau\phi_1}\right)^\alpha} - \phi_1 = \frac{1}{1 + \left(1 + \frac{\tau\phi_2 - \tau\phi_1}{1+\tau\phi_1}\right)^\alpha} - \phi_1 \\ &= \frac{1}{1 + \left(1 - \frac{2\phi_1 - 1}{\phi_1 + \frac{1}{\tau}}\right)^\alpha} - \phi_1, \end{aligned} \tag{4.5}$$

where we have used that $\phi_2 = 1 - \phi_1$.

Rearranging in (4.5) we get

$$\begin{aligned} \tau\frac{d\phi_1}{d\tau} &= \frac{1}{1 + \left(1 - \frac{2\phi_1 - 1}{\frac{\tau\phi_1 + 1}{\tau}}\right)^\alpha} - \phi_1 = \frac{1}{1 + \left(\frac{2 + \tau - 1 - \tau\phi_1}{\tau\phi_1 + 1}\right)^\alpha} - \phi_1 \\ &= \frac{1}{1 + \left(\frac{2+\tau}{\tau\phi_1 + 1} - 1\right)^\alpha} - \phi_1 \approx \frac{1}{1 + \left(-1 + \phi_1^{-1}\right)^\alpha} - \phi_1 \end{aligned} \tag{4.6}$$

where he have done an approximation using the following Taylor's expansion since $1 \ll \tau, \phi_1 \gg \tau^{-1}$

$$\frac{1}{1 - x} = \sum_{j=0}^{\infty} x^j, |x| < 1,$$

If we do the change $\eta = \log(\tau)$ in (4.6) we have

$$\boxed{\frac{d\phi_1}{d\eta} = \frac{1}{1+\left(\frac{1}{\phi_1}-1\right)^{\alpha}} - \phi_1} \tag{4.7}$$

To find the equilibrium points we calculate

$$\frac{d\phi_1}{d\eta} = 0 \Leftrightarrow \phi_1 + (1-\phi_1)^{\alpha}\phi_1^{(1-\alpha)} = 1,$$

and we get, in a straightforward manner, the following three roots

$$\phi_1 = 1, \qquad \phi_1 = 0, \qquad \phi_1 = \frac{1}{2}.$$

Hence, the equilibrium points are

$$(1,0), \qquad (0,1), \qquad (\frac{1}{2},\frac{1}{2}).$$

We study in detail the behavior at each equilibrium point.

Case $\phi_1 = \frac{1}{2}$. We consider the approximation

$$\phi_1 = \frac{1}{2} + \tilde{\phi_1}.$$

Introducing this value into equation (4.7) we have

$$\begin{aligned}\frac{d\tilde{\phi_1}}{d\eta} &= \frac{1}{1+\left(\frac{2}{1+2\tilde{\phi_1}}-1\right)^{\alpha}} - \frac{1}{2} - \tilde{\phi_1} \approx \frac{1}{1+(2-4\tilde{\phi_1}-1)^{\alpha}} - \frac{1}{2} - \tilde{\phi_1} \\ &\approx \frac{1}{2-4\alpha\tilde{\phi_1}} - \frac{1}{2} - \tilde{\phi_1} \approx \frac{1}{2}(1+2\alpha\tilde{\phi_1}) - \frac{1}{2} - \tilde{\phi_1} = (\alpha-1)\tilde{\phi_1}\end{aligned}$$

where we have used Taylor's expansions.

Then, we have two different cases:

a) If $\alpha < 1$,

$$\frac{d\tilde{\phi_1}}{d\eta} = \overbrace{(\alpha-1)}^{<0}\tilde{\phi_1} \Rightarrow \tilde{\phi_1} \approx Ce^{(-|\alpha-1|\eta)}$$

$\phi_1 = \frac{1}{2}$ is STABLE

b) If $\alpha > 1$,

$$\frac{d\tilde{\phi_1}}{d\eta} = \overbrace{(\alpha-1)}^{>0}\tilde{\phi_1} \Rightarrow \tilde{\phi_1} \approx Ce^{(|\alpha-1|\eta)}$$

$\phi_1 = \frac{1}{2}$ is UNSTABLE

Case $\phi_1 = 1$. We consider the approximation

$$\phi_1 = 1 - \tilde{\phi_1}.$$

Introducing this value into equation (4.7) we have

$$\begin{aligned} -\frac{d\tilde{\phi_1}}{d\eta} &= \frac{1}{1 + \left(\frac{1}{1-\tilde{\phi_1}} - 1\right)^{\alpha}} + \tilde{\phi_1} - 1 \approx \frac{1}{1 + (1 + \tilde{\phi_1} - 1)^{\alpha}} - 1 + \tilde{\phi_1} \\ &\approx 1 - \tilde{\phi_1}^{\alpha} - 1 + \tilde{\phi_1} = \tilde{\phi_1} - \tilde{\phi_1}^{\alpha} \end{aligned}$$

where we have used Taylor's expansions.

We have the following cases:

a) If $\alpha > 1$, since $\tilde{\phi_1} \gg \tilde{\phi_1}^{\alpha}$

$$\frac{d\tilde{\phi_1}}{d\eta} = -\tilde{\phi_1} \Rightarrow \tilde{\phi_1} \approx Ce^{-\eta}$$

$\phi_1 = 1$ is STABLE

b) If $\alpha < 1$, since $\tilde{\phi_1} \ll \tilde{\phi_1}^{\alpha}$

$$\frac{d\tilde{\phi_1}}{d\eta} = \tilde{\phi_1}^{\alpha} \Rightarrow \tilde{\phi_1} \approx C\eta^{\frac{1}{1-\alpha}}$$

$\phi_1 = 1$ is UNSTABLE

Case $\phi_1 = 0$. We consider the approximation

$$\phi_1 = \tilde{\phi_1}.$$

Introducing this value into equation (4.7) we have

$$\begin{aligned} \frac{d\tilde{\phi_1}}{d\eta} &= \frac{1}{1 + \left(\frac{1}{\tilde{\phi_1}} - 1\right)^{\alpha}} - \tilde{\phi_1} = \frac{\tilde{\phi_1}\alpha}{\tilde{\phi_1}^{\alpha} + (1 - \tilde{\phi_1})^{\alpha}} - \tilde{\phi_1} \\ &\approx \tilde{\phi_1}^{\alpha} - \tilde{\phi_1} \end{aligned}$$

where we have used Taylor's expansions.

We have the following cases:

a) If $\alpha > 1$, since $\tilde{\phi_1} \gg \tilde{\phi_1}^{\alpha}$,

$$\frac{d\tilde{\phi_1}}{d\eta} = -\tilde{\phi_1} \Rightarrow \tilde{\phi_1} \approx Ce^{-\eta}$$

$\phi_1 = 0$ is STABLE

b) If $\alpha < 1$, since $\tilde{\phi_1} \ll \tilde{\phi_1}^{\alpha}$,

$$\frac{d\tilde{\phi_1}}{d\eta} = \tilde{\phi_1}^{\alpha} \Rightarrow \tilde{\phi_1} \approx C\eta^{\frac{1}{1-\alpha}}$$

$\phi_1 = 0$ is UNSTABLE

Therefore, α appears as a critical parameter for reinforcement of edges. If $\alpha < 1$ then non-reinforcement will take place since the state $(\phi_1, \phi_2) = (\frac{1}{2}, \frac{1}{2})$ is stable. On the other hand, if $\alpha > 1$ then one edge or the other will be reinforced since both $(\phi_1, \phi_2) = (1, 0)$ and $(\phi_1, \phi_2) = (0, 1)$ become stable. The result, of course, supports the numerical observations in chapter 3. Specifically, the linearized analysis clearly supports the numerical observations that the super-linear non-linearities in the reinforcement yield path selection while sub-linear non-linearities do not.

4.2 Network with three nodes

We consider a three node network with the following constraints: if the ant is at node 1 or 2, it can move to the other two nodes. If the ant is at node 3 and the previous node is node 1, then it must move to node 2; if the previous node is node 2, then it must move to node 1 (directionality constraint).

4.2.1 Analytical study for a reinforced three node network

We consider a three node network as in figure (4.2) with reinforcement. With this constraint we have four different states for our system: being at node 1 (with associated probability p_1), being at node 2 (with associated probability p_2), being at node 3 coming from node 1 (with associated probability $p_{3\uparrow 1}$) and being at node 3 coming from node 2 (with associated probability $p_{3\downarrow 2}$). The transition probabilities are $p_{i,j}$ probability of moving from node i to node j. If we denote by $\omega_i(t)$ the quantity of pheromone at link W_i, at time t ($i = 1, 2, 3$), then the probabilities at step t are given by:

$$\begin{aligned}
p_{1,2}(t) &= \frac{(k+\omega_1(t))^{\alpha}}{(k+\omega_1(t))^{\alpha} + (k+\omega_2(t))^{\alpha}} \\
p_{1,3}(t) &= \frac{(k+\omega_2(t))^{\alpha}}{(k+\omega_1(t))^{\alpha} + (k+\omega_2(t))^{\alpha}} \\
p_{2,1}(t) &= \frac{(k+\omega_1(t))^{\alpha}}{(k+\omega_1(t))^{\alpha} + (k+\omega_3(t))^{\alpha}} \\
p_{2,3}(t) &= \frac{(k+\omega_3(t))^{\alpha}}{(k+\omega_1(t))^{\alpha} + (k+\omega_3(t))^{\alpha}}.
\end{aligned} \tag{4.8}$$

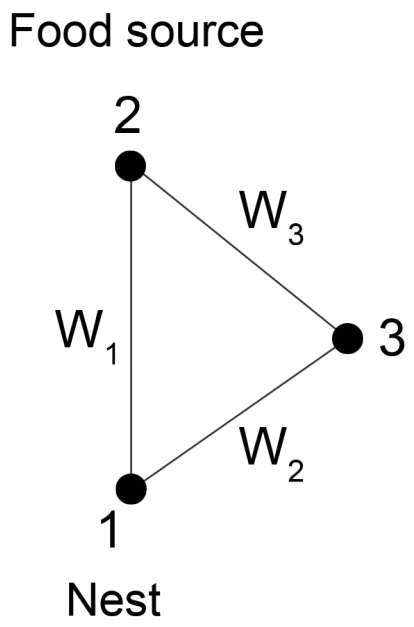

Figure 4.2: Three node network

In the case with directionality constraint, since an ant in node 3 is forced to go to node 2 if it is coming from node 1 and to node 1 if it is coming from node 2, one must take $p_{3,1} = 1$ and $p_{3,2} = 1$.

We recall that Δt is the time between two consecutive steps. Suppose that $t \gg 1$, then since ω_i is reinforced at each time step ω_i is put of order t. Let us assume now that the ants perform N steps with $N\Delta t \gg 1$ and $N\Delta t \ll t$. Since the characteristic time ω_i is of order t, we have that in the N iterations the ω_i can be assumed to be frozen. Therefore the evolution of the ants can be described with a markov chain with constant probabilities. Hence in times larger than $N\Delta t$ the occupancy times of the different nodes are proportional to the equilibrium probabilities for the markov chain. Since the size of the networks is of order one, the number of iterations needed for the system to approach equilibrium is of order one, and therefore the system can be assume to be at the equilibrium.

We can then compute the rate of change of the ω_i using these equilibrium distributions:

$$\omega_1(t + N\Delta t) - \omega_1(t) = N(p_{2,1}p_2 + p_{1,2}p_1),$$

$$\omega_2(t + N\Delta t) - \omega_2(t) = N(p_{1,3}p_1 + p_{3\downarrow 2}),$$

$$\omega_3(t + N\Delta t) - \omega_3(t) = N(p_{2,3}p_2 + p_{3\uparrow 1}),$$

where the p_1, p_2, $p_{3\downarrow 2}$ and $p_{3\uparrow 1}$ are at equilibrium.

Asymptotically, taking $\Delta t = 1$ and approximating $\frac{1}{N}(\omega_i(t+N\Delta t) - \omega_i(t)) \approx \frac{d\omega_i}{dt}, i = 1, 2, 3$, we get

$$\begin{cases} \dfrac{d\omega_1}{dt} = p_{2,1}p_2 + p_{1,2}p_1, \\ \dfrac{d\omega_2}{dt} = p_{1,3}p_1 + p_{3\downarrow 2}, \\ \dfrac{d\omega_3}{dt} = p_{2,3}p_2 + p_{3\uparrow 1}, \end{cases} \tag{4.9}$$

with $p_{1,3}p_1 + p_{3\downarrow 2} + p_{2,1}p_2 + p_{1,2}p_1 + p_{2,3}p_2 + p_{3\uparrow 1} = 1$, since we are working with probabilities, and $\omega_1 + \omega_2 + \omega_3 = t$.

The equations for the probabilities of the four different states are then

$$\begin{cases} p_1 = p_2 \dfrac{(k+\omega_1)^\alpha}{(k+\omega_1)^\alpha + (k+\omega_3)^\alpha} + p_{3\downarrow 2}, \\ p_2 = p_1 \dfrac{(k+\omega_1)^\alpha}{(k+\omega_1)^\alpha + (k+\omega_2)^\alpha} + p_{3\uparrow 1}, \\ p_{3\uparrow 1} = p_1 \dfrac{(k+\omega_2)^\alpha}{(k+\omega_1)^\alpha + (k+\omega_2)^\alpha}, \\ p_{3\downarrow 2} = p_2 \dfrac{(k+\omega_3)^\alpha}{(k+\omega_1)^\alpha + (k+\omega_3)^\alpha}. \end{cases} \tag{4.10}$$

If we do the change $\omega_i = k\Omega_i, i = 1, 2, 3, t = k\tau$ then system (4.9) becomes

$$\begin{cases} \dfrac{d\Omega_1}{d\tau} = \dfrac{(k\Omega_1 + k)^\alpha}{(k\Omega_1 + k)^\alpha + (k\Omega_3 + k)^\alpha} p_2 + \dfrac{(k\Omega_1 + k)^\alpha}{(k\Omega_1 + k)^\alpha + (k\Omega_2 + k)^\alpha} p_1, \\ \dfrac{d\Omega_2}{d\tau} = \dfrac{(k\Omega_2 + k)^\alpha}{(k\Omega_1 + k)^\alpha + (k\Omega_2 + k)^\alpha} p_1 + p_{3\downarrow 2}, \\ \dfrac{d\Omega_3}{d\tau} = \dfrac{(k\Omega_3 + k)^\alpha}{(k\Omega_1 + k)^\alpha + (k\Omega_3 + k)^\alpha} p_2 + p_{3\uparrow 1}, \end{cases} \tag{4.11}$$

and $\Omega_1 + \Omega_2 + \Omega_3 = \tau$.

Similarly, for $N \gg 1$, system (4.10) becomes

$$\begin{cases} p_1 = p_2 \dfrac{\Omega_1^\alpha}{\Omega_1^\alpha + \Omega_3^\alpha} + p_{3\downarrow 2}, & (4.12) \\ p_2 = p_1 \dfrac{\Omega_1^\alpha}{\Omega_1^\alpha + \Omega_2^\alpha} + p_{3\uparrow 1}, & (4.13) \\ p_{3\uparrow 1} = p_1 \dfrac{\Omega_2^\alpha}{\Omega_1^\alpha + \Omega_2^\alpha}, & (4.14) \\ p_{3\downarrow 2} = p_2 \dfrac{\Omega_3^\alpha}{\Omega_1^\alpha + \Omega_3^\alpha}. & (4.15) \end{cases}$$

Since $\tau \gg 1$, then by writing $\Omega_i = \phi_i \tau$, $i = 1, 2, 3$ asymptotically the system (4.11) becomes

$$\begin{cases} \phi_1 = \dfrac{\phi_1^\alpha}{\phi_1^\alpha + \phi_3^\alpha} p_2 + \dfrac{\phi_1^\alpha}{\phi_1^\alpha + \phi_2^\alpha} p_1, & (4.16) \\ \phi_2 = \dfrac{\phi_2^\alpha}{\phi_1^\alpha + \phi_2^\alpha} p_1 + p_{3\downarrow 2}, & (4.17) \\ \phi_3 = \dfrac{\phi_3^\alpha}{\phi_1^\alpha + \phi_3^\alpha} p_2 + p_{3\uparrow 1}, & (4.18) \end{cases}$$

and system (4.12)-(4.15) holds with Ω_i replaced by ϕ_i:

$$\begin{cases} p_1 = p_2 \dfrac{\phi_1^\alpha}{\phi_1^\alpha + \phi_3^\alpha} + p_{3\downarrow 2}, & (4.19) \\ p_2 = p_1 \dfrac{\phi_1^\alpha}{\phi_1^\alpha + \phi_2^\alpha} + p_{3\uparrow 1}, & (4.20) \\ p_{3\uparrow 1} = p_1 \dfrac{\phi_2^\alpha}{\phi_1^\alpha + \phi_2^\alpha}, & (4.21) \\ p_{3\downarrow 2} = p_2 \dfrac{\phi_3^\alpha}{\phi_1^\alpha + \phi_3^\alpha}. & (4.22) \end{cases}$$

Substituting (4.21) into (4.20) we get

$$p_1 \frac{\phi_1^\alpha}{\phi_1^\alpha + \phi_2^\alpha} + p_1 \frac{\phi_2^\alpha}{\phi_1^\alpha + \phi_2^\alpha} - p_2 = 0 \Rightarrow \boxed{p_1 = p_2} \tag{4.23}$$

and introducing (4.23), (4.21), (4.22) into (4.17) and (4.18) we have

$$\begin{cases} \phi_2 = \dfrac{\phi_2^\alpha}{\phi_1^\alpha + \phi_2^\alpha} p_1 + \dfrac{\phi_3^\alpha}{\phi_1^\alpha + \phi_3^\alpha} p_1, \\ \phi_3 = \dfrac{\phi_3^\alpha}{\phi_1^\alpha + \phi_3^\alpha} p_1 + \dfrac{\phi_2^\alpha}{\phi_1^\alpha + \phi_2^\alpha} p_1, \end{cases} \Rightarrow \boxed{\phi_2 = \phi_3} \tag{4.24}$$

By substituting (4.23) and (4.24) into (4.21) and (4.22) we have

$$\boxed{p_{3\downarrow 2} = p_{3\uparrow 1}} \tag{4.25}$$

Finally, introducing (4.23) and (4.24) into (4.20) we have

$$p_1 \left(1 - \frac{(1 - 2\phi_2)^\alpha}{(1 - 2\phi_2)^\alpha + \phi_2^\alpha} \right) = p_{3\uparrow 1}. \tag{4.26}$$

Since $p_1 + p_2 + p_{3\uparrow 1} + p_{3\downarrow 2} = 1$ and $p_1 = p_2, p_{3\uparrow 1} = p_{3\downarrow 2}$ we have

$$\frac{1}{2} - p_1 = p_{3\uparrow 1}. \tag{4.27}$$

Putting (4.27) into (4.26) we get

$$p_1 \left(1 - \frac{(1 - 2\phi_2)^\alpha}{(1 - 2\phi_2)^\alpha + \phi_2^\alpha} \right) = \frac{1}{2} - p_1 \Rightarrow p_1 = \frac{1}{2} \left(\frac{1}{1 + \frac{\phi_2^\alpha}{\phi_2^\alpha + \phi_1^\alpha}} \right). \tag{4.28}$$

Now, we study the equilibrium points for system (4.11) as well as their stability. Since $\phi_1 + \phi_2 + \phi_3 = 1$ and $\phi_2 = \phi_3$ by (4.24), we only take into account the equation for Ω_1. Hence

$$\frac{d\Omega_1}{d\tau} = \frac{d}{d\tau}(\tau\phi_1) = \phi_1 + \tau\frac{d\phi_1}{d\tau} = 2p_1\left(\frac{(1+\tau\phi_1)^\alpha}{(1+\tau\phi_1)^\alpha + (1+\tau\phi_2)^\alpha}\right). \tag{4.29}$$

Introducing the value of p_1 into (4.29) and approximating for $\tau \gg 1$ we get

$$\tau\frac{d\phi_1}{d\tau} \approx \frac{1}{1+2\left(\frac{\phi_2}{\phi_1}\right)^\alpha} - \phi_1 = \frac{1}{1+2\left(\frac{\frac{1-\phi_1}{2}}{\phi_1}\right)^\alpha} - \phi_1 \tag{4.30}$$

where we have used that $\phi_2 = \frac{1-\phi_1}{2}$.

Therefore, (4.30) becomes

$$\tau\frac{d\phi_1}{d\tau} = \frac{1}{1+2^{(1-\alpha)}(-1+\phi_1^{-1})^\alpha} - \phi_1, \tag{4.31}$$

which provides an equation for ϕ_1 provided that $1 \ll \tau, \phi_1 \gg \tau^{-1}$.

If we do the change $\eta = \log(\tau)$ in (4.31) we have

$$\boxed{\frac{d\phi_1}{d\eta} = \frac{1}{1+2^{(1-\alpha)}\left(\frac{1}{\phi_1}-1\right)^\alpha} - \phi_1} \tag{4.32}$$

To find the equilibrium points we calculate

$$\frac{d\phi_1}{d\eta} = 0 \Leftrightarrow (2\phi_1)^{(\alpha-1)} = (2\phi_1)^{(\alpha-1)}\phi_1 + (1-\phi_1)^\alpha,$$

and by straightforward calculations we get

$$\phi_1 = 1, \qquad \phi_1 = 0, \qquad \phi_1 = \frac{1}{3}.$$

Hence, the equilibrium points are

$$(1,0,0), \qquad (0,\frac{1}{2},\frac{1}{2}), \qquad (\frac{1}{3},\frac{1}{3},\frac{1}{3}).$$

We study in detail the behavior at each equilibrium point.

Case $\phi_1 = \frac{1}{3}$. We consider the approximation

$$\phi_1 = \frac{1}{3} + \tilde{\phi_1}.$$

Introducing this value into equation (4.32) we have

$$\begin{aligned}\frac{d\tilde{\phi}_1}{d\eta} &= \frac{1}{1+2\left(\frac{\frac{2}{3}-\tilde{\phi}_1}{\frac{2}{3}+2\tilde{\phi}_1}\right)^{\alpha}} - \frac{1}{3} - \tilde{\phi}_1 = \frac{1}{1+2\left(\frac{1}{1+3\tilde{\phi}_1} - \frac{1}{2}\frac{\tilde{\phi}_1}{\frac{1}{3}+\tilde{\phi}_1}\right)^{\alpha}} - \frac{1}{3} - \tilde{\phi}_1 \\ &\approx \frac{1}{1+2\left(1-3\tilde{\phi}_1 - \frac{1}{2}\frac{3\tilde{\phi}_1}{1+3\tilde{\phi}_1}\right)^{\alpha}} - \frac{1}{3} - \tilde{\phi}_1 \approx \frac{1}{1+2\left(1-\frac{9}{2}\tilde{\phi}_1\right)^{\alpha}} - \frac{1}{3} - \tilde{\phi}_1 \\ &\approx \frac{1}{1+2(1-\frac{9}{2}\alpha\tilde{\phi}_1)} - \frac{1}{3} - \tilde{\phi}_1 = \frac{1}{3}\frac{1}{1-3\alpha\tilde{\phi}_1} - \frac{1}{3} - \tilde{\phi}_1 \\ &\approx \frac{1}{3}(1+3\alpha\tilde{\phi}_1) - \frac{1}{3} - \tilde{\phi}_1 = \alpha\tilde{\phi}_1 - \tilde{\phi}_1 = (\alpha-1)\tilde{\phi}_1\end{aligned}$$

where we have used Taylor's expansions.

Then, we have two different cases:

a) If $\alpha < 1$,

$$\frac{d\tilde{\phi}_1}{d\eta} = \overbrace{(\alpha-1)}^{<0}\tilde{\phi}_1 \Rightarrow \tilde{\phi}_1 \approx Ce^{(-|\alpha-1|\eta)}$$

$\phi_1 = \frac{1}{3}$ is STABLE

b) If $\alpha > 1$,

$$\frac{d\tilde{\phi}_1}{d\eta} = \overbrace{(\alpha-1)}^{>0}\tilde{\phi}_1 \Rightarrow \tilde{\phi}_1 \approx Ce^{(|\alpha-1|\eta)}$$

$\phi_1 = \frac{1}{3}$ is UNSTABLE

Case $\phi_1 = 1$. We consider the approximation

$$\phi_1 = 1 - \tilde{\phi}_1.$$

Introducing this value into equation (4.32) we have

$$\begin{aligned}-\frac{d\tilde{\phi}_1}{d\eta} &= \frac{1}{1+2\left(\frac{1}{2}\frac{\tilde{\phi}_1}{1-\tilde{\phi}_1}\right)^{\alpha}} - 1 + \tilde{\phi}_1 = \frac{1}{1+2\left(\frac{1}{2}\tilde{\phi}_1(1+\tilde{\phi}_1)\right)^{\alpha}} - 1 + \tilde{\phi}_1 \\ &\approx 1 - 2\left(\frac{1}{2}\tilde{\phi}_1\right)^{\alpha} - 1 + \tilde{\phi}_1 = -2^{1-\alpha}{\tilde{\phi}_1}^{\alpha} + \tilde{\phi}_1,\end{aligned}$$

where we have used Taylor's expansions.

We have the following cases:

a) If $\alpha > 1$, since $\tilde{\phi_1} \gg \tilde{\phi_1}^{\alpha}$

$$\frac{d\tilde{\phi_1}}{d\eta} = -\tilde{\phi_1} \Rightarrow \tilde{\phi_1} \approx Ce^{-\eta}$$

$\phi_1 = 1$ is STABLE

b) If $\alpha < 1$, since $\tilde{\phi_1} \ll \tilde{\phi_1}^{\alpha}$

$$\frac{d\tilde{\phi_1}}{d\eta} = 2^{(1-\alpha)}\tilde{\phi_1}^{\alpha} \Rightarrow \tilde{\phi_1} \approx C\eta^{\frac{1}{1-\alpha}}$$

$\phi_1 = 1$ is UNSTABLE

Case $\phi_1 = 0$. We consider the approximation

$$\phi_1 = \tilde{\phi_1}.$$

Introducing this value into equation (4.32) we have

$$\frac{d\tilde{\phi_1}}{d\eta} = \frac{1}{1 + 2\left(\frac{1-\tilde{\phi_1}}{2\tilde{\phi_1}}\right)^{\alpha}} - \tilde{\phi_1} = \frac{1}{1 + 2^{(1-\alpha)}\left(\frac{1-\tilde{\phi_1}}{\tilde{\phi_1}}\right)^{\alpha}} - \tilde{\phi_1} =$$

$$\approx 1 - 2^{(1-\alpha)}\left(\frac{1-\tilde{\phi_1}}{\tilde{\phi_1}}\right)^{\alpha} - \tilde{\phi_1} = 1 - 2^{(1-\alpha)}(1 - \tilde{\phi_1}^{-\alpha}) - \tilde{\phi_1},$$

where we have used Taylor's expansions.

We have the following cases:

a) If $\alpha > 1$, since $\tilde{\phi_1} \gg \tilde{\phi_1}^{\alpha}$

$$\frac{d\tilde{\phi_1}}{d\eta} = -\tilde{\phi_1} \Rightarrow \tilde{\phi_1} \approx Ce^{-\eta}$$

$\phi_1 = 0$ is STABLE

b) If $\alpha < 1$, since $\tilde{\phi_1} \ll \tilde{\phi_1}^{\alpha}$

$$\frac{d\tilde{\phi_1}}{d\eta} = 1 - 2^{(1-\alpha)}\tilde{\phi_1}^{-\alpha} \Rightarrow \tilde{\phi_1} \approx C\eta^{\frac{\alpha}{1+\alpha}}$$

$\phi_1 = 0$ is UNSTABLE

As a conclusion of the analysis of the three node network, if $\alpha < 1$ then the three edges are run with identical probability since the only stable equilibrium is $(\phi_1, \phi_2, \phi_3) = (\frac{1}{3}, \frac{1}{3}, \frac{1}{3})$, while for $\alpha > 1$ the states $(\phi_1, \phi_2, \phi_3) = (1, 0, 0)$ and $(\phi_1, \phi_2, \phi_3) = (0, \frac{1}{2}, \frac{1}{2})$, corresponding to the shortest and longest paths respectively, are the stable ones. This result implies that for $\alpha > 1$ one particular path, the short or the long one, will be reinforced and our random walker will end up walking on it with a probability that tends to one as time goes to infinity. Nevertheless,

the analysis does not provide a reason for the shortest one to be selected preferably with respect to the longest one. In the next sections, we will see that such a selection takes place in the first stages of the evolution when more than one ant are running through the network. In order to perform this analysis, we will linearize the probabilities given by (4.8) using as a small parameter α/k and solve the resulting evolution problem. By assuming $\alpha/k \ll 1$ we are considering the case where reinforcement remains very weak up to times when $\omega_i = \mathcal{O}(k)$. We will show that the difference in the amount of pheromone between the shortest path and any of the links in the longest path has a probability distribution that evolves according to a convection equation. The convection velocity, when there is more than one ant, is always in the direction of increasing the value of the difference in the amount of pheromone and hence the shortest path will be increasingly reinforced. This breaking of symmetry occurs faster with increasing number of ants due to the fact that the convection velocity grows very quickly with the number of ants.

4.2.2 Reinforced and non-reinforced network with one ant

Considering the three node network in figure (4.2) for one ant, we have two possible states:

- The ant is at food source (node 2) or nest (node 1), case $\mathcal{A}$;
- The ant is at node 3, case $\mathcal{B}$;

To simplify the analysis we restrict the problem to times t so that $\omega_j = \mathcal{O}(t) \ll \frac{k}{\alpha}$ and we can approximate the probability $p_{1,2}$ in formula (4.8) by

$$\begin{aligned} p_{1,2} &= \frac{(k+\omega_1)^\alpha}{(k+\omega_1)^\alpha + (k+\omega_2)^\alpha} \approx \frac{1+\alpha\frac{\omega_1}{k}}{2+\alpha\left(\frac{\omega_1}{k}+\frac{\omega_2}{k}\right)} \approx \frac{1}{2}\left(1+\alpha\frac{\omega_1}{k}\right)\left(1-\frac{\alpha}{2}\left(\frac{\omega_1}{k}+\frac{\omega_2}{k}\right)\right) \\ &\approx \frac{1}{2}\left(1+\alpha\frac{\omega_1}{k}-\frac{\alpha}{2}\left(\frac{\omega_1}{k}+\frac{\omega_2}{k}\right)\right) = \frac{1}{2}\left(1+\alpha\frac{\omega_1-\omega_2}{2k}\right) = \frac{1+\varepsilon\Delta}{2}, \end{aligned}$$

where $\varepsilon = \frac{\alpha}{2k}$ and $\Delta = \omega_1 - \omega_2$

Analogously,

$$p_{1,3} \approx \frac{1-\varepsilon\Delta}{2}, \qquad p_{2,1} \approx \frac{1+\varepsilon\Delta}{2}, \qquad p_{2,3} \approx \frac{1-\varepsilon\Delta}{2}.$$

Notice that we have approximated $\omega_2 = \omega_3$ since both edges W_2, W_3 are run the same number of times due to the directionality constraint imposed. Considering the cases $\mathcal{A}$ and $\mathcal{B}$, we can describe any possible evolution as a sequence of the following states:

1. From state $\mathcal{A}$ to state $\mathcal{A}$: $p = \frac{1+\varepsilon\Delta}{2}, \Delta \to \Delta + 1$;
2. From state $\mathcal{A}$ to state $\mathcal{A}$ passing through state $\mathcal{B}$: $p = \frac{1-\varepsilon\Delta}{2}, \Delta \to \Delta - 1$;

Then the equation for the probability is:

$$p(\Delta, N+1) = \frac{1}{2}(1-\varepsilon\Delta)p(\Delta+1, N) + \frac{1}{2}(1+\varepsilon\Delta)p(\Delta-1, N). \tag{4.33}$$

Equations at $\mathcal{O}(\varepsilon^0)$

From (4.33) we have that

$$p(\Delta, N+1) = \frac{1}{2}p(\Delta+1, N) + \frac{1}{2}p(\Delta-1, N). \tag{4.34}$$

If we subtract $p(\Delta, N)$ at both sides in (4.34), we get

$$\frac{\partial p}{\partial t} \approx p(\Delta, N+1) - p(\Delta, N) = \frac{p(\Delta+1, N) + p(\Delta-1, N) - 2p(\Delta, N)}{2} \approx \frac{1}{2}\frac{\partial^2 p}{\partial \Delta^2}.$$

This is a diffusion equation without transport terms (i.e. terms involving $\frac{\partial p}{\partial x}$) and hence the solution is such that if $p(\Delta, 0)$ is centered at $\Delta = \Delta_0$ then $p(\Delta, t)$ will also be centered at $\Delta = \Delta_0$. Therefore, the maximum probability will always be at $\Delta = \Delta_0$ and hence no path will be reinforced.

Equations at $\mathcal{O}(\varepsilon^1)$

From (4.33) we have that

$$p(\Delta, N+1) = \frac{-\varepsilon\Delta}{2}p(\Delta+1, N) + \frac{\varepsilon\Delta}{2}p(\Delta-1, N) + \frac{1}{2}p(\Delta+1, N) + \frac{1}{2}p(\Delta-1, N). \tag{4.35}$$

Hence, if we subtract $p(\Delta, N)$ at both sides in (4.35), we get

$$\frac{\partial p}{\partial t} \approx \frac{1}{2}\frac{\partial^2 p}{\partial \Delta^2} - \varepsilon\Delta\frac{\partial p}{\partial \Delta},$$

where we have done the following approximations

$$\frac{\partial p}{\partial t} \approx p(\Delta, N+1) - p(\Delta, N), \qquad \frac{\partial p}{\partial \Delta} \approx \frac{p(\Delta+1, N) - p(\Delta-1, N)}{2},$$

$$\frac{\partial^2 p}{\partial \Delta^2} \approx p(\Delta+1, N) + p(\Delta-1, N) - 2p(\Delta, N).$$

If $p(\Delta, 0)$ is centered at $\Delta = \Delta_0$ then the presence of a connective term with velocity $\varepsilon\Delta$ will produce a shift of the movement of $p(\Delta, t)$ to increasing (if $\Delta_0 > 0$) values of Δ or to decreasing (if $\Delta_0 < 0$) values of Δ. Hence, one of the paths, the short or the long one, will be reinforced depending on the initial condition. This agrees with our previous numerical simulations concerning the fact that only one ant is able to reinforce one of the paths but more than one ant is necessary to actually reinforce the shortest one preferably.

4.2.3 Reinforced and non-reinforced network with two ants

In this section, we consider at the same time both the reinforced and non-reinforced cases for two ants in a three node network with directionality constraints. We will split the analysis into two parts: equations at $\mathcal{O}(\varepsilon^0)$ (non-reinforced case) and $\mathcal{O}(\varepsilon^1)$ (reinforced case).

We show that it is enough to consider both directionality constraint and reinforcement to reproduce ant's behavior concerning choice of the shortest path.

Considering the three node network in figure (4.2) for two ants, we can classify any state into these four different states:

1. Both ants at nest (node 1) or food source (node 2), case $\mathcal{A}^+$;
2. One ant at nest and the other at food source, case $\mathcal{A}^-$;
3. Both ants at node 3, case $\mathcal{B}$;
4. One ant at nest/food source and the other at node 3, case $\mathcal{C}$.

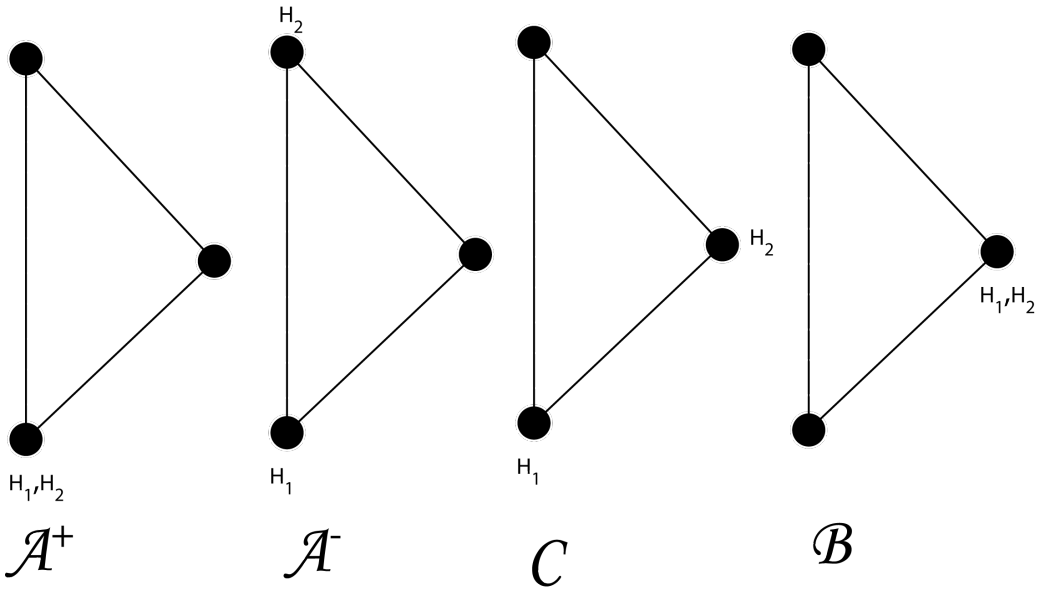

Figure 4.3: Different ant's states. State $\mathcal{A}^+$ also represents the situation where both ants are at the food source. The state $\mathcal{C}$ also represents the situation where one ant is at the food source and the other at node three.

By employing these 4 states, we can describe any possible evolution as a sequence of such states. The probability of being at one of the states at a certain time will depend on the probabilities of having previously been at other states. In order to arrive to a simple way to compute such probabilities, we find a representation of the evolution as a markovian process where one can write the probability to reach a certain state at time $N+1$ merely as a function

of the probabilities to be at each state at time N. The directionality imposed in the problem reduces drastically the number of possible transitions from one state to the other so that any evolution of the system can be viewed as a sequence of "syllables"

$$\mathcal{A}^+\mathcal{A}^+, \qquad \mathcal{A}^-\mathcal{A}^-, \qquad \mathcal{A}^+\mathcal{B}\mathcal{A}^+, \qquad \mathcal{A}^-\mathcal{B}\mathcal{A}^-, \qquad \mathcal{A}^+\mathcal{C}^{(2j)}\mathcal{A}^+,$$
$$\mathcal{A}^+\mathcal{C}^{(2j+1)}\mathcal{A}^-, \qquad \mathcal{A}^-\mathcal{C}^{(2j+1)}\mathcal{A}^+, \qquad \mathcal{A}^-\mathcal{C}^{(2j)}\mathcal{A}^-,$$

where $\mathcal{C}^n$ means that state C is repeated n times. Notice that any of the syllables leaves the system at $\mathcal{A}^+$ or $\mathcal{A}^-$ state and implies a certain change in the relative amount of pheromone Δ and hence, in the probabilities for the transition from one state to the other. Therefore, we can compute the probabilities of being left in state $\mathcal{A}^+$(resp. $\mathcal{A}^-$) with a certain value of Δ after the syllable $\ell+1$ as a function of the probabilities of each syllable to occur and the change in Δ that they produce. These can be easily computed, by induction, to be:

1. From state $\mathcal{A}^+$ to state $\mathcal{A}^+$: $p = \frac{(1+\varepsilon\Delta)^2}{4}$, $\Delta \mapsto \Delta + 2$;
2. From state $\mathcal{A}^-$ to state $\mathcal{A}^-$: $p = \frac{(1+\varepsilon\Delta)^2}{4}$, $\Delta \mapsto \Delta + 2$;
3. From state $\mathcal{A}^+$ to state $\mathcal{A}^+$ passing through state $\mathcal{B}$: $p = \frac{(1-\varepsilon\Delta)^2}{4}$, $\Delta \mapsto \Delta - 2$;
4. From state $\mathcal{A}^-$ to state $\mathcal{A}^-$ passing through state $\mathcal{B}$: $p = \frac{(1-\varepsilon\Delta)^2}{4}$, $\Delta \mapsto \Delta - 2$;
5. From state $\mathcal{A}^-$ to state $\mathcal{A}^+$ passing $n = 2j+1$ times through state $\mathcal{C}$:
$$p = \frac{1}{2^{2j+3}} + \varepsilon\frac{2j^2-4j}{2^{2j+3}} - \varepsilon\Delta\frac{2j-1}{2^{2j+3}} + \mathcal{O}(\varepsilon^2), j = 0, 1, \ldots,$$
$$\Delta \mapsto \Delta - (2j-1), j = 0, 1, \ldots;$$
6. From state $\mathcal{A}^+$ to state $\mathcal{A}^+$ passing $n = 2j$ times through state $\mathcal{C}$:
$$p = \frac{1}{2^{2j+2}} + \varepsilon\frac{2j^2-6j+2}{2^{2j+2}} - \varepsilon\Delta\frac{2j-2}{2^{2j+2}} + \mathcal{O}(\varepsilon^2), j = 1, 2, \ldots,$$
$$\Delta \mapsto \Delta - (2j-2), j = 1, 2, \ldots;$$
7. From state $\mathcal{A}^+$ to state $\mathcal{A}^-$ passing $n = 2j+1$ times through state $\mathcal{C}$:
$$p = \frac{1}{2^{2j+3}} + \varepsilon\frac{2j^2-4j+1}{2^{2j+3}} - \varepsilon\Delta\frac{2j-1}{2^{2j+3}} + \mathcal{O}(\varepsilon^2), j = 0, 1, \ldots,$$
$$\Delta \mapsto \Delta - (2j-1), j = 0, 1, \ldots;$$
8. From state $\mathcal{A}^-$ to state $\mathcal{A}^-$ passing $n = 2j$ times through state $\mathcal{C}$:
$$p = \frac{1}{2^{2j+2}} + \varepsilon\frac{2j^2-6j+4}{2^{2j+2}} - \varepsilon\Delta\frac{2j-2}{2^{2j+2}} + \mathcal{O}(\varepsilon^2), j = 1, 2, \ldots,$$
$$\Delta \mapsto \Delta - (2j-2), j = 1, 2, \ldots;$$

If we set

$$p(N+1,(\Delta,\mathcal{A}^-)) = p_{N+1}(\Delta^-),$$

$$p(N+1,(\Delta,\mathcal{A}^+)) = p_{N+1}(\Delta^+),$$

for the probabilities of having a relative reinforcement Δ and end after the $N+1$ syllable at state $\mathcal{A}^-$ or $\mathcal{A}^+$ respectively, then the equations for such probabilities are:

$$\begin{aligned}
p_{N+1}(\Delta^-) = {} & \frac{1}{4}\big((1+\varepsilon(\Delta-2))^2\big)p_N\big((\Delta-2)^-\big) + \frac{1}{4}\big((1-\varepsilon(\Delta+2))^2\big)p_N\big((\Delta+2)^-\big) \\
& + 2\sum_{j=0}^{\infty}\frac{1}{2^{2j+3}}p_N\big((\Delta+2j-1)^+\big) + 2\sum_{j=1}^{\infty}\frac{1}{2^{2j+2}}p_N\big((\Delta+2j-2)^-\big) \\
& + 2\varepsilon\sum_{j=0}^{\infty}\frac{2j^2-4j+1}{2^{2j+3}}p_N\big((\Delta+2j-1)^+\big) + 2\varepsilon\sum_{j=1}^{\infty}\frac{2j^2-6j+4}{2^{2j+2}}p_N\big((\Delta+2j-2)^-\big) \\
& - 2\varepsilon\sum_{j=0}^{\infty}\frac{2j-1}{2^{2j+3}}(\Delta+2j-1)p_N\big((\Delta+2j-1)^+\big) \\
& - 2\varepsilon\sum_{j=1}^{\infty}\frac{2j-2}{2^{2j+2}}(\Delta+2j-2)p_N\big((\Delta+2j-2)^-\big),
\end{aligned} \tag{4.36}$$

$$\begin{aligned}
p_{N+1}(\Delta^+) = {} & \frac{1}{4}\big((1+\varepsilon(\Delta-2))^2\big)p_N\big((\Delta-2)^+\big) + \frac{1}{4}\big((1-\varepsilon(\Delta+2))^2\big)p_N\big((\Delta+2)^+\big) \\
& + 2\sum_{j=0}^{\infty}\frac{1}{2^{2j+3}}p_N\big((\Delta+2j-1)^-\big) + 2\sum_{j=1}^{\infty}\frac{1}{2^{2j+2}}p_N\big((\Delta+2j-2)^+\big) \\
& + 2\varepsilon\sum_{j=0}^{\infty}\frac{2j^2-4j}{2^{2j+3}}p_N\big((\Delta+2j-1)^-\big) + 2\varepsilon\sum_{j=1}^{\infty}\frac{2j^2-6j+2}{2^{2j+2}}p_N\big((\Delta+2j-2)^+\big) \\
& - 2\varepsilon\sum_{j=0}^{\infty}\frac{2j-1}{2^{2j+3}}(\Delta+2j-1)p_N\big((\Delta+2j-1)^-\big) \\
& - 2\varepsilon\sum_{j=1}^{\infty}\frac{2j-2}{2^{2j+2}}(\Delta+2j-2)p_N\big((\Delta+2j-2)^+\big).
\end{aligned} \tag{4.37}$$

If we perform the approximation

$$p(\Delta^{+,-}+\delta) = p(\Delta^{+,-}) + \delta\frac{\partial p}{\partial\Delta}(\Delta^{+,-}),$$

then (4.36) becomes

$$
\begin{aligned}
p_{N+1}(\Delta^-) = {} & \frac{1}{4}\big(1+\varepsilon^2(\Delta-2)^2+2\varepsilon(\Delta-2)\big)\big(p_N(\Delta^-)-2\frac{\partial p_N}{\partial\Delta}(\Delta^-)\big) \\
& + \frac{1}{4}\big(1+\varepsilon^2(\Delta+2)^2-2\varepsilon(\Delta+2)\big)\big(p_N(\Delta^-)+2\frac{\partial p_N}{\partial\Delta}(\Delta^-)\big)\big) \\
& + 2\sum_{j=0}^{\infty}\frac{1}{2^{2j+3}}\big(p_N(\Delta^+)+(2j-1)\frac{\partial p_N}{\partial\Delta}(\Delta^+)\big) \\
& + 2\sum_{j=1}^{\infty}\frac{1}{2^{2j+2}}\big(p_N(\Delta^-)+(2j-2)\frac{\partial p_N}{\partial\Delta}(\Delta^-)\big) \\
& + 2\varepsilon\sum_{j=0}^{\infty}\frac{2j^2-4j+1}{2^{2j+3}}\big(p_N(\Delta^+)+(2j-1)\frac{\partial p_N}{\partial\Delta}(\Delta^+)\big) \\
& + 2\varepsilon\sum_{j=1}^{\infty}\frac{2j^2-6j+4}{2^{2j+2}}\big(p_N(\Delta^-)+(2j-2)\frac{\partial p_N}{\partial\Delta}(\Delta^-)\big) \\
& - 2\varepsilon\sum_{j=0}^{\infty}\frac{2j-1}{2^{2j+3}}(\Delta+2j-1)\big(p_N(\Delta^+)+(2j-1)\frac{\partial p_N}{\partial\Delta}(\Delta^+)\big) \\
& - 2\varepsilon\sum_{j=1}^{\infty}\frac{2j-2}{2^{2j+2}}(\Delta+2j-2)\big(p_N(\Delta^-)+(2j-2)\frac{\partial p_N}{\partial\Delta}(\Delta^-)\big) \qquad (4.38) \\
= {} & \frac{1}{4}p_N(\Delta^-)-\varepsilon p_N(\Delta^-)-\varepsilon(\Delta-2)\frac{\partial p_N}{\partial\Delta}(\Delta^-)+\frac{1}{4}p_N(\Delta^-)-\varepsilon p_N(\Delta^-) \\
& - \varepsilon(\Delta+2)\frac{\partial p_N}{\partial\Delta}(\Delta^-)+\frac{1}{3}p_N(\Delta^+)-\frac{1}{4}\frac{\partial p_N}{\partial\Delta}(\Delta^+)+\frac{1}{6}p_N(\Delta^-) \\
& + \frac{1}{9}\frac{\partial p_N}{\partial\Delta}(\Delta^-)+\frac{7}{27}\varepsilon p_N(\Delta^+)+\frac{1}{9}\varepsilon\frac{\partial p_N}{\partial\Delta}(\Delta^+)+\frac{2}{27}\varepsilon p_N(\Delta^-) \\
& + \frac{4}{9}\varepsilon\frac{\partial p_N}{\partial\Delta}(\Delta^-)-\frac{17}{27}\varepsilon p_N(\Delta^+)-2\varepsilon\Delta p_N(\Delta^+)\sum_{j=0}^{\infty}\frac{2j-1}{2^{2j+3}} \\
& - \frac{37}{27}\varepsilon\frac{\partial p_N}{\partial\Delta}(\Delta^+)-2\varepsilon\Delta\frac{\partial p_N}{\partial\Delta}(\Delta^+)\sum_{j=0}^{\infty}\frac{(2j-1)^2}{2^{2j+3}} \\
& - \frac{10}{27}\varepsilon p_N(\Delta^-)-2\varepsilon\Delta p_N(\Delta^-)\sum_{j=1}^{\infty}\frac{2j-2}{2^{2j+2}}-\frac{44}{27}\varepsilon\frac{\partial p_N}{\partial\Delta}(\Delta^-) \\
& - 2\varepsilon\Delta\frac{\partial p_N}{\partial\Delta}(\Delta^+)\sum_{j=1}^{\infty}\frac{(2j-2)^2}{2^{2j+2}}+\mathcal{O}(\Delta^2,\varepsilon^2)
\end{aligned}
$$

$$= \frac{2}{3}p_N(\Delta^-) + \frac{1}{3}p_N(\Delta^+) - \frac{62}{27}\varepsilon p_N(\Delta^-) - \frac{10}{27}\varepsilon p_N(\Delta^+)$$
$$- \langle\delta\Delta\rangle_{A^-\to A^-}\frac{\partial p_N}{\partial\Delta}(\Delta^-) - \langle\delta\Delta\rangle_{A^+\to A^-}\frac{\partial p_N}{\partial\Delta}(\Delta^+) + \mathcal{O}(\Delta^2,\varepsilon^2),$$

where

$$\begin{aligned}
\langle\delta\Delta\rangle_{A^-\to A^-} &= 2\varepsilon\Delta - \frac{1}{9} - \frac{4}{9}\varepsilon + \frac{44}{27}\varepsilon + 2\varepsilon\Delta\sum_{j=1}^{\infty}\frac{(2j-2)^2}{2^{2j+2}} \\
&= -\frac{1}{9} + \frac{32}{27}\varepsilon + \frac{64}{27}\varepsilon\Delta, \\
\langle\delta\Delta\rangle_{A^+\to A^-} &= \frac{1}{9} - \frac{1}{9}\varepsilon + \frac{37}{27}\varepsilon + 2\varepsilon\Delta\sum_{j=0}^{\infty}\frac{(2j-1)^2}{2^{2j+3}} \\
&= \frac{1}{9} + \frac{34}{27}\varepsilon + \frac{17}{27}\varepsilon\Delta,
\end{aligned}$$

and (4.37) becomes

$$\begin{aligned}
p_{N+1}(\Delta^+) = {} & \frac{1}{4}\big(1+\varepsilon^2(\Delta-2)^2 + 2\varepsilon(\Delta-2)\big)\big(p_N(\Delta^+) - 2\frac{\partial p_N}{\partial\Delta}(\Delta^+)\big) \\
& + \frac{1}{4}\big(1+\varepsilon^2(\Delta+2)^2 - 2\varepsilon(\Delta+2)\big)\big(p_N(\Delta^+) + 2\frac{\partial p_N}{\partial\Delta}(\Delta^+)\big)\big) \\
& + 2\sum_{j=0}^{\infty}\frac{1}{2^{2j+3}}\big(p_N(\Delta^-) + (2j-1)\frac{\partial p_N}{\partial\Delta}(\Delta^-)\big) \\
& + 2\sum_{j=1}^{\infty}\frac{1}{2^{2j+2}}\big(p_N(\Delta^+) + (2j-2)\frac{\partial p_N}{\partial\Delta}(\Delta^+)\big) \\
& + 2\varepsilon\sum_{j=0}^{\infty}\frac{2j^2-4j}{2^{2j+3}}\big(p_N(\Delta^-) + (2j-1)\frac{\partial p_N}{\partial\Delta}(\Delta^-)\big) \\
& + 2\varepsilon\sum_{j=1}^{\infty}\frac{2j^2-6j+2}{2^{2j+2}}\big(p_N(\Delta^+) + (2j-2)\frac{\partial p_N}{\partial\Delta}(\Delta^+)\big) \\
& - 2\varepsilon\sum_{j=0}^{\infty}\frac{2j-1}{2^{2j+3}}(\Delta+2j-1)\big(p_N(\Delta^-) + (2j-1)\frac{\partial p_N}{\partial\Delta}(\Delta^-)\big) \\
& - 2\varepsilon\sum_{j=1}^{\infty}\frac{2j-2}{2^{2j+2}}(\Delta+2j-2)\big(p_N(\Delta^+) + (2j-2)\frac{\partial p_N}{\partial\Delta}(\Delta^+)\big)
\end{aligned} \tag{4.39}$$

$$
\begin{aligned}
&= \frac{1}{4}p_N(\Delta^+) - \varepsilon p_N(\Delta^+) - \varepsilon(\Delta-2)\frac{\partial p_N}{\partial \Delta}(\Delta^+) + \frac{1}{4}p_N(\Delta^+) - \varepsilon p_N(\Delta^+) \\
&\quad - \varepsilon(\Delta+2)\frac{\partial p_N}{\partial \Delta}(\Delta^+) + \frac{1}{3}p_N(\Delta^-) - \frac{1}{9}\frac{\partial p_N}{\partial \Delta}(\Delta^-) + \frac{1}{6}p_N(\Delta^+) \\
&\quad + \frac{1}{9}\frac{\partial p_N}{\partial \Delta}(\Delta^+) - \frac{2}{27}\varepsilon p_N(\Delta^-) + \frac{2}{9}\varepsilon\frac{\partial p_N}{\partial \Delta}(\Delta^-) - \frac{7}{27}\varepsilon p_N(\Delta^+) \\
&\quad + \frac{2}{9}\varepsilon\frac{\partial p_N}{\partial \Delta}(\Delta^+) - \frac{17}{27}\varepsilon p_N(\Delta^-) - 2\varepsilon\Delta p_N(\Delta^-)\sum_{j=0}^{\infty}\frac{2j-1}{2^{2j+3}} \\
&\quad - \frac{37}{27}\varepsilon\frac{\partial p_N}{\partial \Delta}(\Delta^-) - 2\varepsilon\Delta\frac{\partial p_N}{\partial \Delta}(\Delta^-)\sum_{j=0}^{\infty}\frac{(2j-1)^2}{2^{2j+3}} \\
&\quad - \frac{10}{27}\varepsilon p_N(\Delta^+) - 2\varepsilon\Delta p_N(\Delta^+)\sum_{j=1}^{\infty}\frac{2j-2}{2^{2j+2}} - \frac{44}{27}\varepsilon\frac{\partial p_N}{\partial \Delta}(\Delta^+) \\
&\quad - 2\varepsilon\Delta\frac{\partial p_N}{\partial \Delta}(\Delta^+)\sum_{j=1}^{\infty}\frac{(2j-2)^2}{2^{2j+2}} + \mathcal{O}(\Delta^2,\varepsilon^2) \\
&= \frac{1}{3}p_N(\Delta^-) + \frac{2}{3}p_N(\Delta^+) - \frac{19}{27}\varepsilon p_N(\Delta^-) - \frac{71}{27}\varepsilon p_N(\Delta^+) \\
&\quad - \langle\delta\Delta\rangle_{A^-\to A^+}\frac{\partial p_N}{\partial \Delta}(\Delta^-) - \langle\delta\Delta\rangle_{A^+\to A^+}\frac{\partial p_N}{\partial \Delta}(\Delta^+) + \mathcal{O}(\Delta^2,\varepsilon^2),
\end{aligned}
$$

where

$$
\begin{aligned}
\langle\delta\Delta\rangle_{A^-\to A^+} &= \frac{1}{9} - \frac{2}{9}\varepsilon + \frac{37}{27}\varepsilon + 2\varepsilon\Delta\sum_{j=0}^{\infty}\frac{(2j-1)^2}{2^{2j+3}} \\
&= \frac{1}{9} + \frac{31}{27}\varepsilon + \frac{17}{27}\varepsilon\Delta, \\
\langle\delta\Delta\rangle_{A^+\to A^+} &= 2\varepsilon\Delta - \frac{1}{9} - \frac{2}{9}\varepsilon + \frac{44}{27}\varepsilon + 2\varepsilon\Delta\sum_{j=1}^{\infty}\frac{(2j-2)^2}{2^{2j+2}} \\
&= -\frac{1}{9} + \frac{38}{27}\varepsilon + \frac{64}{27}\varepsilon\Delta,
\end{aligned}
$$

and the sums in (4.38) and (4.39) have been calculated by using the following formula:

$$
\sum_{j=0}^{\infty}\frac{aj^3+bj^2+cj+d}{4^j} = a\frac{44}{27} + b\frac{20}{27} + c\frac{4}{9} + d\frac{4}{3}.
$$

This formula can be proved by employing

$$
\frac{1}{1-x} = \sum_{j=0}^{\infty}x^j, |x| < 1. \tag{4.40}
$$

By derivation in (4.40) we get

$$
\frac{1}{1-x^2} = \sum_{j=0}^{\infty}(j+1)x^j, |x| < 1 \tag{4.41}
$$

and substituting in $x = \frac{1}{4}$ we have that

$$\sum_{j=0}^{\infty} \frac{j+1}{4^j} = \frac{16}{9}$$

and so

$$\sum_{j=0}^{\infty} \frac{j}{4^j} = \frac{4}{9};$$

Now, if we multiply by x equation (4.41) and derivate once we get that

$$\frac{1+x}{(1-x)^3} = \sum_{j=0}^{\infty}(j+1)^2 x^j, |x| < 1 \tag{4.42}$$

and substituting in $x = \frac{1}{4}$ we have that

$$\sum_{j=0}^{\infty} \frac{(j+1)^2}{4^j} = \frac{80}{27}$$

and so

$$\sum_{j=0}^{\infty} \frac{j^2}{4^j} = \frac{20}{27};$$

Finally, if we multiply by x equation (4.42) and derivate once we get that

$$\frac{1+4x+x^2}{(1-x)^4} = \sum_{j=0}^{\infty}(j+1)^3 x^j, |x| < 1$$

and substituting in $x = \frac{1}{4}$ we have that

$$\sum_{j=0}^{\infty} \frac{(j+1)^3}{4^j} = \frac{176}{27}$$

and so

$$\sum_{j=0}^{\infty} \frac{j^3}{4^j} = \frac{44}{27}.$$

Next we proceed to solve equations (4.38),(4.39) both for $\varepsilon = 0$ and $\varepsilon > 0$.

Equations at $\mathcal{O}(\varepsilon^0)$

From (4.38) and (4.39) we have that

$$p_{N+1}(\Delta^-) = \frac{2}{3}p_N(\Delta^-) + \frac{1}{3}p_N(\Delta^+) + \frac{1}{9}\frac{\partial p_N}{\partial \Delta}(\Delta^-) - \frac{1}{9}\frac{\partial p_N}{\partial \Delta}(\Delta^+), \tag{4.43}$$

$$p_{N+1}(\Delta^+) = \frac{1}{3}p_N(\Delta^-) + \frac{2}{3}p_N(\Delta^+) - \frac{1}{9}\frac{\partial p_N}{\partial \Delta}(\Delta^-) + \frac{1}{9}\frac{\partial p_N}{\partial \Delta}(\Delta^+). \tag{4.44}$$

By adding (4.43) and (4.44) we get

$$p_{N+1} \equiv p_{N+1}(\Delta^-) + p_{N+1}(\Delta^+) = p_N(\Delta^-) + p_N(\Delta^+) \equiv p_N. \tag{4.45}$$

Subtracting (4.44) and (4.43) we have

$$\begin{aligned} \delta p_{N+1} \equiv p_{N+1}(\Delta^+) - p_{N+1}(\Delta^-) = -\frac{1}{3}p_N(\Delta^-) + \frac{1}{3}p_N(\Delta^+) \\ - \frac{2}{9}\frac{\partial p_N}{\partial \Delta}(\Delta^-) + \frac{2}{9}\frac{\partial p_N}{\partial \Delta}(\Delta^+) \equiv \frac{1}{3}\delta p_N + \frac{2}{9}\frac{\partial \delta p_N}{\partial \Delta}. \end{aligned} \tag{4.46}$$

Since

$$\delta p_{N+1} - \delta p_N \simeq \frac{\partial \delta p}{\partial t}$$

then (4.46) becomes

$$\frac{\partial \delta p}{\partial t} = -\frac{2}{3}\delta p + \frac{2}{9}\frac{\partial \delta p}{\partial \Delta}, \tag{4.47}$$

and so

$$\delta p = \exp(-\frac{2}{3}t)\delta p_0(\Delta + \frac{2}{9}t) \tag{4.48}$$

where δp_0 is the initial data. This solution shows us an exponential decay for the difference of probabilities $p_N(\Delta^+) - p_N(\Delta^-)$ while the sum of probabilities remains constant for any Δ (4.45). As a consequence, no preferential selection of any edge takes place. Directionality persistence is not sufficient for shortest path's selection.

Equations at $\mathcal{O}(\varepsilon^1)$

From (4.38) and (4.39) we have that

$$\begin{aligned} p_{N+1}(\Delta^-) = \frac{2}{3}p_N(\Delta^-) + \frac{1}{3}p_N(\Delta^+) - \frac{62}{27}\varepsilon p_N(\Delta^-) - \frac{10}{27}\varepsilon p_N(\Delta^+) \\ - \frac{\partial p_N}{\partial \Delta}(\Delta^-)\big(-\frac{1}{9} + \frac{32}{27}\varepsilon + \frac{64}{27}\varepsilon\Delta\big) - \frac{\partial p_N}{\partial \Delta}(\Delta^+)\big(\frac{1}{9} + \frac{34}{27}\varepsilon + \frac{17}{27}\varepsilon\Delta\big), \end{aligned} \tag{4.49}$$

$$\begin{aligned} p_{N+1}(\Delta^+) = \frac{1}{3}p_N(\Delta^-) + \frac{2}{3}p_N(\Delta^+) - \frac{19}{27}\varepsilon p_N(\Delta^-) - \frac{71}{27}\varepsilon p_N(\Delta^+) \\ - \frac{\partial p_N}{\partial \Delta}(\Delta^-)\big(\frac{1}{9} + \frac{31}{27}\varepsilon + \frac{17}{27}\varepsilon\Delta\big) - \frac{\partial p_N}{\partial \Delta}(\Delta^+)\big(-\frac{1}{9} + \frac{38}{27}\varepsilon + \frac{64}{27}\varepsilon\Delta\big). \end{aligned} \tag{4.50}$$

Subtracting $p_N(\Delta^-)$ from (4.49) and $p_N(\Delta^+)$ from (4.50) we have

$$\begin{aligned} \frac{\partial p^-}{\partial t} = \frac{1}{3}(p^+ - p^-) - \frac{1}{9}(p^+ - p^-)_\Delta \\ - p^-_\Delta\big(\frac{32}{27}\varepsilon + \frac{64}{27}\varepsilon\Delta\big) - p^+_\Delta\big(\frac{34}{27}\varepsilon + \frac{17}{27}\varepsilon\Delta\big), \end{aligned} \tag{4.51}$$

$$\begin{aligned}\frac{\partial p^+}{\partial t} &= \frac{1}{3}(p^- - p^+) - \frac{1}{9}(p^- - p^+)_\Delta \\ &\quad - p^-_\Delta\big(\frac{31}{27}\varepsilon + \frac{17}{27}\varepsilon\Delta\big) - p^+_\Delta\big(\frac{38}{27}\varepsilon + \frac{64}{27}\varepsilon\Delta\big),\end{aligned} \tag{4.52}$$

where

$$\frac{\partial p^-}{\partial t} = p_{N+1}(\Delta^-) - p_N(\Delta^-), \qquad \frac{\partial p^+}{\partial t} = p_{N+1}(\Delta^+) - p_N(\Delta^+),$$

$$p^+ = p_N(\Delta^+), \qquad p^- = p_N(\Delta^-), \qquad (p^+)_\Delta = \frac{\partial p_N}{\partial \Delta}(\Delta^+), \qquad (p^-)_\Delta = \frac{\partial p_N}{\partial \Delta}(\Delta^-).$$

Adding equations (4.51) and (4.52), putting $p = p^+ + p^-$ and making the approximations $p^+ = \frac{p}{2} + \frac{\delta p}{2}, p^- = \frac{p}{2} - \frac{\delta p}{2}$ we have

$$\begin{aligned}\frac{\partial p}{\partial t} &= -\big(\frac{7}{3}\varepsilon + 3\varepsilon\Delta\big)(p^-)_\Delta - \big(\frac{8}{3}\varepsilon + 3\varepsilon\Delta\big)(p^+)_\Delta \\ &= -\frac{1}{2}\big(5\varepsilon + 6\varepsilon\Delta\big)p_\Delta - \frac{1}{6}\varepsilon(\delta p)_\Delta,\end{aligned} \tag{4.53}$$

where we have also approximated the derivatives by

$$p^+_\Delta = \frac{1}{2}p_\Delta + \frac{1}{2}(\delta p)_\Delta, \qquad p^-_\Delta = \frac{1}{2}p_\Delta - \frac{1}{2}(\delta p)_\Delta,$$

and δp is given by (4.48). Neglecting δp which is exponentially decreasing in time, equation (4.53) becomes a transport equation that can be solved using the characteristics method. The characteristics are the solution of

$$\frac{d\Delta}{dt} = \frac{5}{2}\varepsilon + 3\varepsilon\Delta \Rightarrow \Delta = \frac{5}{6}(\kappa\exp(3\varepsilon t) - 1),$$

and hence

$$p = (\exp(3\varepsilon t)p_0\big(\Delta - \frac{5}{6}(\exp(3\varepsilon t) - 1)\big) \simeq (\exp(3\varepsilon t)p_0(\Delta - \frac{5}{6}3\varepsilon t) = (\exp(3\varepsilon t)p_0(\Delta - \frac{5}{2}\varepsilon t), \tag{4.54}$$

since $\varepsilon t \ll 1$ and p_0 is the initial data.

Notice that the probability distribution shifts towards increasing values of Δ at a velocity $\frac{5}{2}\varepsilon$, (4.54). Hence, we conclude that shortest path (the one producing increase of Δ) is progressively reinforced. This result provides an analytical proof of the fact that both reinforcement and persistence are sufficient to produce shortest path selection at least for two ants. Remind that such shortest path selection was not possible with only one ant. In the next section we will consider the problem for larger number of ants.

4.2.4 Non-reinforced network with H ants

Now, we consider the three node network in figure (4.2) but for H ants. Our analysis with two ants without reinforcement lead, from formulas (4.38) and (4.39) to a system that can be written in the form

$$\begin{pmatrix} P(\Delta^-) \\ P(\Delta^+) \end{pmatrix}_{N+1} = A \begin{pmatrix} P(\Delta^-) \\ P(\Delta^+) \end{pmatrix}_N + B\frac{\partial}{\partial\Delta} \begin{pmatrix} P(\Delta^-) \\ P(\Delta^+) \end{pmatrix}_N$$

where

$$A = \begin{pmatrix} \frac{2}{3} & \frac{1}{3} \\ \frac{1}{3} & \frac{2}{3} \end{pmatrix},\ B = \begin{pmatrix} \frac{1}{9} & -\frac{1}{9} \\ -\frac{1}{9} & \frac{1}{9} \end{pmatrix}$$

and the states $\mathcal{A}^-$ and $\mathcal{A}^+$ correspond to 1 or 2 ants in the nest respectively. Notice that the elements of both the rows and columns of matrix A sum one and they are positive (since they correspond to probabilities). Moreover, matrix A is symmetric. These properties are also verified when considering H ants and, therefore, H possible states $\mathcal{A}^1, \mathcal{A}^2, \ldots, \mathcal{A}^H$ corresponding to $1, 2, \ldots, H$ ants at the nest respectively. We can also write the system

$$\begin{pmatrix} P(\Delta^1) \\ P(\Delta^2) \\ \vdots \\ P(\Delta^H) \end{pmatrix}_{N+1} = A \begin{pmatrix} P(\Delta^1) \\ P(\Delta^2) \\ \vdots \\ P(\Delta^H) \end{pmatrix}_N + B\frac{\partial}{\partial\Delta} \begin{pmatrix} P(\Delta^1) \\ P(\Delta^2) \\ \vdots \\ P(\Delta^H) \end{pmatrix}_N \tag{4.55}$$

with A a symmetric matrix with positive entries such that any row and column sums one. This characterizes A as an stochastic matrix which is, moreover, symmetric. The Perron-Frobenius theorem implies then that there exists an eigenvalue $\lambda = 1$ and all other eigenvalues λ are such that $|\lambda| < 1$. Since the matrix is symmetric, such eigenvalues are real. The eigenvector corresponding to the eigenvalue 1, called the Perron-Frobenius eigenvector, is $(1, 1, \ldots, 1)^T$. This implies that $A = Q^{-1}DQ$ with D the matrix of eigenvalues. The lack of reinforcement implies that the probabilities $P(\Delta^1), P(\Delta^2), \ldots, P(\Delta^H)$ are indeed independent of Δ and therefore we will denote them as $P_1, P_2, \ldots, P_H$. For all these reasons, (4.55) can be written in the form

$$\widetilde{P}_{N+1} = D\widetilde{P}_N \tag{4.56}$$

where $\widetilde{P}_{N+1} = Q\,(P_1, P_2, \ldots, P_H)^T_{N+1}$.

Notice that (4.56) is the discretized version of the following system of equations

$$\frac{\partial\widetilde{P}}{\partial t} = (D - I)\widetilde{P}, \tag{4.57}$$

with solution $\widetilde{P}(t) = \exp((D-I)t)\widetilde{P}_0$. Notice that all components of $D - I$, except for the first

one (corresponding to the Perron-Frobenius eigenvalue $\lambda = 1$ for A) are negative and hence

$$e^{(D-I)t} = \begin{pmatrix} 1 & 0 & \cdots & 0 \\ 0 & e^{(\lambda_2 - 1)t} & 0 & \vdots \\ \vdots & 0 & \ddots & 0 \\ 0 & \cdots & 0 & e^{(\lambda_H - 1)t} \end{pmatrix}$$

with $\lambda_j < 1$, $j = 2, \ldots, H$. The eigenvectors e_j corresponding to eigenvalues λ_j , $j = 2, ..., H$, are orthogonal to the Perron-Frobenius eigenvector. Hence the vectors with all entries equal to 0 except for a 1 at position k and a -1 at position l, which are orthogonal to the vector $(1, 1, ..., 1)^T$, are linear combinations of the eigenvectors e_j, $j > 1$. This implies that

$$|P_{k,N} - P_{l,N}| \leq Ce^{-\inf_{j>1}\{|(\lambda_j - 1)|\}t} \text{ for all } k, l. \tag{4.58}$$

Since the probability distribution converge to equilibrium exponentially fast, we will not make distinction among different states in what follows and we will merely write equations for

$$p(N) = \sum_{j=1}^{H} P_j$$

or, in other words, for the component of the probability vector $(P_1, P_2, \ldots, P_H)_{N+1}^T$ on the Perron-Frobenius eigenstate (all the other components converge exponentially fast to zero by (4.58)).

4.2.5 Reinforced network with H ants

Finally, we consider the three node network in figure 3.8 right with reinforcement and for H ants. As in the case for two ants, we can decompose the evolution as a sequence of syllables starting and ending in a state $\mathcal{A}$ at which all ants are at the nest or the food source. All the possible syllables are of the form $\mathcal{AA}$, $\mathcal{ABA}$ and $\mathcal{AC}^(j)\mathcal{A}$, where the state $\mathcal{B}$ consists of all ants in the node that is not nest nor food source and state $\mathcal{C}$ can be any possible combination of n_1 ants at the nest or food source and n_2 ants at the other vertex. Since there are arbitrary long sequences of $\mathcal{C}$ states we will denote by $n_1^(1), n_1^(2), \ldots$ the number of ants that are at the nest or the food source at each of the $\mathcal{C}$ states of the sequence. Similarly, we denote by $n_2^(1), n_2^(2), \ldots$ the number of ants that are not at the nest nor at the food source. Notice then that $n_1^(j) + n_2^(j) = H$. Following the same steps as in the case for two ants, we can then write

the following equation for the probability:

$$\begin{aligned} & p(\Delta, N+1) \\ = \quad & \frac{(1+\varepsilon\Delta)^H}{2^H} p(\Delta - H, N) + \frac{(1-\varepsilon\Delta)^H}{2^H} p(\Delta + H, N) \\ & + \sum \frac{1}{2^{(S+1)H-x}} \left(\prod_{j=1}^{S+1} \binom{H - n_2^{(j-1)}}{H - (n_2^{(j)} + n_2^{(j-1)})} \right) \\ & \left(1 + \varepsilon \mathcal{Q}^H_{\{S, n_2^{(1)}, \ldots, n_2^{(S)}\}}(\Delta)\right) p(\Delta - ((S+1)H - 3x), N), \end{aligned} \tag{4.59}$$

where the sum goes over all S from 1 to ∞ and over all the $S-$uplas $\left\{n_2^{(1)}, n_2^{(2)}, \ldots, n_2^{(S)}\right\}$ such that $1 \leq n_2^{(k)} < H$, $n_2^{(k)} + n_2^{(k+1)} \leq H, \forall k \geq 1$, $x = \sum_{k=1}^{S} n_2^{(k)}$ and

$$\begin{aligned} & \mathcal{Q}^H_{\{S, n_2^{(1)}, \ldots, n_2^{(S)}\}}(\Delta) \\ & = (n_1^{(1)} - n_2^{(1)})(\Delta - (S+1)H + 3x) \\ & + \sum_{j=1}^{S} \left((n_1^{(j)} - 2n_2^{(j+1)}) \Big(\sum_{k=1}^{j} (n_1^{(k-1)} - n_2^{(k)}) \right. \\ & \left. - \frac{1}{2} \left(\sum_{k=1}^{j} n_2^{(k)} + n_2^{(k-1)} \right) + (\Delta - (S+1)H + 3x) \Big) \right). \end{aligned} \tag{4.60}$$

Applying Taylor's expansion in (4.59) and using the relations

$$\frac{2}{2^H} + \sum \frac{1}{2^{(S+1)H-x}} \left(\prod_{j=1}^{S+1} \binom{H - n_2^{(j-1)}}{H - (n_2^{(j)} + n_2^{(j-1)})} \right) = 1, \tag{4.61}$$

$$\sum \frac{(S+1)H - 3x}{2^{(S+1)H-x}} \left(\prod_{j=1}^{S+1} \binom{H - n_2^{(j-1)}}{H - (n_2^{(j)} + n_2^{(j-1)})} \right) = 0, \tag{4.62}$$

(see remark at the end of this chapter for a proof of this formulas) we arrive, keeping up to $\mathcal{O}(\varepsilon)$ terms, at the equation

$$p(\Delta, N+1) = p(\Delta, N) + c(\Delta)\varepsilon \frac{\partial p}{\partial \Delta}(\Delta, N), \tag{4.63}$$

where

$$c(\Delta) = -\sum \frac{(S+1)H - 3x}{2^{(S+1)H-x}} \left(\prod_{j=1}^{S+1} \binom{H - n_2^{(j-1)}}{H - (n_2^{(j)} + n_2^{(j-1)})} \right) \mathcal{Q}^H_{\{S, n_2^{(1)}, \ldots, n_2^{(S)}\}}(\Delta).$$

Equation (4.63) is a discretized version of the transport equation

$$\frac{\partial p(\Delta, t)}{\partial t} = c\varepsilon \frac{\partial p}{\partial \Delta}(\Delta, t).$$

The constant $c(0)$ is computed numerically from formulas (4.59) and (4.60) using Fortran. Since we are considering the early times when the maximum of the probability distribution is close to $\Delta = 0$, it is the convection produced by $c(0)$ what breaks the symmetry and shifts the probability distribution towards increasing/decreasing values of Δ at a velocity $c(0)$ provided it is strictly positive/negative. Our numerical computations yield the values for the velocity $c(0) = 11.2476$ for 3 ants and $c(0) = 28.2320$ for 4 ants. Hence, the shortest path will be progressively reinforced and this will occur at a velocity that increases with the number of ants. The convergence is shown in tables (4.1) and (4.2) and as well as figure (4.4) at the end of the chapter.

The limit $\varepsilon = 0$

By considering $\varepsilon = 0$ in (4.59) we return to the problem without reinforcement and the equation for the probability is:

$$\begin{aligned} p(\Delta, N+1) &= \frac{1}{2^H} p(\Delta - H, N) + \frac{1}{2^H} p(\Delta + H, N) \\ &+ \sum \frac{1}{2^{(S+1)H-x}} \left(\prod_{j=1}^{S+1} \binom{H - n_2^{(j-1)}}{H - (n_2^{(j)} + n_2^{(j-1)})} \right) p(\Delta - ((S+1)H - 3x), N) \end{aligned} \tag{4.64}$$

where the sum goes over all S from 1 to ∞ and over all the $S-$uplas $\left\{ n_2^{(1)}, n_2^{(2)}, \ldots, n_2^{(S)} \right\}$ such that $1 \leq n_2^{(k)} < H$ and $n_2^{(k)} + n_2^{(k+1)} \leq H, \forall k \geq 1$ and $x = \sum_{k=1}^{S} n_2^{(k)}$. We suppose that $n_2^{(0)} = n_2^{(S+1)} = 0$.

Applying Taylor's expansion in (4.64) we have that

$$\begin{aligned} p(\Delta, N+1) &= \frac{1}{2^H} p(\Delta, N) + \frac{1}{2^H} p(\Delta, N) \\ &+ \sum \frac{1}{2^{(S+1)H-x}} \left(\prod_{j=1}^{S+1} \binom{H - n_2^{(j-1)}}{H - (n_2^{(j)} + n_2^{(j-1)})} \right) p(\Delta, N) \\ &- \left[\sum \frac{(S+1)H - 3x}{2^{(S+1)H-x}} \left(\prod_{j=1}^{S+1} \binom{H - n_2^{(j-1)}}{H - (n_2^{(j)} + n_2^{(j-1)})} \right) \right] \frac{\partial p}{\partial \Delta}(\Delta, N) + \mathcal{O}(\Delta^2) \end{aligned} \tag{4.65}$$

As a final remark, we note that without reinforcement the convection velocity vanishes by formula (4.62), $p(\Delta, N+1) = p(\Delta, N)$ by formula (4.61), and hence no path selection takes place. Formula (4.61) follows from the fact that the sum of all the probabilities must to be one and formula (4.62) must necessarily be true due to the following:

1. If there is not reinforcement, the movement of just one ant does not affect the others.

2. If the initial position for all ants is at node 1, we have with probability 1 that all the ants will be at node 1 at a subsequent time t.

3. The mean Δ change produced by an ant with initial position at node 1 and coming for the first time also to node 1 is

$$\begin{aligned}\langle \delta\Delta \rangle &= 2p_{1,2,1} + (-2)p_{1,3,2,3,1} + 0p_{1,3,2,1} + 0p_{1,2,3,1} \\ &= 2\frac{1}{4} + (-2)\frac{1}{4} + 0 + 0 = 0.\end{aligned}$$

When all the ants meet at node 1, each ant has done a certain number of elementary paths: $(1,2,1), (1,3,2,3,1), (1,3,2,1), (1,2,3,1)$. Since the mean change $\langle \delta\Delta \rangle = 0$, then (4.62) must be true.

The computational time grows exponentially with H so that we can only compute a few values of S when $H < 5$. Nevertheless, the tendency to reach larger values of $c(0)$ can be clearly appreciated at least for $H = 5, 6, 7$.

As a result of analytical results presented above, we conclude that reinforcement, persistence and a relatively large (in fact, more than one) number of ants are necessary for shortest selection in our three node network. The effect is stronger increasing number of ants (the convergence is exponentially fast).

Table 4.1: Values for 3 ants (S is the number of summands)

S=1,. . . ,10	**S=11,. . . ,20**	**S=21,. . . ,30**	**S=31,. . . ,39**
-1.68750000000000	6.34836387634277	10.7769719472562	11.2217437880206
-2.53125000000000	7.23112392425537	10.8874437563791	11.2290148067098
-2.32031250000000	7.98751652240753	10.9732685254639	11.2344497060999
-1.79296875000000	8.62515860795975	11.0395933880391	11.2385015073743
-0.777832031250000	9.15521809458733	11.0905997799873	11.2415147184009
0.402099609375000	9.59050320088863	11.1296495417419	11.2438
1.69079589843750	9.94414290413260	11.1594210533052	11.2455
2.97784423828125	10.2287268061191	11.1820310238697	11.2467
4.20721435546875	10.4557968000881	11.1991402542278	11.2476
5.33770751953125	10.6355926024262	11.2120434019826	

Table 4.2: Values for 4 ants (S is the number of summands)

S=1,...,10	**S=11,...,20**	**S=21,...,25**
-2.92187500000000	4.50025232967164	24.1563390572839
-5.59375000000000	6.94225190742145	25.3594091989049
-6.54614257812500	9.34652319722341	26.4334158012737
-7.22521972656250	11.6709826334469	27.3877
-6.77570724487305	13.8851470442689	28.2320
-5.84203720092773	15.9680644072455	
-4.31725507974625	17.9067495095693	
-2.43186268210411	19.6946205757634	
-0.262493065558374	21.3301454339337	
2.07489867508411	22.8156550080546	

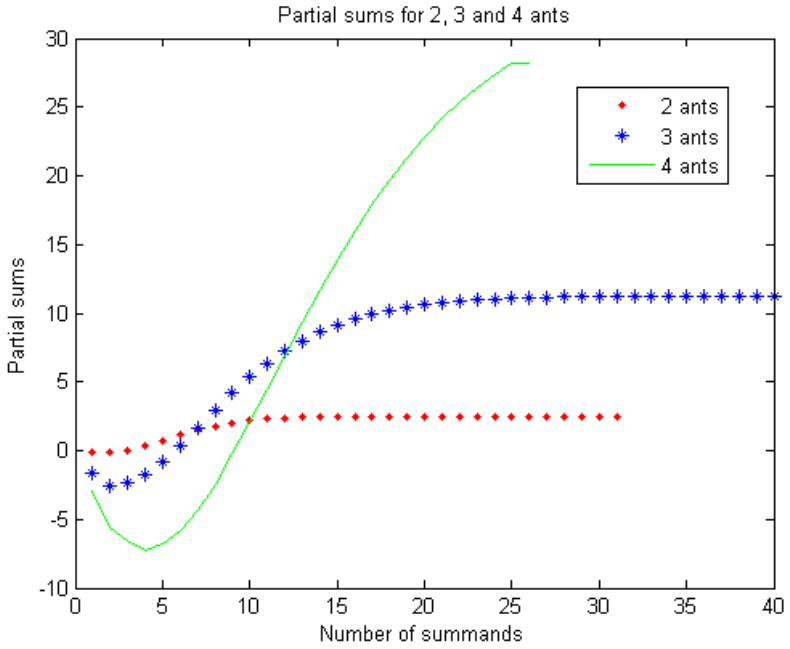

Figure 4.4: Partial sums for the velocity $c(0)$ as a function of the number of summands for $H = 2, 3, 4$ ants.

4.3 Conclusions

We have presented a model for ants to simulate their behavior when foraging. It is well know that social insects, as for example ants, leave a trail to coordinate the group and to communicate to each other. This pheromone plays an important role to recruit the individuals and reinforce the shortest path between nest and food source. In this chapter, we have proved:

- In order for the ants to follow the geodesic path in a two or three node network, it is necessary not only to invoke the pheromone-induced reinforcement but also to have a directionality constraint (persistence of motion). Such constraint is so that ants prefer to maintain their direction of motion to turn back and return.

- More than one ant is also needed to reinforce the geodesic path, with the velocity of reinforcement increasing fast with the number of ants.

- The possibility of choosing a path of minimal length requires super-linearity ($\alpha > 1$) in the law for the reinforcement.

- It is expected that the combined effect of reinforcement and persistence is able to induce the formation of ant trails of minimal length not only in simple networks, but also in more complex networks, in the plane or in surfaces of general topology. This is the subject of the next chapters in this thesis.

Bibliography

[1] J. L. Deneubourg, S. Aron, S. Goss and J. M. Pasteels, The Self-Organizing Exploratory Pattern of the Argentine Ant. J. Insect Behav. **3(2)**, (1990), 159-168.

[2] K. Kang, A. Stevens and J. J. L. Velazquez, Qualitative behavior of a Keller-Segel model with non-diffusive memory. Communications in PDE **35(2)**, (2010), 245-274.

[3] S. Garnier, S. Guérécheau, M. Combe, V. Fourcassié and G. Theraulaz, Path selection and foraging efficiency in Argentine ant transport networks. Behav. Ecol. Sociobiol. **63**, (2009), 1167-1179.

Chapter 5

Simulations in complex networks

Goals of this chapter

- Make simulations for complex networks as an eight node network, polarized and non-polarized mazes, regular lattices and non regular lattices.

5.1 Simulations in complex networks

In this section we simulate the behavior of ants when foraging from nest to food source in different complex networks: network with two triangles (appeared in [1]) and with several hexagons (appeared in [2]). Furthermore, we also study the case of some regular lattices: triangle regular mesh, square regular mesh and hexagonal regular mesh. Finally, we consider some irregular meshes. We show that for some symmetrical regular lattices (triangular and square) ants do not always follow the geodesic path. On the other hand, for a general mesh, the geodesic path is selected in most cases.

We have studied numerically the collective behavior of a variable number of ants in complex networks in the form of graphs with E edges, $w_1, w_2, \ldots, w_E$. The experiments are done using a Monte Carlo method with the random number generator *binornd* from MATLAB. This random number generator returns numbers from a binomial distribution with parameters N (number of Yes/No experiments) and p (probability of success). We do a certain number of simulations for a different number of time steps and for a number H of ants. For a general complex network with reinforcement we have that the probability of moving from node i to node j coming from node v at step t is:

$$p_{i,j}^{v}(t) = \frac{(\theta_{ij}^{v})^{\beta}(k+\omega_{ij}(t))^{\alpha}}{\sum_{\ell=1}^{deg(i)}(\theta_{i\ell}^{v})^{\beta}(k+\omega_{i\ell}(t))^{\alpha}},$$

where $\omega_{i\ell}(t)$ are the quantities of pheromone at each incident link $W_{i\ell}$ to node i at time t, $\theta^v_{i\ell}$ is the angle coefficient between the link W_{vi} (the previous link of the ant) and the link $W_{i\ell}$ (the following link), $deg(i)$ is the degree of node i, k is a positive constant, $\alpha \geq 1$ is the exponent of the non-linearity and β is the angle exponent. The value of $\omega_{i\ell}(t)$ is increased in one unit each time the ant moves along the edge $W_{i\ell}$, representing the deposit of pheromone by the ant. The angle coefficients are computed as $\theta^v_{i\ell}(\pi - \widehat{W_{vi}W_{i\ell}})/\pi$ and they are equal to 1 at the food source and the nest.

In the numerical experiments, we count the number of times that the links of the path of minimal length (that is, of minimum number of links) are run by ants and compute the ratio between this number and the total number of steps taken by all the ants. This number will be called *the selection of shortest path ratio* and will be denoted by r.

5.2 Simulations for an eight node network

We consider a network with two triangles as in figures 5.1 and 5.2. It is based on the network appeared in [1]. This network has the same directionality constraints as the triangle network appeared in chapter 3 but for each triangle. That is, if the ant is at node 1 it must move to node 2; if it is at node 2, it can move to nodes 3 or 4 if it comes from node 1, whereas if it comes from node 4 it can move to nodes 3 or 1 and if it comes from node 3 it can move to nodes 1 or 4. If the ant is at node 3 coming from node 2 it must move to node 4, whereas if it is at node 3 coming from node 4 it must move to node 2. If the ant is at node 4 coming from node 2 it can move to nodes 3 or 5, whereas if the preceding node is 3 it can move to nodes 2 or 5 and if the preceding node is 5 it can move to nodes 2 or 3. Similarly, for the symmetric subnetwork.

We employ different MATLAB program simulations to show:

a) Temporal evolution graphics to show the number of times several ants go through the geodesic path without taking into account the angles. We conclude that reinforcement and directionality constraint for this network are not enough to reproduce ant's behavior (see figure 5.3).

b) Temporal evolution graphics to show the number of times several ants go through the geodesic path taking into account the angles between the links. We conclude that reinforcement, angles and directionality constraint for this network are enough to reproduce ant's behavior (figures 5.4,5.5). It is showed that even if we increase the number of ants the convergence is not much faster but the dispersion decreases. Moreover, the convergence to the geodesic path is exponentially fast, ratio $\simeq 0.3329 \times e^{-2.4\times 10^{-3}t}$.

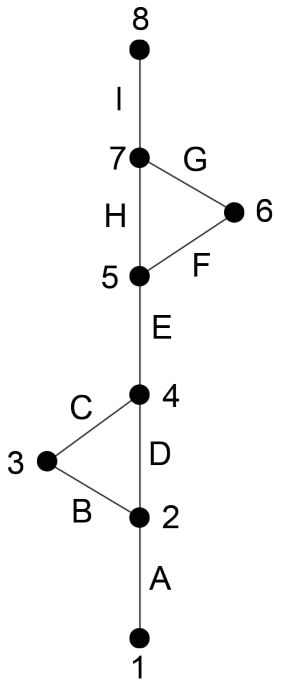

Figure 5.1: Network with two triangles.

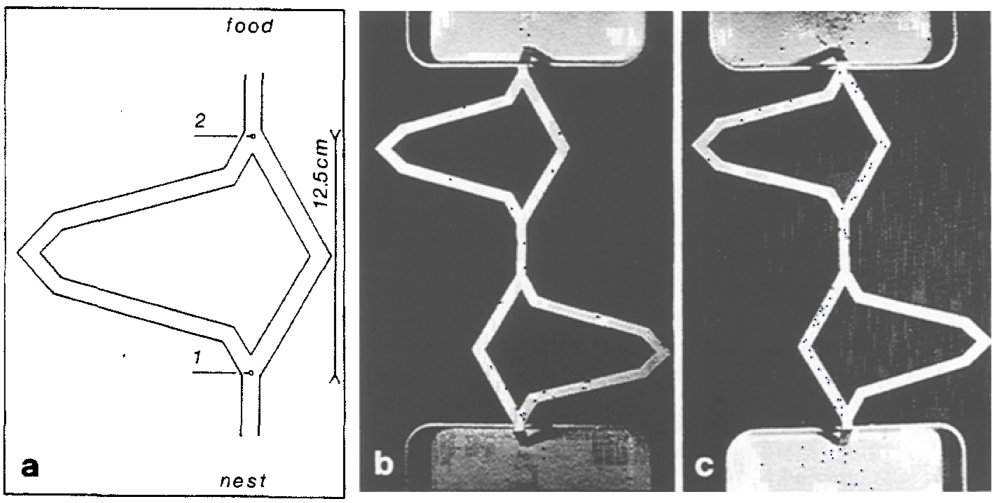

Figure 5.2: Network employed in the experiment. Figure from [1].

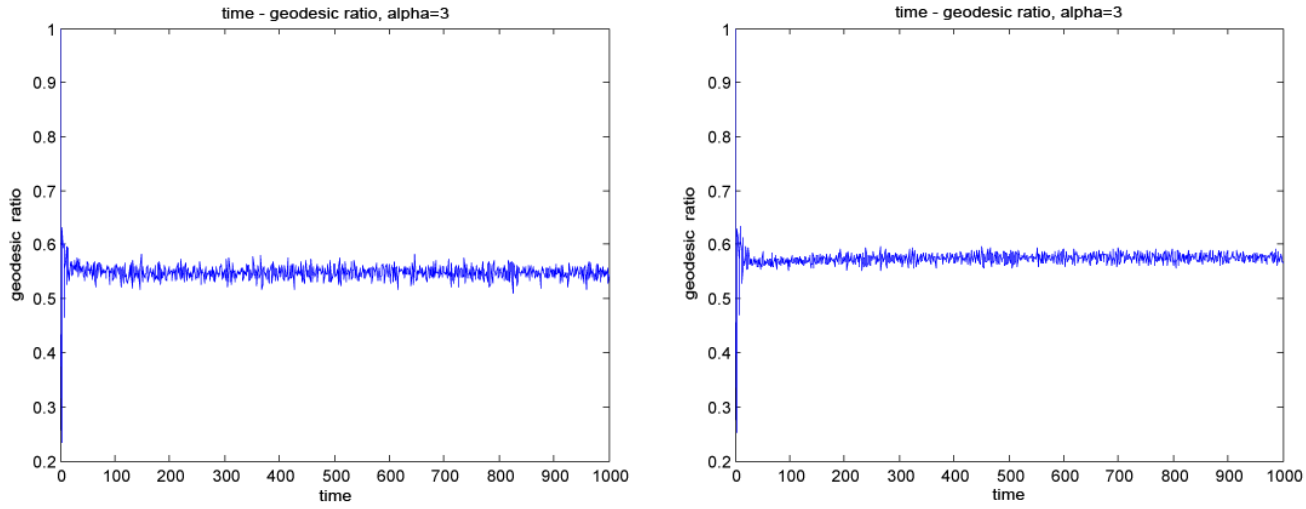

Figure 5.3: Temporal evolution for the selection of shortest path ratio r, 100 ants (left figure), 50 ants (right figure), $k = 20$; network without weighted angles. The experiment is repeated 100 times.

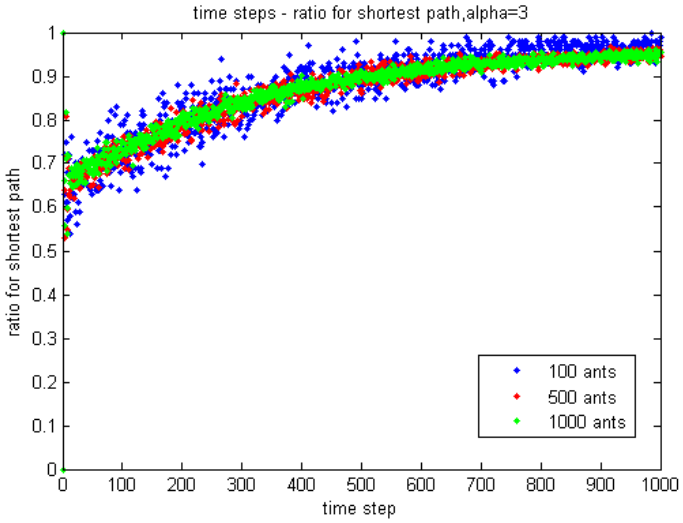

Figure 5.4: Temporal evolution for r, $\alpha = 3$, $k = 20$; 100 ants (blue color), 500 ants (red color), 1000 ants (green color) and 1000 time steps; network with weighted angles. If we increase the number of ants, the convergence is not much faster but the dispersion decreases.

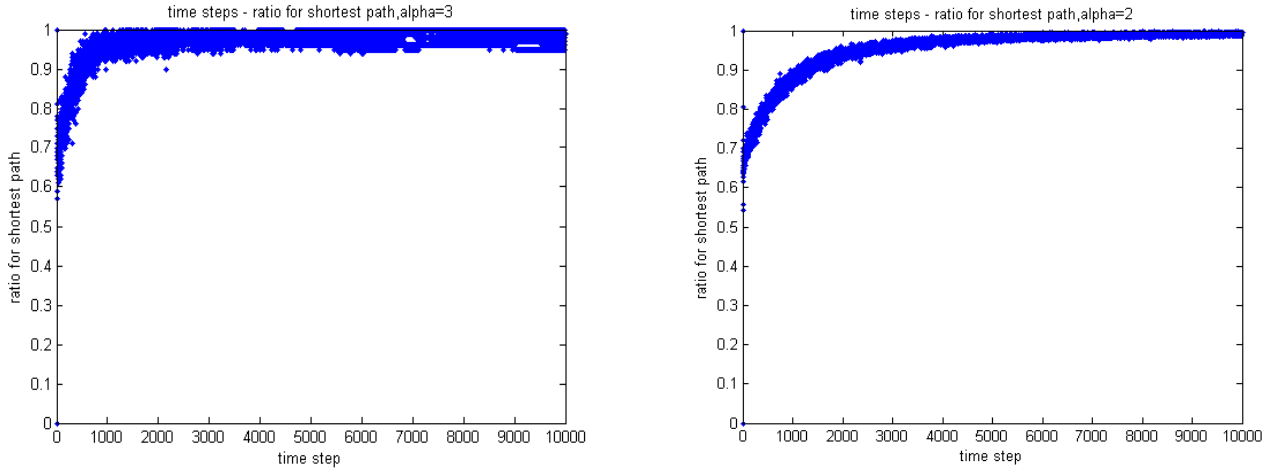

Figure 5.5: Temporal evolution for r, $k = 20$, 10000 time steps; 100 ants, $\alpha = 3$ (left figure) and 1000 ants, $\alpha = 2$ (right figure); network with weighted angles.

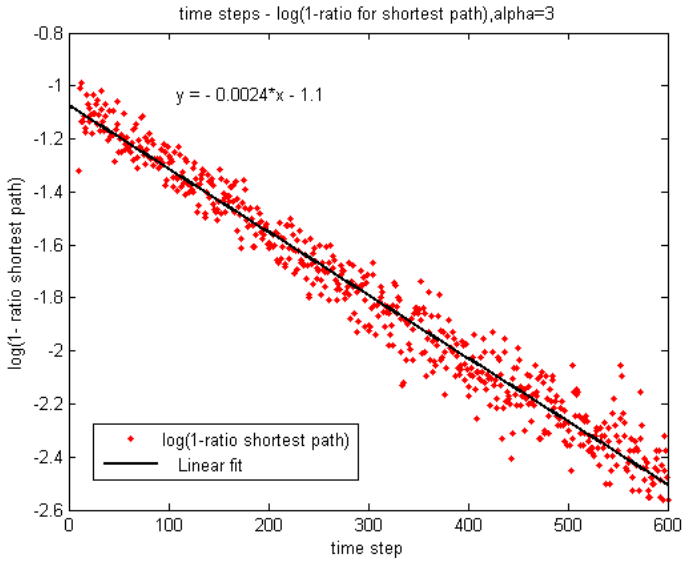

Figure 5.6: Temporal evolution of $\log(1 - r)$ for $k = 20$, 600 time steps; 1000 ants, $\alpha = 3$; network with weighted angles. The convergence to the geodesic path is exponentially fast: $r \simeq 1 - 0.3329 \times e^{-2.4\times 10^{-3}t}$.

5.3 Simulations for polarized and non-polarized mazes

We consider next a network with several hexagons as in figure 5.7. It is based on the network appeared in the study of [2]. We do different experiments for the polarized maze (P-Maze) and for the non-polarized maze (NP-maze). In the P-maze ants go from nest (N) to source food (A) with an angle of 30 degrees from the horizontal (we also consider the cases of 20 and

10 degrees). Hence, when coming back from the food to the nest there is an asymmetrical bifurcation (one exit branch deviates by 30 degrees while the other deviates by 120 degrees from the access branch for the first case; the exit branch deviates by 20 degrees while the other deviates by 140 from the access branch for the second case; the exit branch deviates by 10 degrees while the other deviates by 160 degrees for the third case). On the other hand, in the NP-maze, the angle between the three branches is always the same, 60 degrees.

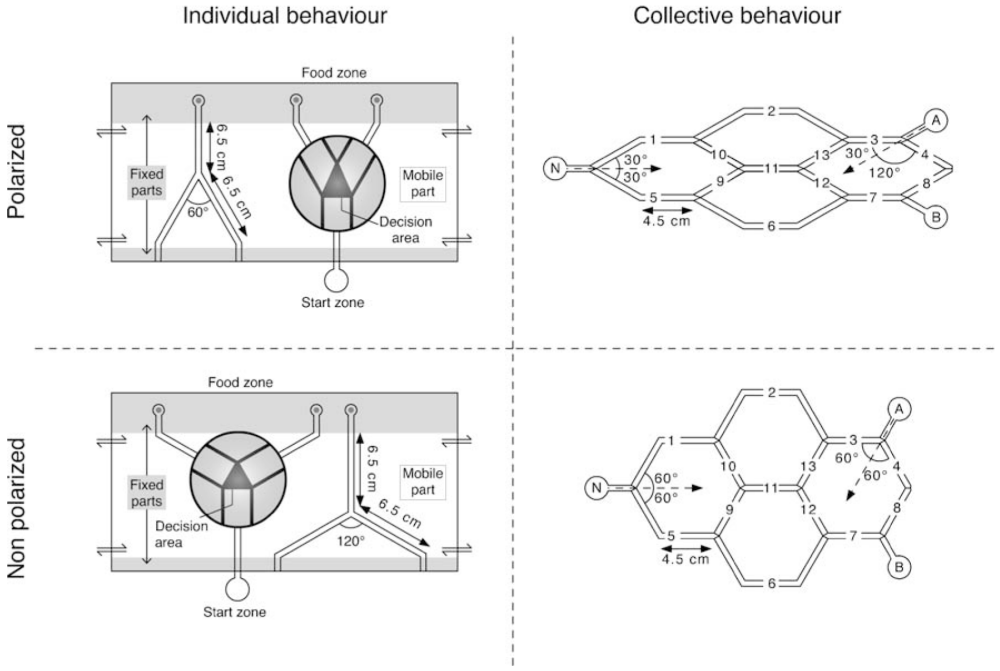

Figure 5.7: Schematic representation of the experimental setups. Figure from [2].

We implement different MATLAB program simulations to show:

a) Temporal evolution graphics to show the number of times several ants go through one of the geodesic path in the NP-maze. Temporal evolution graphics to show the number of times several ants go through one of the geodesic path in the P-maze of 30 degrees. We conclude that ants choose less times the geodesic path in the NP-maze than in the P-maze (figure 5.8).

b) Temporal evolution graphics to show the number of times several ants go through one of the geodesic path in the P-maze of 20 and 10 degrees. We conclude that ants choose more or less the same number of times the geodesic path in the P-maze of 30 degrees as in the 20 or 10 degrees (figure 5.9).

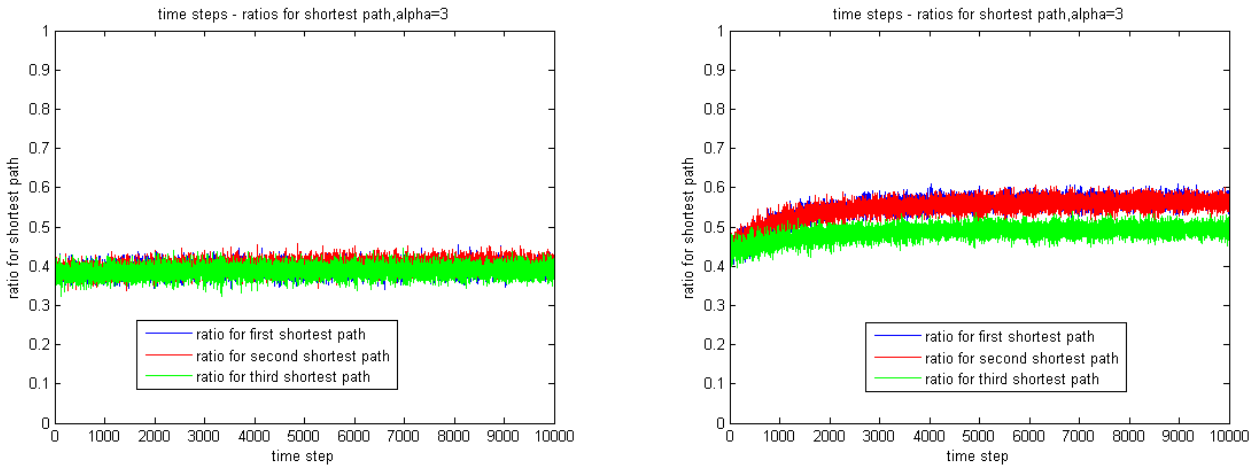

Figure 5.8: Temporal evolution for r, 10000 ants, $k = 20$, $\alpha = 3$, NP-maze (left figure), P-maze (right figure).

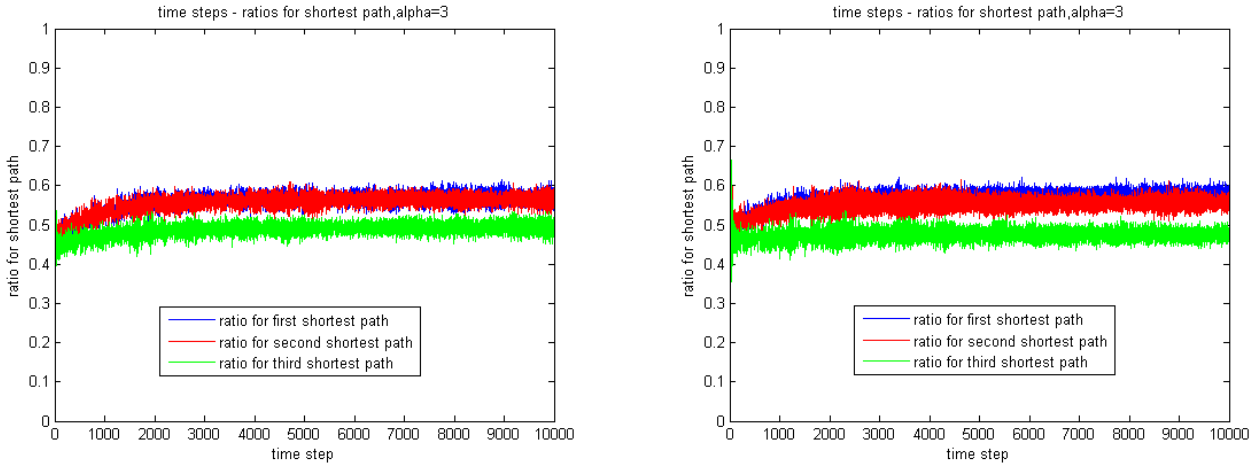

Figure 5.9: Temporal evolution for r, 10000 ants, $k = 20$, $\alpha = 3$, P-maze of 20 degrees (left figure), P-maze of 10 degrees (right figure).

5.4 Simulations for some regular lattices

When ants move in a regular lattice, the effects of reinforcement and persistence make enter into competition as demonstrated in section 5.3. The reason is that, in general, the shortest path between two vertices may require the ants to turn a large angle at some intermediate vertex. Taking such a turn, instead of another possible turn with a smaller angle, might be difficult due to the persistence effect. This phenomenon is evident when considering large regular lattices as we will demonstrate in this section.

5.4.1 Simulations for square regular lattice

Now we consider the case of a square mesh in a (10×10) lattice as in figure 5.10. We impose periodical conditions in the boundaries. To do so we create "ghost" links in the boundaries to have the geometry as in a torus.

We do different simulations to show:

a) Ants usually move through the boundaries, even if the nest or food are in the middle of the lattice. To show that we do Monte Carlo simulations of several ants and we calculate the average number of times they follow one path. We plot the paths that are followed most times by ants.

b) Ants usually reinforce straight lines even though they do not connect nest and food.

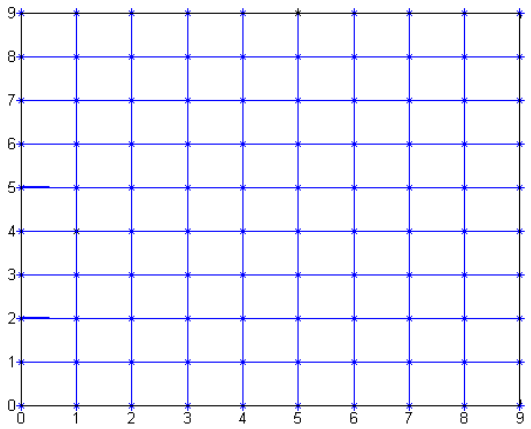

Figure 5.10: Regular squared lattice network.

5.4.2 Simulations for triangular regular lattice

Next, we consider the case of a triangular mesh in a (10×10) lattice as in figure 5.11. We impose periodical conditions in the boundaries. To do so we create "ghost" links in the boundaries to have the geometry as in a torus.

We do different simulations to show:

a) Ants usually reinforce straight lines even tough they do not connect nest and food (they are like periodical orbits). To show that we do Monte Carlo simulations of several ants and we calculate the average number of times they follow one path. We plot in red the paths between nest and food that are followed most times (see figure 5.12).

b) The shortest path is not always selected.

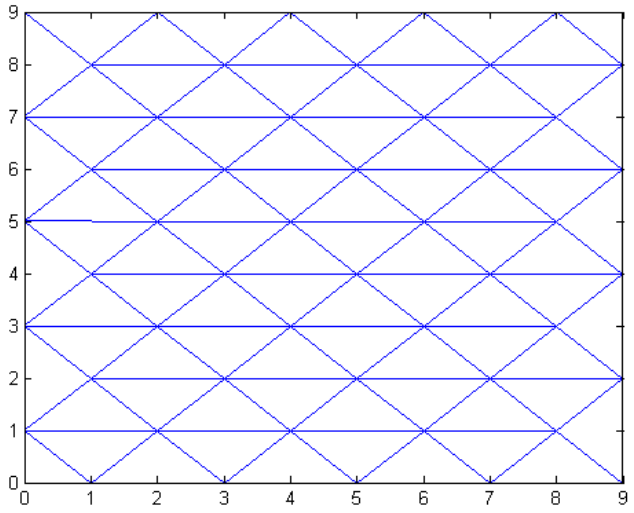

Figure 5.11: Regular triangular lattice network.

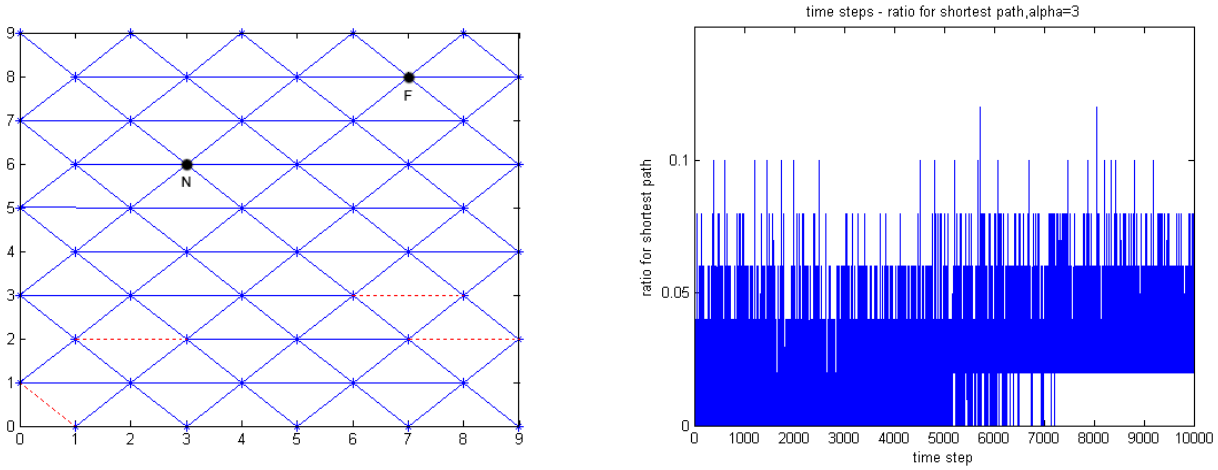

Figure 5.12: Most reinforced paths (in red dashed lines, left figure) and temporal evolution for r (right figure), 10000 time steps, $k = 20$, $\alpha = 3$, $\beta = 0.8$ and 50 ants. Nest at node N and food source at node F.

5.4.3 Simulations for hexagonal regular lattice

Now we consider the case of an hexagonal mesh in a (11×10) lattice as in figure 5.13. We work with polarized mazes of 30 degrees, with polarized mazes of 20 degrees and with non polarized mazes as in the previous hexagonal case. Indeed, we impose periodical conditions in the boundaries by creating "ghost" links in the boundaries.

We do different simulations to show:

a) Ants usually reinforce straight lines between the nest and food. To show that we do Monte Carlo simulations of several ants and we calculate the average number of times they follow one path. We plot in red the paths between nest and food that are followed most times. Furthermore, we plot temporal evolution graphs with the number of times that edges belonging to a geodesic path are selected with respect to the total number of steps taken by all the ants (see figure 5.14). Observe the clear tendency to increase, implying that a majority of ants is tending to follow the geodesic path.

b) The shortest path is selected in most cases. The number of times a geodesic path is selected is larger for the cases of polarized mazes. The more polarized is the mesh the more times is selected a geodesic path (see figure 5.14).

c) Even if the nest and food are separated by a certain distance, ants choose straight lines between the nest and food and the shortest path is selected many times (see figures 5.15, 5.16).

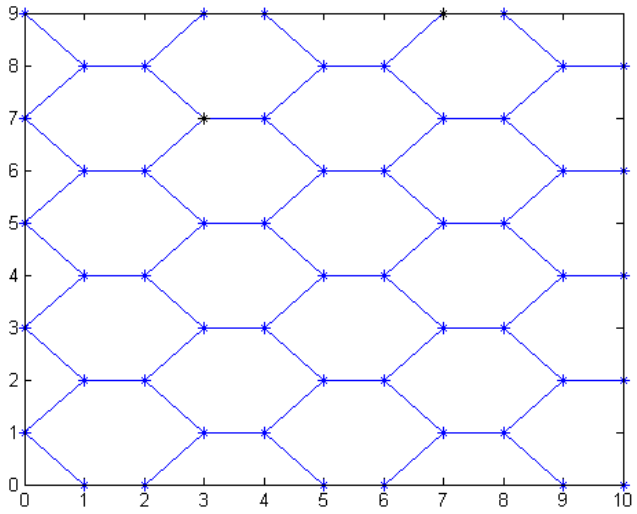

Figure 5.13: Regular hexagonal lattice network.

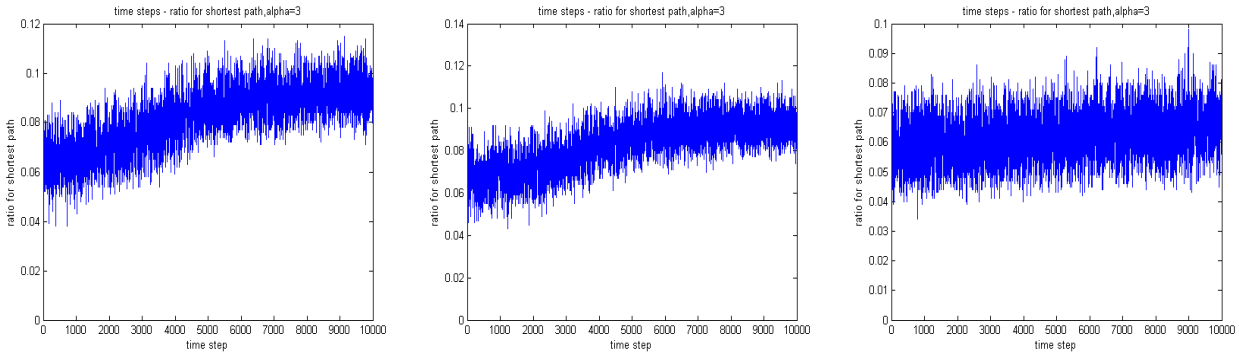

Figure 5.14: Temporal evolution for r plots for polarized maze (left, angle= 20°), more polarized maze (center, angle= 30°) and non polarized maze (right), 10000 time steps, $k = 20$, $\alpha = 3$, $\beta = 0.8$ and 1000 ants.

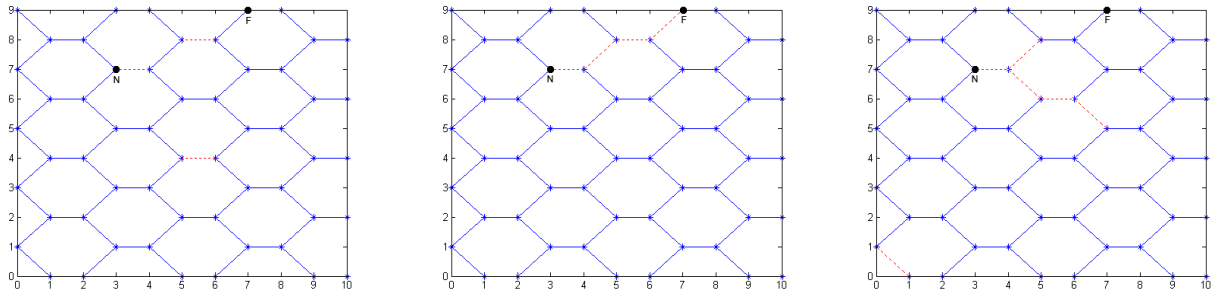

Figure 5.15: Most reinforced paths (in red dashed lines) for polarized maze (left, angle= 20°), more polarized maze (center, angle= 30°) and non polarized maze (right), 10000 time steps, $k = 20$, $\alpha = 3$, $\beta = 0.8$ and 50 ants. Nest at node N and food source at node F.

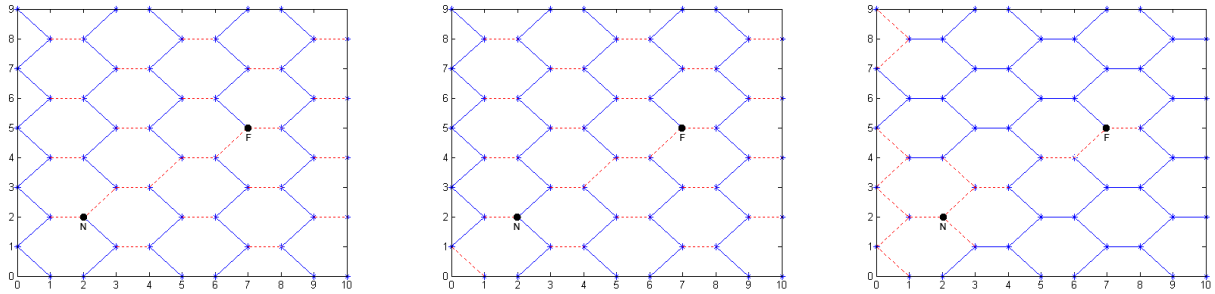

Figure 5.16: Most reinforced paths (in red dashed lines) for polarized maze (left, angle= 20°), more polarized maze (center, angle= 30°) and non polarized maze (right), 10000 time steps, $k = 20$, $\alpha = 3$, $\beta = 0.8$ and 1000 ants. Nest at node N and food source at node F.

5.5 Simulations for some non-regular lattices

We use the pdetool from Matlab to create an irregular mesh in a (10×10) lattice as in figure 5.17. We impose periodical conditions in the boundaries. To do so we create "ghost" links in the boundaries to have the geometry as in a torus.

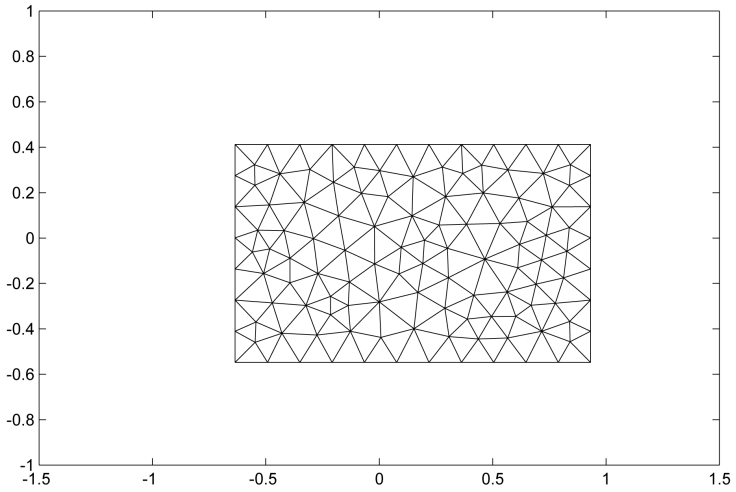

Figure 5.17: Irregular mesh in a squared lattice network.

5.5.1 Non-bounced conditions

We do different simulations to show:

a) Ants usually move through the boundaries, even if the nest or food are in the middle of the lattice. They also reinforce straight lines even though they do not connect nest and food. To show that we do Monte Carlo simulations of several ants and we calculate the average number of times they follow one path (see figure 5.18). We plot the most passed paths (see figure 5.19).

b) Several ants follow the shortest path between nest and food.

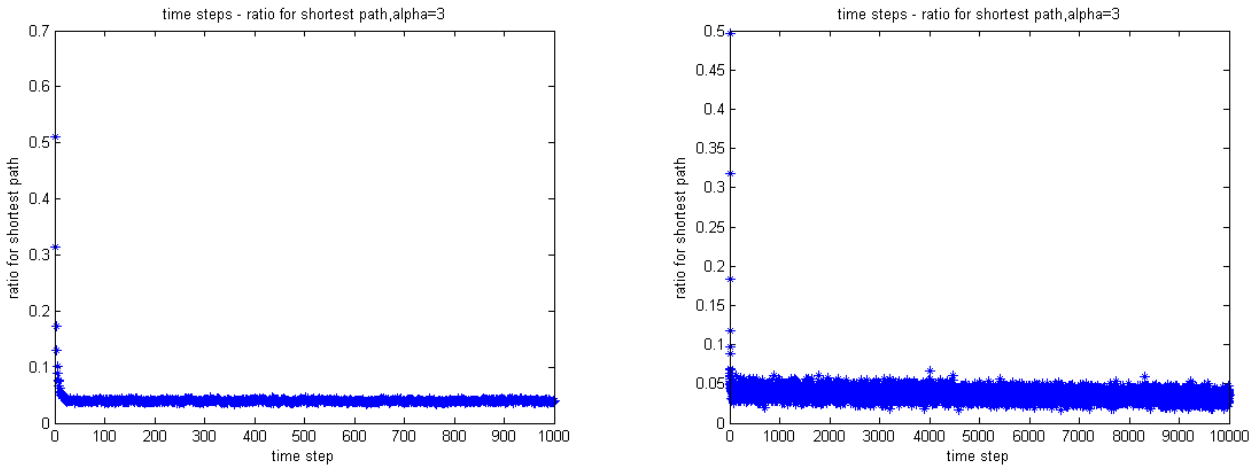

Figure 5.18: Temporal evolutions plots, $k = 20$, $\alpha = 3$, $\beta = 0.8$; 1000 time steps and 10000 ants (left), and 10000 time steps and 1000 ants (right).

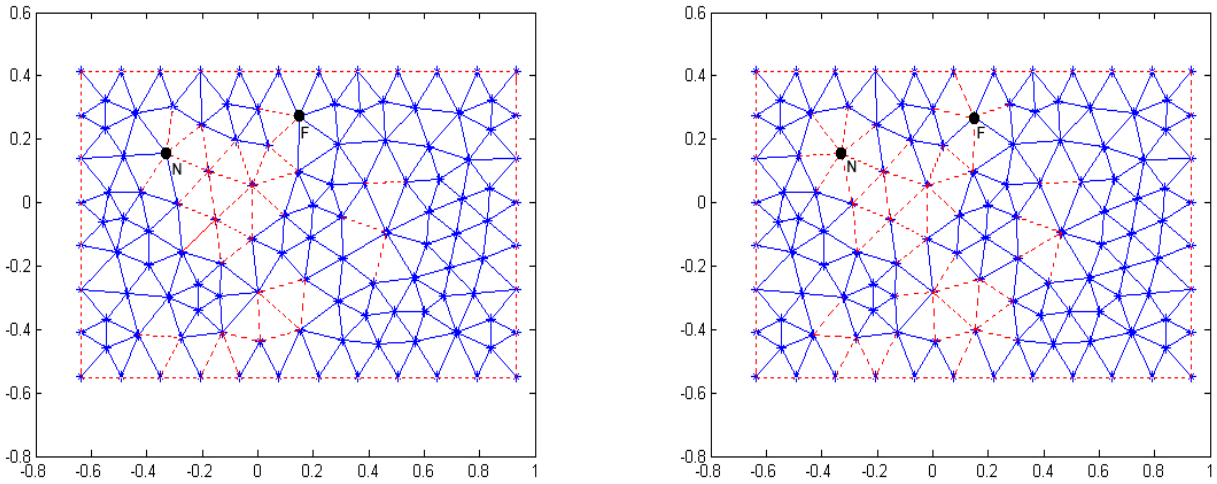

Figure 5.19: Most reinforced paths, $k = 20$, $\alpha = 3$, $\beta = 0.8$; 1000 time steps and 10000 ants (left), and 10000 time steps and 1000 ants (right). Nest at node N and food source at node F.

5.5.2 Bounced conditions

If we impose the condition for the ants to bounce when arriving to the boundaries, we get that:

a) Ants usually reinforce straight lines even though they do not connect nest and food. They do not get trapped in the boundaries (see figures 5.20) and 5.21).

b) More ants than in the case of non-bounced conditions follow the shortest path between nest and food.

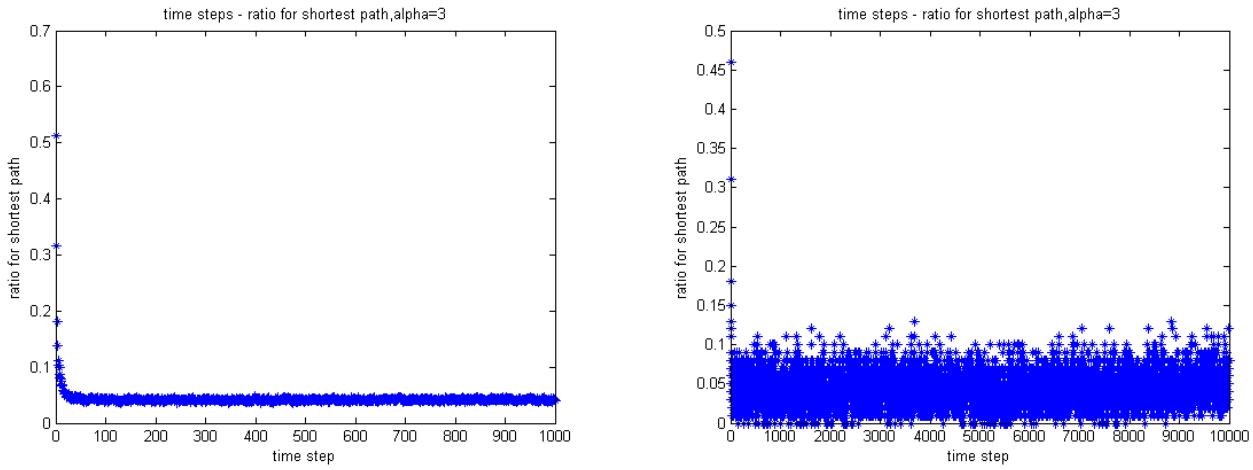

Figure 5.20: Temporal evolutions for r plots, $k = 20$, $\alpha = 3$, $\beta = 0.8$; 1000 time steps and 10000 ants (left), and 10000 time steps and 1000 ants (right).

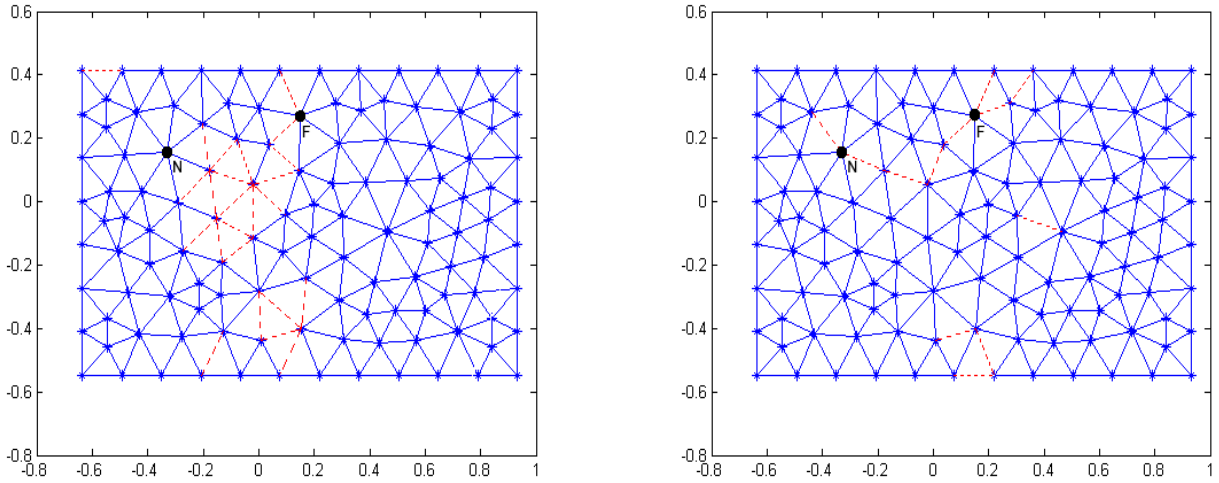

Figure 5.21: Most reinforced paths, $k = 20$, $\alpha = 3$, $\beta = 0.8$; 1000 time steps and 10000 ants (left), and 10000 time steps and 1000 ants (right). Nest at node N and food source at node F.

5.6 Conclusions

In this chapter, we have considered mazes of general geometry and topology in order to investigate whether the same rules for the creation of geodesic paths that we proved to be sufficient for simple graphs, are also sufficient in more general situation or not. Our conclusion, in agreement with experimental observations by previous authors, is that the effect of preferential reinforcement of minimal paths is also present in these cases but can be more or less accentuated strongly depending on the geometry of the network. More precisely:

- In the case of a maze consisting of two triangular networks as considered in the experi-

ments by [1], the effect is clear and all ants end up following the minimal path between nest and food source and this path is created exponentially fast in time.

- In the case of regular hexagonal mazes as considered in [2] we have found, in agreement with experimental observations, a strong dependence on the relative angles between edges at every vertex of the maze. In the case of non-polarized mazes, although a certain number of ants end up following the minimal path, many of them follow cycles inside the maze. In polarized mazes, those cycles tend to disappear and a much larger number of ants end up following minimal paths.

- In the case of triangular meshes, there is a certain reinforcement of minimal paths, but many ants end up following periodic trajectories (if periodic boundary conditions are imposed) that do not touch the nest nor the food source. Imposing Neumann type boundary conditions so that ants "rebound" at the boundaries, alleviate the formation of the cycles but the effect is still present.

Bibliography

[1] S. Goss, S. Aron, J. L. Deneubourg and J. M. Pasteels , Self-organized Shortcuts in the Argentine Ant. Naturwissenschaften **76**, (1989), 579-581.

[2] S. Garnier, S. Guérécheau, M. Combe, V. Fourcassié and G. Theraulaz, Path selection and foraging efficiency in Argentine ant transport networks. Behav. Ecol. Sociobiol. **63**, (2009), 1167-1179.

Chapter 6

Monte Carlo simulations

Goals of this chapter

- Make Monte Carlo simulations to find the best algorithm that reproduces ants' behavior when moving from nest to food source in a continuous plane of size 100×100.

6.1 Monte Carlo approach to the continuous problem

In previous chapters we have shown that the combination of reinforcement and persistence are key to the choice of shortest paths in graphs for a collective of ants undergoing random walks. In this chapter we study whether the same principles are also determinant for the choice of shortest paths in the continuum situation. In order to do that we consider groups of ants undergoing random walks in the plane. We also consider that ants produce a certain quantity of pheromone at a constant rate and this pheromone is deposited at a certain neighborhood of each ant's location. Without reinforcement each ant would jump a finite given distance in an arbitrary direction at any time step. Reinforcement is produced by means of a certain bias in the choice of directions so that ants tend to move preferably towards regions of higher concentration of pheromone. Finally, we will impose a certain persistence so that the choice of direction for an ant's jump without reinforcement is not really random but follows a certain probability distribution with its maximum at the direction of the previous jump.

These principles are the natural extension to the continuum of the rules that where imposed in the case of graphs in previous chapters. Here we will consider a collective of N ants, with N sufficiently large and move them in the plane following the principles stated above.

To summarize, we superpose to the random motion of a finite number of ants in our numerical simulations (henceforth the name of Monte Carlo), the effects of persistence and rein-

forcement produced by the concentration of pheromone. In the next sections we present the technical details of the numerical method together with the results of the simulations.

6.2 Implementation of the Monte Carlo simulations

In this section we simulate the behavior of ants when foraging from nest to food source in different square lattices: 1000×1000 and 100×100. We impose periodic boundary conditions. To do so we create "ghost" links in the boundaries to have the geometry as in a torus.

6.2.1 Algorithm rules

Algorithm I

The algorithm is based on the previous analytical studies of section 4. For the representation of the flow chart for this algorithm see figure (6.1).

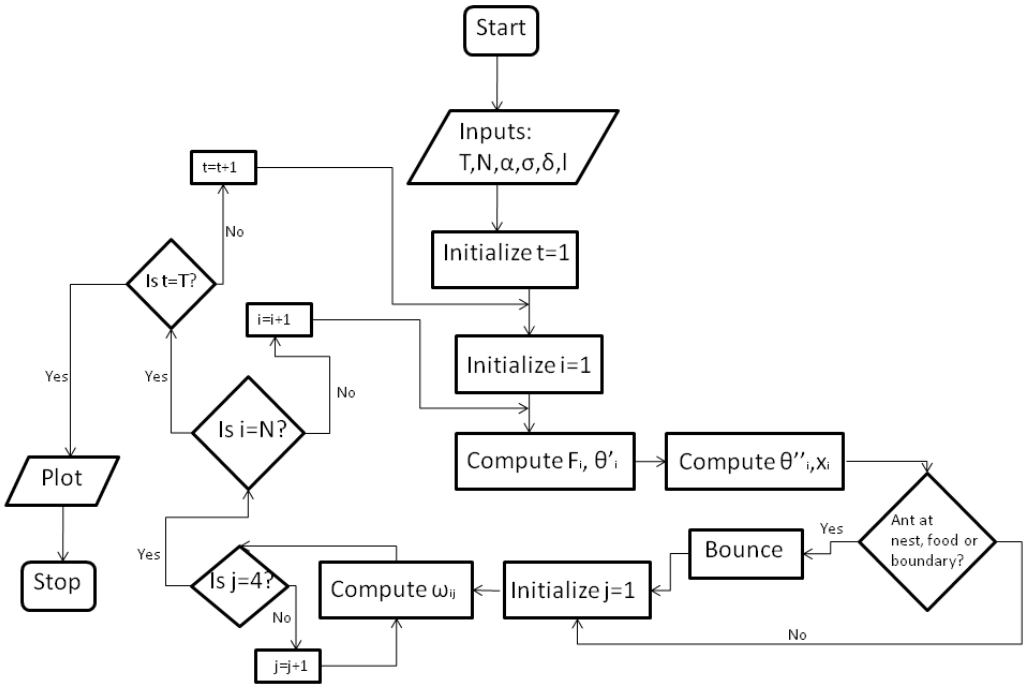

Figure 6.1: Representation of flow chart of Algorithm I.

We consider a continuous plane of size 100×100 and the squared lattice with edges of length $h = 1$. We simulate a certain number of ants $(100, 200, 1000)$ and represent their location as well as the pheromone concentration at various times $(1.000, 5.000, 10.000, 100.000, 1000.000)$. For the shake of simplicity the deposit of pheromone will not be on the neighborhood of each

ant but only on the ant's closest neighbors in a square lattice. Notice that the concentration of pheromone is only defined in the nodes of the lattice. In some sense, we are approximating the concentration of pheromone, which is a continuous function, buy its discretization. When computing an ant's new direction, only the amount of pheromone in the lattice of closest ant's neighbors will be consider. We let the ants move in the continuous plane having positions $\overrightarrow{x_n} = (x_n, y_n)$, where $x_n, y_n \in \mathbb{R} \bigcap [1, 100]$ but they are only allowed to deposit pheromone ω_{ij} at the integer points (i, j) where $i, j \in \mathbb{Z} \bigcap [1, 100]$. We select two special regions in the plane: the nest and the food source where the ants behave in a different way as they do in the rest of the plane.

Initially, ants leave the nest with an angle between $[-10°, 10°]$ measured from the positive X axis. To do so, we consider the rand command (random number generator of a uniform distribution) from MATLAB and we fit the parameters to this range. Once all the ants have leaved the nest we perform the following time steps for each ant i, with direction vector $\overrightarrow{\theta_i}$ and position $\overrightarrow{x_i}$:

Step 1. We calculate the Euclidean distance from its position to the four nearest integer nodes in the lattice: d_{i1}, d_{i2}, d_{i3} and d_{i4}. Once we know these distances, we calculate the $\overrightarrow{F_i}$ vector as follows:

$$\overrightarrow{F_i} = \sum_{j=1}^{4} \overrightarrow{e_{ij}} \frac{\frac{\omega_{ij}}{d_{ij}}}{\left(\sum_{k=1}^{4} \frac{1}{d_{ik}}\right)\left(\sum_{h=1}^{4} \omega_{ih}\right)},$$

where $\overrightarrow{e_{ij}}$ is the unit vector in the direction of the vector connecting the ant i with the node j. For the case $\omega_{ih} = 0 \ \forall h$, we take $\overrightarrow{F_i} = 0$. Let us notice that $\overrightarrow{F_i}$ is the center of mass when considering the amount of pheromone as a mass. This vector points to the preferential direction taking into account only the amount of pheromone the ant is able to sense.

Step 2. We calculate next the new direction vector $\overrightarrow{\theta_i'}$ as follows:

$$\overrightarrow{\theta_i'} = \frac{\overrightarrow{\theta_i} + \delta \overrightarrow{F_i}}{|\overrightarrow{\theta_i} + \delta \overrightarrow{F_i}|}, \tag{6.1}$$

where $\delta \ll 1$ is a small parameter measuring the change of direction due to the anisotropy in the concentration of pheromone. We consider now a small stochastic perturbation of this vector by taking a normal distribution with mean zero and variance σ. To do so, we employ the MATLAB command randn (random number generator of a normal distribution with mean zero and variance one) and multiply the result times σ, that is $prob = randn \times \sigma$. Hence, we can calculate the new direction vector $\overrightarrow{\theta_i''}$ as follows:

$$\overrightarrow{\theta_i''} = [\cos(\theta_i' + prob), \sin(\theta_i' + prob)],$$

where θ_i' is the angle between vector $\overrightarrow{\theta_i'}$ and the positive X axis.

For the two special cases, ant being at nest or food source, we change the new vector direction by considering, as at the beginning, a random direction vector with angle between $[-10°, 10°]$ pointing in the outward direction. As we will see below, computing the new directions in this way produces results that agree with experimental observations but are not fully satisfactory in order to select paths of minimal length. Following the observations in [1], we introduce *saturation* effects so that the deviation of the directions cannot be larger than a certain maximum value. This is achieved by using the formula:

$$\overrightarrow{\theta_i'} = \frac{\overrightarrow{\theta_i} + \frac{\delta\overrightarrow{F_i}}{1+\alpha\delta|\overrightarrow{F_i}|}}{\left|\overrightarrow{\theta_i} + \frac{\delta\overrightarrow{F_i}}{1+\alpha\delta|\overrightarrow{F_i}|}\right|}, \tag{6.2}$$

instead of (6.1). The parameter α is introduced in order to set the maximum possible deviation. It is simple to show that the maximum deviation in the direction vector is $\pm \arctan(\frac{1}{\alpha})$.

Step 3. We can calculate the new position for the ant i as follows:

$$\overrightarrow{x_i}' = \overrightarrow{x_i} + \ell \frac{\overrightarrow{\theta_i''}}{|\overrightarrow{\theta_i''}|},$$

where ℓ is the jump length (to simplify the algorithm we always consider this value equals to one).

Before depositing the pheromone, we have to check if the ant is in the boundary, at nest or at food source. When the ant is in the boundary, we consider a new position following the periodic conditions: we identify the extremes as in a torus. For the two special cases, ant being at nest or food source, we also modify the ant new position by considering the last position for the ant. In this way, we make the ant to bounce at the nest/food.

Step 4. In order to deposit the pheromone in the four nearest nodes to the ant, we calculate the distance d_{ij} from the ant's position to each nearest nodes $j = 1, 2, 3, 4$. We do not add any pheromone to the other nodes.

The amount of pheromone the ant leaves in each node is inversely proportional to the distance to that node j. That is:

$$\omega_{ij} = \frac{\frac{1}{d_{ij}}}{\sum_{k=1}^{4} \frac{1}{d_{ik}}}\Omega,$$

where Ω is the total amount of pheromone deposit by an ant at each step. Notice that, $\sum_j \omega_{ij} = \Omega$. If the ant is at the boundary, we deposit only the half of this quantity. In this way, we avoid to deposit the double of pheromone at the boundary.

Algorithm II

Algorithm II mainly differs from Algorithm I in the deposit of pheromone. Figure (6.2) shows the representation of the flow chart for this algorithm.

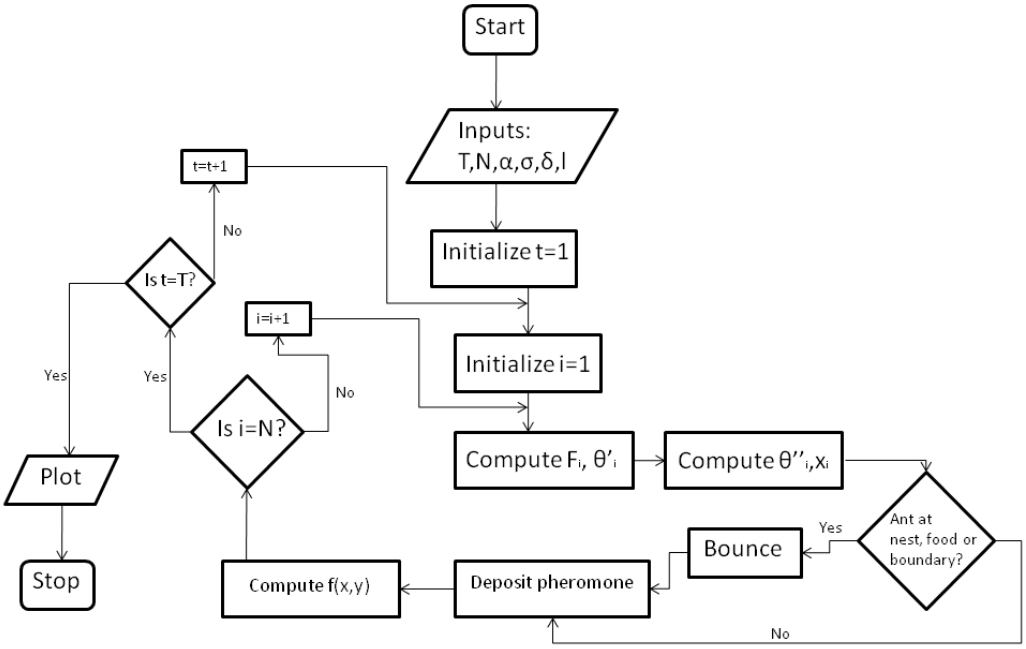

Figure 6.2: Representation of flow chart of Algorithm II.

We consider a continuous plane of size 100×100 and the squared lattice with edges of length $h = 1$. We simulate a certain number of ants $(100, 1000)$ and represent their location as well as the pheromone concentration at various times $(1.000, 5.000, 10.000)$. The deposit of pheromone will be at each ant's position. Notice that the concentration of pheromone is defined in the hole lattice. When computing an ant's new direction, we take into account the complete amount of pheromone in the lattice. We let the ants move in the continuous plane having positions $\overrightarrow{x_n} = (x_n, y_n)$, where $x_n, y_n \in \mathbb{R} \bigcap [1, 100]$ and they are allowed to deposit pheromone ω_{ij} at all real points (i, j) where $i, j \in \mathbb{R} \bigcap [1, 100]$. We select two special regions in the plane: the nest and the food source where the ants behave in a different way as they do in the rest of the plane.

Initially, ants leave the nest with an angle between $[-10°, 10°]$ measured from the positive X axis. To do so, we consider the rand command (random number generator of a uniform distribution) from MATLAB and we fit the parameters to this range. Once all the ants have leaved the nest we perform the following time steps for each ant i, with direction vector $\overrightarrow{\theta_i}$ and position $\overrightarrow{x_i}$:

Step 1. For each ant i being at position (x_i, y_i), we consider the pheromone concentration

function $f(x,y)$ as:

$$f(x,y) = \sum_j e^{-\frac{(x-x_j)^2+(y-y_j)^2}{\beta}}. \tag{6.3}$$

This choice of $f(x,y)$ as the sum of gaussian functions with standard deviation $\sqrt{\beta}$ is inspired on the fact that pheromone is transported by diffusion (the fundamental solution of a diffusion equation is gaussian) with a time scale much larger than the time scale for the motion of ants. Hence, β is taken to be a constant. Making β slowly ranging in time does not change the results significantly. We calculate the $\overrightarrow{F_i}$ vector as the gradient of function f (largest increase):

$$\overrightarrow{F_i} = \nabla f(x,y) = -\frac{2}{\beta}\sum_j (x-x_j, y-y_j) e^{-\frac{(x-x_j)^2+(y-y_j)^2}{\beta}}.$$

This vector points to the preferential direction taking into account only the amount of pheromone the ant is able to sense.

Step 2. We calculate next the new direction vector $\overrightarrow{\theta_i'}$ as follows:

$$\overrightarrow{\theta_i'} = \frac{\overrightarrow{\theta_i} + \delta\overrightarrow{F_i}}{|\overrightarrow{\theta_i} + \delta\overrightarrow{F_i}|}, \tag{6.4}$$

where $\delta \ll 1$ is a small parameter measuring the change of direction due to the anisotropy in the concentration of pheromone. We consider now a small stochastic perturbation of this vector by taking a normal distribution with mean zero and variance σ. To do so, we employ the MATLAB command randn (random number generator of a normal distribution with mean zero and variance one) and multiply the result times σ, that is $prob = randn \times \sigma$. Hence, we can calculate the new direction vector $\overrightarrow{\theta_i''}$ as follows:

$$\overrightarrow{\theta_i''} = [\cos(\theta_i' + prob), \sin(\theta_i' + prob)],$$

where θ_i' is the angle between vector $\overrightarrow{\theta_i'}$ and the positive X axis.

For the two special cases, ant being at nest or food source, we change the new vector direction by considering, as at the beginning, a random direction vector with angle between $[-10°, 10°]$ pointing in the outward direction. As in algorithm I, we can also introduce saturation effects by replacing (6.4) by (6.2).

Step 3. We can calculate the new position for the ant i as follows:

$$\overrightarrow{x_i}' = \overrightarrow{x_i} + \ell\frac{\overrightarrow{\theta_i''}}{|\overrightarrow{\theta_i''}|},$$

where ℓ is the jump length (to simplify the algorithm we always consider this value equals to one).

Before depositing the pheromone, we have to check if the ant is in the boundary, at nest or at food source. When the ant is in the boundary, we consider a new position following the periodic conditions: we identify the extremes as in a torus. For the two special cases, ant being at nest or food source, we also modify the ant's new position by considering the last position for the ant. In this way, we make the ant to bounce at the nest/food.

Step 4**.** We deposit the pheromone in the real point of the plane where the ant has moved to. Hence, we have a new summand in (6.3).

6.3 Numerical results without saturation

6.3.1 Numerical results for Algorithm I

We employ different MATLAB program simulations to show:

a) The amount of pheromone for small time t is spread on the complete plane for both cases: nest in front of food source or nest not in front of food source (figures 6.3, 6.5, left).

b) The amount of pheromone for time t sufficiently great is concentrated between nest and food source for both cases. For the case nest in front of food source it is much more concentrated than for the case nest not in front of food source (figures 6.4, 6.6, left).

c) Ants follow the geodesic path between nest and food much more times when time t is sufficiently large (see figures 6.3, 6.4, 6.5, 6.6).

d) Ants make cycles when applying a modification in Algorithm I and we take not only the values at 4 nearest nodes but at 6 nearest nodes (see figure 6.7). Remarkably, this kind of behavior has been observed experimentally in [1] (see figure 6.8).

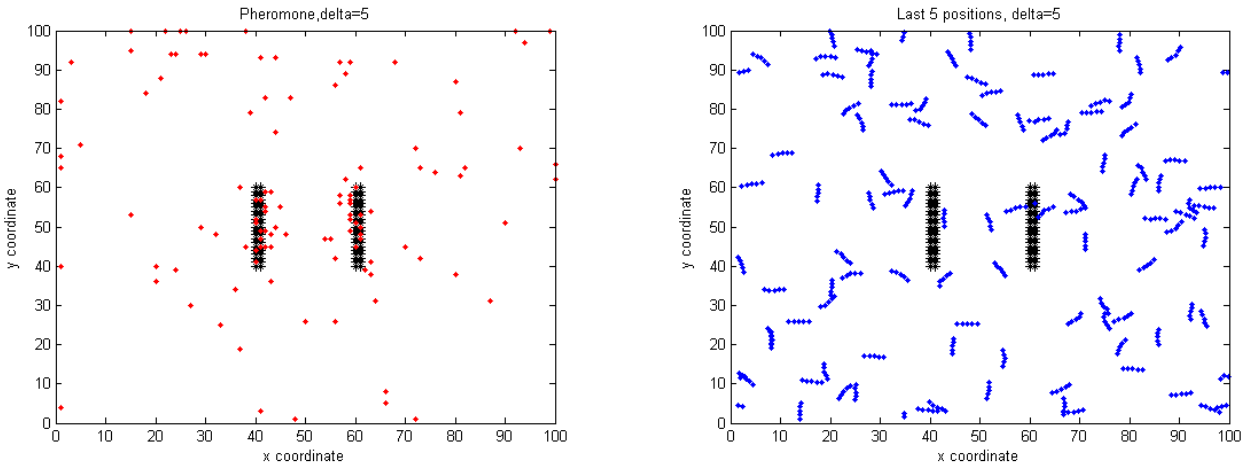

Figure 6.3: Pheromone (left) and last five ants' position (right) for $t = 1000$ simulations, $n = 100$ ants, $\delta = 5$, $\sigma = 0.01$. Nest at $(40-41, 40-60)$ and food source at $(60-61, 40-60)$. Ants start their motion, at $t = 0$, from the center of the nest.

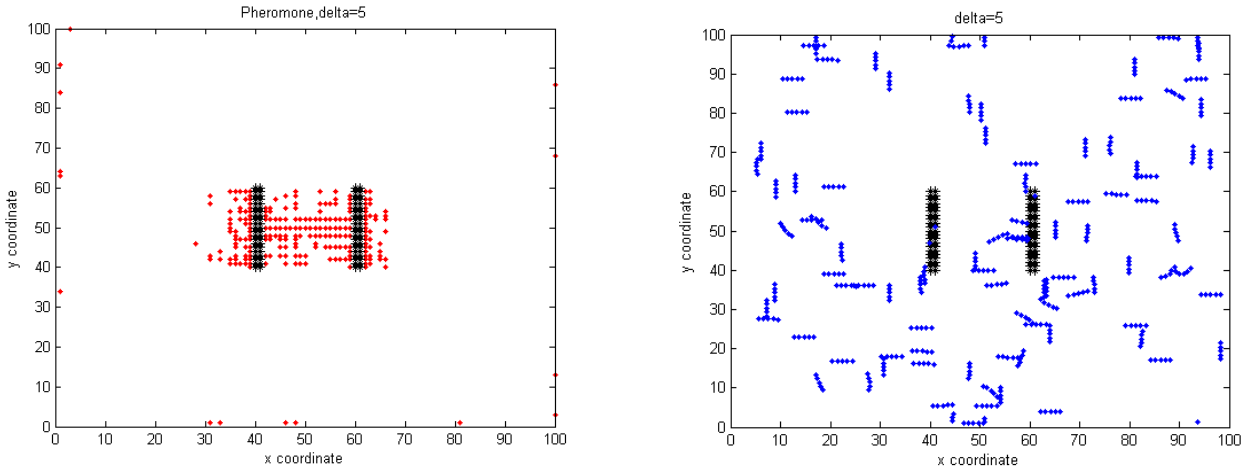

Figure 6.4: Pheromone (left) and last five ants' position (right) for $t = 100000$ simulations, $n = 100$ ants, $\delta = 5$, $\sigma = 0.01$. Nest at $(40-41, 40-60)$ and food source at $(60-61, 40-60)$. Ants start their motion, at $t = 0$, from the center of the nest.

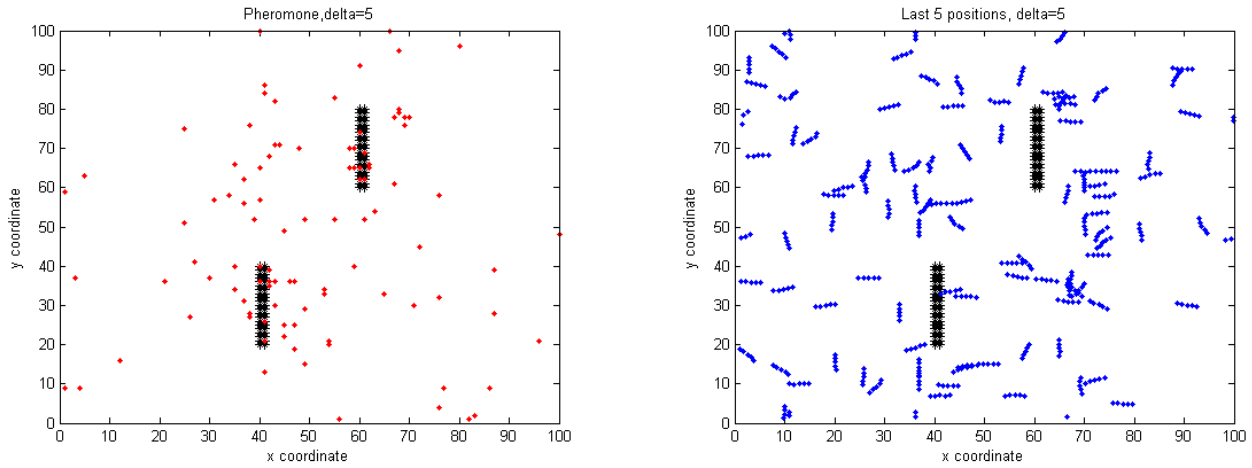

Figure 6.5: Pheromone (left) and last five ants' position (right) for $t = 1000$ simulations, $n = 100$ ants, $\delta = 5$, $\sigma = 0.01$. Nest at $(40-41, 20-40)$ and food source at $(60-61, 60-80)$. Ants start their motion, at $t = 0$, from the center of the nest.

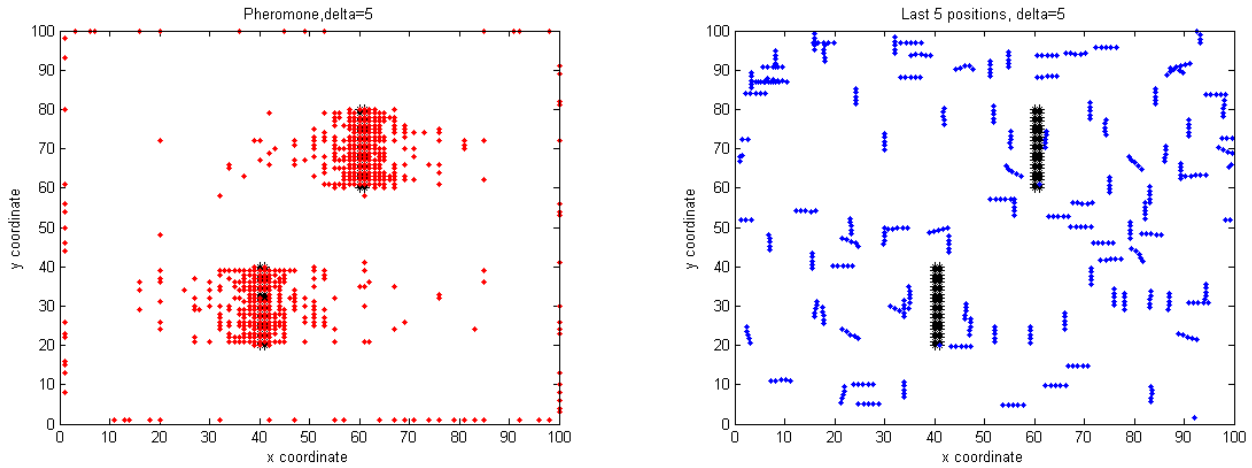

Figure 6.6: Pheromone (left) and last five ants' position (right) for $t = 100000$ simulations, $n = 100$ ants, $\delta = 5$, $\sigma = 0.01$. Nest at $(40-41, 20-40)$ and food source at $(60-61, 60-80)$. Ants start their motion, at $t = 0$, from the center of the nest.

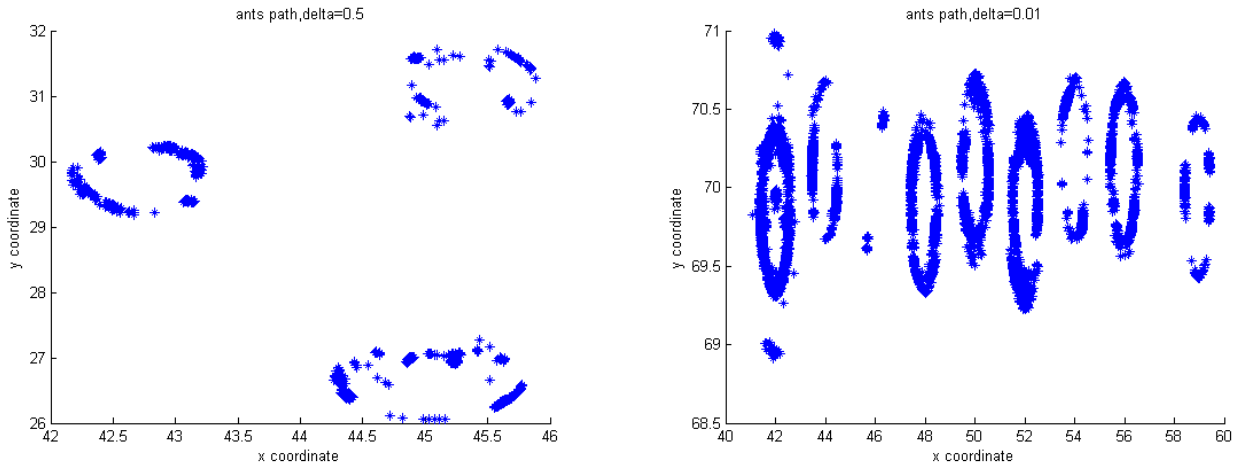

Figure 6.7: Last five ants' position for $t = 1000$ simulations, $n = 100$ ants, $\delta = 0.5$, $\sigma = 0.01$ (left); $t = 1000$ simulations, $n = 100$ ants, $\delta = 0.01$, $\sigma = 0.01$ (right). Nest at $(40-41, 40-60)$ and food source at $(60-61, 40-60)$. Ants start their motion, at $t = 0$, from the center of the nest.

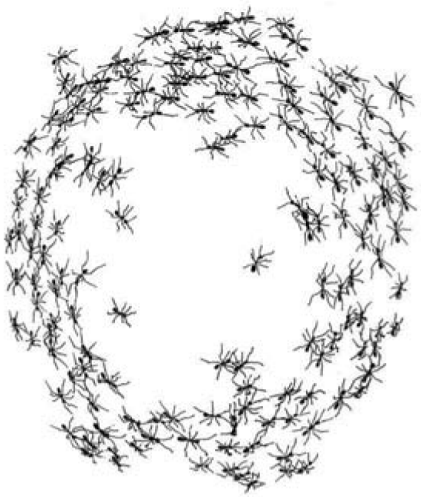

Figure 6.8: Circular milling. Figure from [1].

6.3.2 Numerical results for Algorithm II

We use different MATLAB program simulations to show:

a) The amount of pheromone for small time t is spread on the complete plane (figure 6.9, left).

b) The amount of pheromone for time t sufficiently great is concentrated between nest and food source (figure 6.10, left).

c) Ants try to follow circular mills (see figures 6.11 and 6.12) as in figure 6.8 from [1].

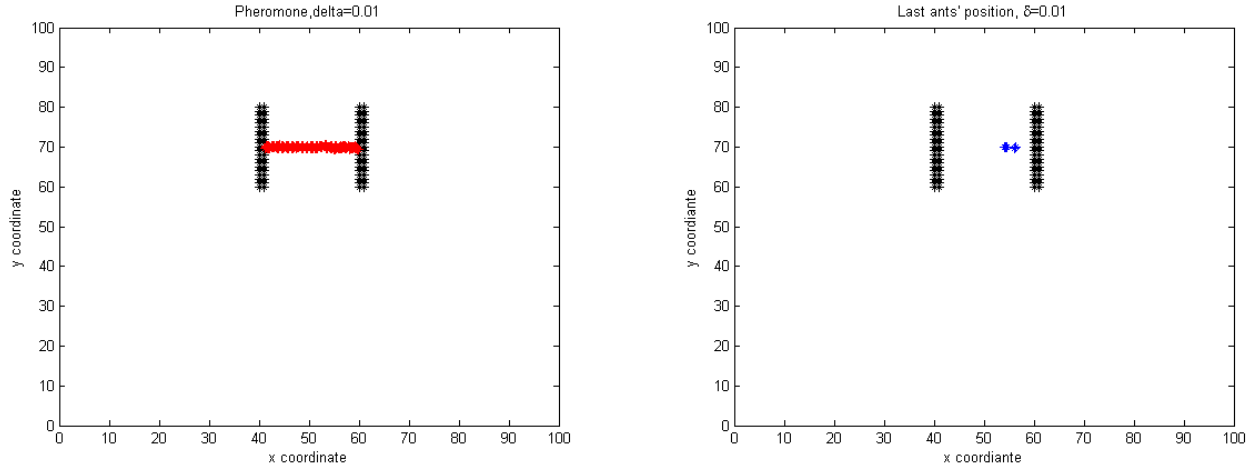

Figure 6.9: Pheromone (left) and last ants' position (right) for $t = 100$ simulations, $n = 10$ ants, $\delta = 0.01$, $\sigma = 0.01$. Nest at $(40-41, 40-60)$ and food source at $(60-61, 40-60)$. Ants start their motion, at $t = 0$, from the center of the nest.

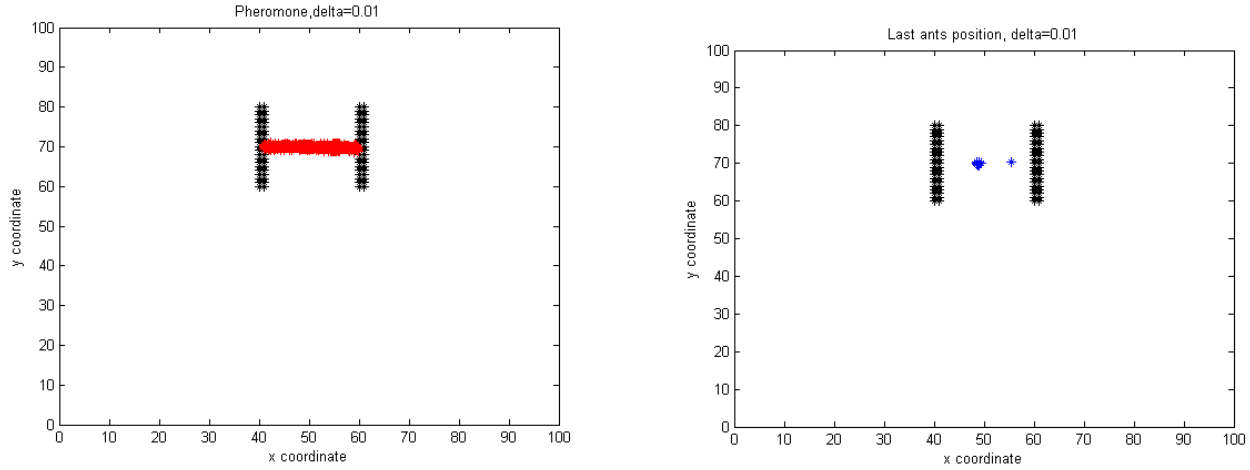

Figure 6.10: Pheromone (left) and last ants' position (right) for $t = 1000$ simulations, $n = 10$ ants, $\delta = 0.01$, $\sigma = 0.01$. Nest at $(40-41, 40-60)$ and food source at $(60-61, 40-60)$. Ants start their motion, at $t = 0$, from the center of the nest.

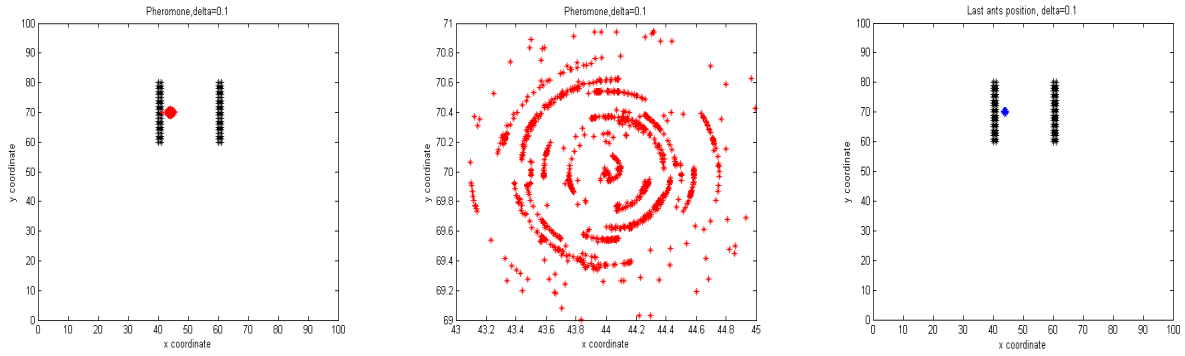

Figure 6.11: Pheromone (left, middle) and last ants' position (right) for $t = 100$ simulations, $n = 10$ ants, $\delta = 0.1$, $\sigma = 0.01$. Nest at $(40-41, 40-60)$ and food source at $(60-61, 40-60)$. Notice that the maximum pheromone concentration is in concentric circles, indicating that ants tend to follow circular paths. Ants start their motion, at $t = 0$, from the center of the nest.

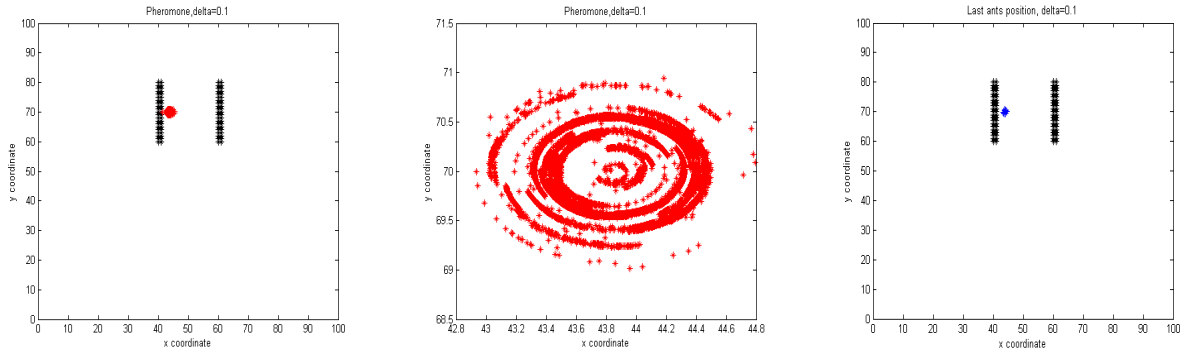

Figure 6.12: Pheromone (left, middle) and last ants' position (right) for $t = 1000$ simulations, $n = 10$ ants, $\delta = 0.1$, $\sigma = 0.01$. Nest at $(40-41, 40-60)$ and food source at $(60-61, 40-60)$. Notice that the maximum pheromone concentration is in concentric circles, indicating that ants tend to follow circular paths. By comparing with the previous figure, we can see that ants tend to concentrate in a unique circular path. Ants start their motion, at $t = 0$, from the center of the nest.

6.4 Numerical results with saturation

As reported in [1], some ant species, as Army ants, are not only good at following trails but also have a propensity to form circular mills when moderate numbers are separated from a colony and restricted to a confined area (see figure 6.8). After a period of disorder, the ants all begin moving in the same direction. This behavior is likely to reflect the ability of Army ant colonies to select a raid direction. In order to avoid this circular milling, we have given less weight to the chemotaxis component, and so more importance to the directionality, as it was done in [1].

This is achieved by introducing saturation into the directionality change, i.e. by using formula (6.2) instead of (6.1) in Algorithm I and (6.2) instead of (6.4) in Algorithm II. By using the value $\alpha = 2$ in Monte Carlo simulations, we are able to avoid the formation of cycles of ants and then intent to create paths of minimal length between nest and food source. See figures 6.13, 6.14 and 6.15 by using Algorithm I with saturation and figures 6.16, 6.17 and 6.18 by using Algorithm II with saturation. It is interesting to observe that ants tend to create paths of minimal length but their trajectory is not purely straight but presents a small sinusoidal oscillation around the minimal path as represented in figure 6.19 from [1]. This effect is also observed in our numerical simulations.

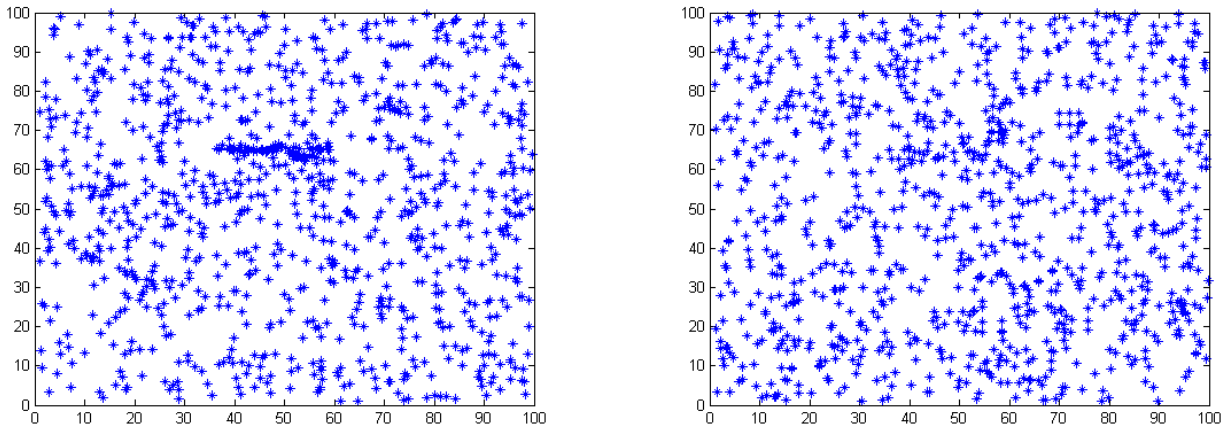

Figure 6.13: Last ants' position for $t = 10000$ simulations, $n = 1000$ ants, $\delta = 0.5$, $\sigma = 0.01$, with (left) and without (right) reinforcement. Nest at $(40 - 41, 40 - 60)$ and food source at $(60 - 61, 40 - 60)$. Ants leave nest with equidistance angles and start their motion, at $t = 0$, from the center of the nest. Algorithm I.

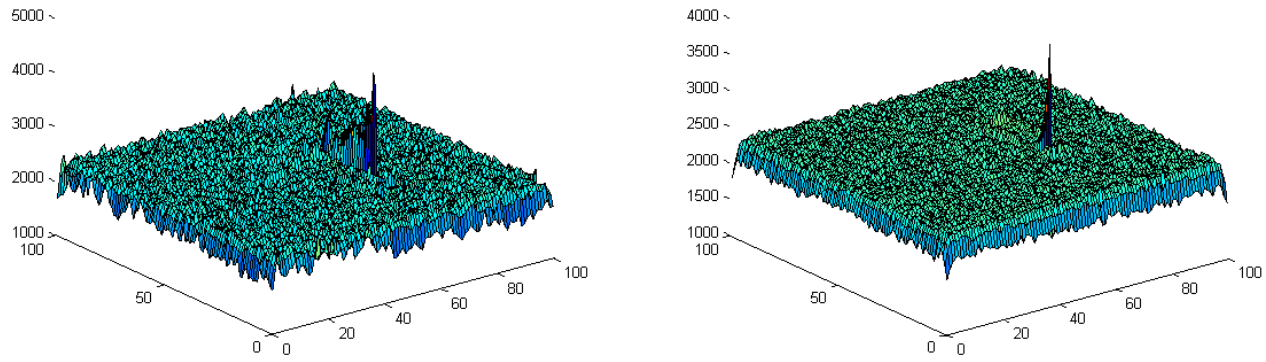

Figure 6.14: Pheromone for $t = 10000$ simulations, $n = 1000$ ants, $\delta = 0.5$, $\sigma = 0.01$, with (left) and without (right) reinforcement. Nest at $(40-41, 40-60)$ and food source at $(60-61, 40-60)$. Ants leave nest with equidistance angles and start their motion, at $t = 0$, from the center of the nest. Algorithm I.

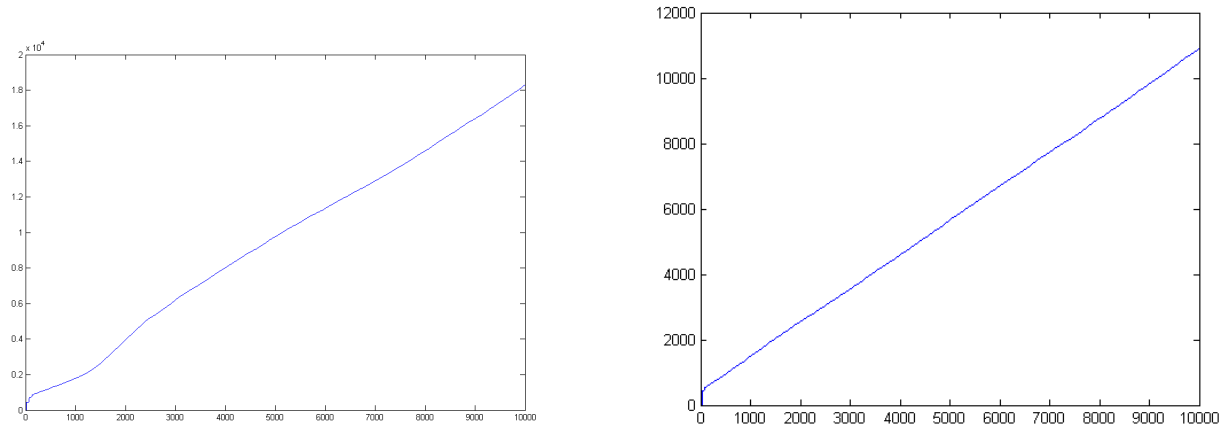

Figure 6.15: Function for the number of visits to food source for $t = 10000$ simulations, $n = 1000$ ants, $\delta = 0.5$, $\sigma = 0.01$, with (left) and without (right) reinforcement. Nest at $(40-41, 40-60)$ and food source at $(60-61, 40-60)$. Ants leave nest with equidistance angles and start their motion, at $t = 0$, from the center of the nest. Algorithm I.

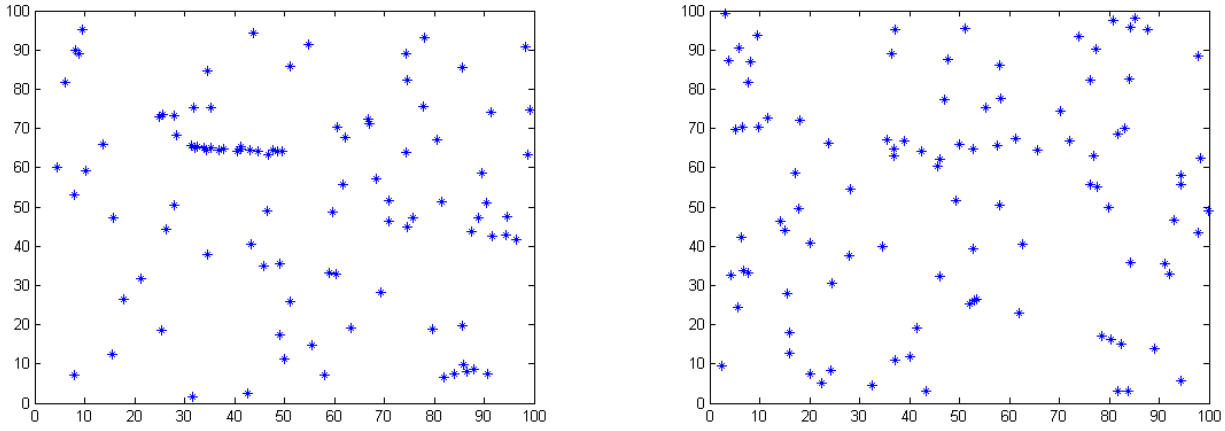

Figure 6.16: Last ants' position for $t = 700$ simulations, $n = 100$ ants, $\delta = 0.5$, $\sigma = 0.07$, with (left) and without (right) reinforcement. Nest at $(40 - 41, 40 - 60)$ and food source at $(60 - 61, 40 - 60)$. Ants leave nest with equidistance angles and start their motion, at $t = 0$, from the center of the nest. Algorithm II.

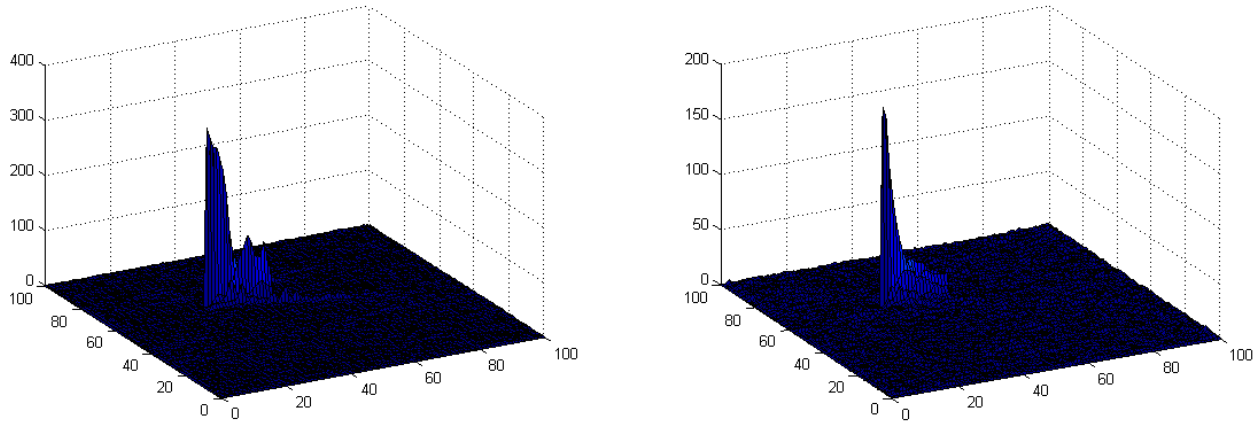

Figure 6.17: Pheromone for $t = 700$ simulations, $n = 100$ ants, $\delta = 0.5$, $\sigma = 0.07$, with (left) and without (right) reinforcement. Nest at $(40-41, 40-60)$ and food source at $(60-61, 40-60)$. Ants leave nest with equidistance angles and start their motion, at $t = 0$, from the center of the nest. Algorithm II.

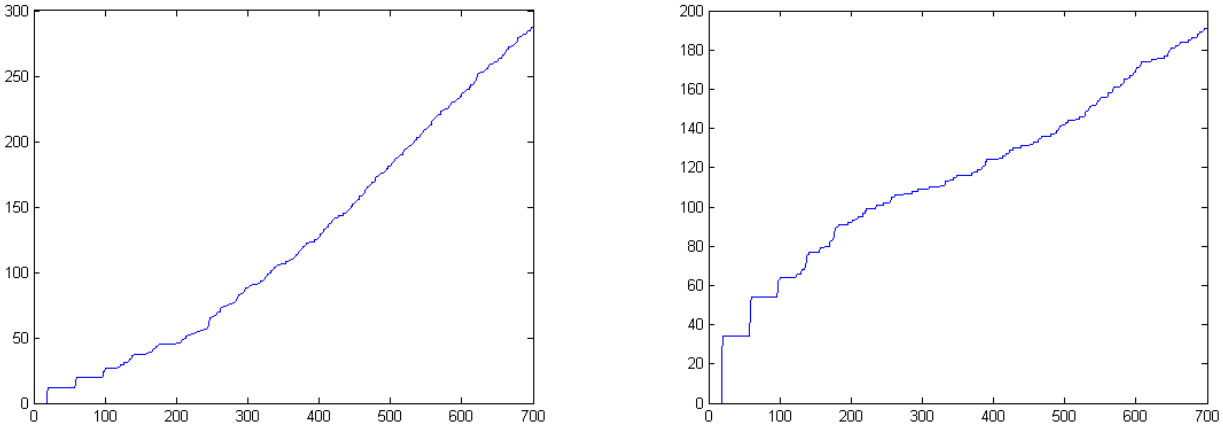

Figure 6.18: Function for the number of visits to food source for $t = 700$ simulations, $n = 100$ ants, $\delta = 0.5$, $\sigma = 0.07$, with (left) and without (right) reinforcement. Nest at $(40-41, 40-60)$ and food source at $(60-61, 40-60)$. Ants leave nest with equidistance angles and start their motion, at $t = 0$, from the center of the nest. Algorithm II.

Figure 6.19: Typical trajectories of simulated ants. Figure from [1].

6.5 Conclusions

We have shown by means of numerical simulations that in order for the ants to follow the geodesic path in the plane, it is necessary not only to invoke the pheromone-induced reinforcement but also to have a directionality constraint and a saturation effect to avoid large deviations with respect to the straight line direction. Furthermore, more than one ant is also needed to reinforce the geodesic path. We have done this by implementing two different algorithms based on Monte Carlo type simulations:

- In Algorithm I, we deposit pheromone in discrete points of the plane and ants measure at each time step the concentration of pheromone at neighbor nodes. Depending on these concentrations and the direction of the ant, it decides the new direction to move according to a certain reinforced stochastic law. Minimal paths are created so that most of the ants end up following it.

- In Algorithm II, pheromone is deposited according to a gaussian law for the concentration that is centered at the ants location. In this way, the amount of pheromone is a sum of gaussians from which one can compute the change in direction according to a law similar to Algorithm I. The observations concerning creation of minimal paths are identical although this algorithm is much more expensive from the computational point of view.

- If directionality constraint (or persistence in the notation introduced in previous chapters) is removed from both algorithms, then ants end up forming circular milling, as reported in experiments from [1].

Bibliography

[1] I. D. Couzin and N. R. Franks, Self-organized lane formation and optimized traffic flow in army ants. Proc. R. Soc. Lond. B **270(22)**, (2003), 139-146.

Chapter 7

Conclusiones

Destacamos las siguientes conclusiones extraídas de esta monografía:

Descripción del problema

- Se han descrito en detalle los resultados experimentales para 4 tipos diferentes de hormigas.
- Se han estudiado en detalle algunos modelos aparecidos en la literatura.

Resultados analíticos

- Se han resuelto de forma analítica los modelos propuestos para redes con reforzamiento con dos y tres nodos para una hormiga.
- Se ha resuelto de forma analítica el modelo para una red con 3 nodos sin reforzamiento y con direccionalidad para dos hormigas.
- Se ha resuelto de forma analítica el modelo para una red con 3 nodos con reforzamiento y con direccionalidad para dos hormigas.

Experiencia computacional

- Se ha realizado una extensa experiencia computacional con redes simples, redes complejas y simulaciones de Montecarlo.
- Se han comparado los resultados obtenidos con los existentes en la literatura.

Chapter 8

Conclusions

Problem description and previous results in the literature

- We have described some interesting experimental results for 4 different types of ants.
- We have described in detail some models appeared in the literature.

Analytical results

- We have solved analytically some models for networks of two and three nodes for one ant.
- We have solved analytically the model for a three node network without reinforcement and with directionality constraint for two ants.
- We have solved analytically the model for a three node network with reinforcement and with directionality constraint for two ants.

Computational experiments

- We have developed numerical algorithms and performed extensive numerical computations in various situations: simple networks, complex networks and Monte Carlo simulations to show that both directionality constraint and reinforcement are needed in order for the ants to follow the shortest paths. Moreover, we have developed a model for the motion of ants in a general planar domain and solve it numerically to show the tendency for the ants to create shortest paths.
- We have compared our results with the ones appeared in the literature.

List of Figures

List of Tables